CO_2 Storage Efficiency in Deep Saline Formations – Stage 2

IEAGHG Technical Report
2018-02
January 2018

IEA GREENHOUSE GAS R&D PROGRAMME

International Energy Agency

The International Energy Agency (IEA), an autonomous agency, was established in November 1974. Its primary mandate was – and is – two-fold: to promote energy security amongst its member countries through collective response to physical disruptions in oil supply, and provide authoritative research and analysis on ways to ensure reliable, affordable and clean energy for its 30 member countries and beyond. Within its mandate, the IEA created Technology Collaboration Programmes (TCPs) to further facilitate international collaboration on energy related topics. To date, there are 38 TCPs who carry out a wide range of activities on energy technology and related issues.

ACKNOWLEDGEMENTS AND CITATIONS

This report describes research commissioned by IEAGHG. This report was prepared by:

- Energy & Environmental Research Center
- University of North Dakota

The principal researchers were:
- Lawrence J. Pekot
- Nicholas W. Bosshert
- Chantsalmaa Dalkhaa
- Neil W Dotzenrod
- Scott C Ayash
- Wesley D. Peck
- Charles D Gorecki

To ensure the quality and technical integrity of the research undertaken by IEAGHG each study is managed by an appointed IEAGHG manager. The report is also reviewed by a panel of independent technical experts before its release.

The IEAGHG managers for this report were:
- James Craig

The expert reviewers for this report were:
- Seyyed A Hosseini, BEG, University of Texas
- Curtis M Oldenberg, LLBL
- Jerry Carr, NETL US DOE
- Ton Wildenborg, TNO
- Stefan Bachu, Alberta Innovates
- Owain Tucker, Shell
- Sarah Gasda, University of Bergen
- Sylvain Thibeau, Total

The report should be cited in literature as follows: 'IEAGHG, "CO_2 Storage Efficiency in Deep Saline Formations – Stage 2", 2018/02, January, 2018.'

Further information or copies of the report can be obtained by contacting IEAGHG at:

IEAGHG, Pure Offices, Cheltenham Office Park, Hatherley Lane, Cheltenham, GLOS., GL51 6SH, UK
Tel: +44 (0)1242 802911 E-mail: mail@ieaghg.org Internet: www.ieaghg.org

CO_2 Storage Efficiency in Deep Saline Formations – Stage 2

A key determinant for CO_2 storage in deep saline formations (DSFs) is dynamic efficiency (E factor) – that is the effect that increased pressure caused by fluid injection has on the storage capacity of a formation. The storage capacity will always be limited by the pressure limit imposed by the geomechanical strength of the caprock, which is defined as the fracture pressure. If a formation is bounded by faults or other low permeability barriers, then excess pressure could limit the dynamic efficiency, a condition referred to as a closed boundary. In contrast formations that extend over several 100 square kilometres without significant barriers can enable pressure to be dissipated, a condition known as an open boundary. In a previous study commissioned by IEAGHG the effects of dynamic efficiency were compared between two contrasting onshore basins (one open and the other closed), but over a long hypothetical time-scale of 2,000 years. Although the previous study[1] showed the effects of boundary conditions, the dynamic efficiency was based on very large areas extending of several thousands of square kilometres. The results did not reflect the more likely conditions of much shorter timescales and injection over limited areas that would be experienced in early CO_2 storage sites. The aim of this second study is to improve the estimated dynamic storage of DSFs based on a modelled 50 year injection period and over comparatively limited areas of ~1,000 km^2. Two well researched formations were selected: one from an onshore basin (the Minnelusa Formation in the USA) and the other form an offshore basin (the Bunter Formation in the North Sea). This study also includes a cost development model to determine how the number of wells affects the cost-effectiveness of each storage site.

Key Messages

- The impact of water extraction on the Minnelusa over a 50 year period raised the storage efficiency from 4.7% to 5.9%. This is equivalent to an estimated increase in storage capacity from 242 Mt to 302 Mt of CO_2. Extending injectivity for a further 50 years would increase storage capacity to over 400 Mt of CO_2.
- The impact of water extraction on the Bunter was profound raising storage efficiency from 4.7% to 7.4%. This is equivalent to raising the estimated storage capacity from 1,770 Mt to 2,806 Mt of CO_2. The difference between these two formations in terms of storage capacity can be attributed to the highly favourable permeability across the Bunter compared with the Minnelusa.
- As the number of injection wells increases in a designated storage system, more of the wells become influenced by pressure interference from their neighbours and the injectivity rate per well declines.
- The closer a DSF approaches full development, the more its efficiency approaches that of a closed system, even if it has open boundaries.
- The differences between open and closed boundaries clearly signifies the importance of defining or conducting a careful preliminary assessment of boundary conditions.
- Well configuration and structural settings can have a significant influence on storage efficiency.
- The annual injection rate profile is a critical parameter in the design of an optimised injection plan for a multiwell project. The rate of injection will gradually decline with time.

[1] CO_2 Storage Efficiency in Deep Saline Formations: A Comparison of Volumetric and Resource Estimation Methods, 2014-09

- In both cases 20% of all the wells in the cost model were able to deliver more than 60% of the total CO_2 injected. In both modelled formations the number of wells was the primary variable in determining the cost factor. Delivering the amount of injected CO_2 by increasing the number of wells becomes proportionately less cost-effective.
- The E factor only applies to the modelled areas, as in these cases, and cannot be extended to the full aquifer unless the model boundaries are coincident with the periphery of the formation.
- There are variations in modelled predictions based on the model grid cell size for the same level of salinity which is a significant parameter that controls CO_2 solubility.
- Heterogeneity and different model projections can substantially influence the quantity of injected CO_2. It is important to understand and separate the effects of the choices of simulation parameters from the physical effects in a storage formation.
- It is recommended that key parameters used for initial dynamic storage estimates are clearly stated and should include: domain dimensions, formation boundaries, caprock threshold limits and the duration of injection.

Background to the Study

A key parameter that will determine the viability of large-scale geological storage of CO_2 is the capacity of extensive deep saline formations (DSFs). Initial estimates have relied on volumetric estimates of formation pore volume, but this approach does not take account of dynamic effects created by the injection of CO_2 and the related pressure build-up. In a previous study EERC modelled the capacity of two DSFs from two contrasting basins (the Minnelusa Formation in the Powder River Basin of the United States and the Qingshankou–Yaojia system of the Songliao Basin of China) based on dynamic conditions. This Stage 1 study was extended over a 2,000 year period and included 820 injection wells distributed across the Minnelusa. Over this time span dynamic resource estimates obtained were comparable to volumetric estimates. Although the Stage 1 study indicated what might be hypothetically achievable a more realistic scenario, based on a 50 year horizon over a limited area of a basin, was necessary to provide greater certainty on dynamic storage estimates.

Scope of the Study

The aim of this Stage 2 study is to investigate the range of storage efficiency that is practically achievable within a 50-year injection period and assess key factors that may influence the effectiveness of CO_2 storage within that shorter time frame.

In Stage 2 two DSFs previously considered for CO_2 storage were investigated. The Minnelusa Formation was re-examined on a sector model scale to provide continuity with the previous work and to allow for direct comparison of the new work with previous efforts. The Stage 2 study has also investigated a sector of the Bunter Sandstone located in the UK's sector of the Southern North Sea Basin to provide an offshore and European counterpoint to the continental setting of the Minnelusa. Additionally, cost estimation methods have been investigated to provide some guidance for CO_2 storage development costs (CAPEX and OPEX for the life cycle of a hypothetical CO_2 storage scenario). The cost evaluation has incorporated results of the modelling exercises to produce cost–benefit indices for onshore and offshore storage development.

Dynamic calculations using reservoir simulation software were based on geological criteria for each study area and then run over a 50 year period. These methods generally provide lower estimates of storage capacity because the software can account for the limitations that

geological conditions place on the ability of injection wells to displace the saline pore water, such as pressure interference between storage sites, model boundary conditions and general pressure buildup in the reservoir.

Existing geological models were used for the two areas that were studied. For the Minnelusa Formation, a 50-km × 25-km sector was selected from a basin-scale model of the formation. For the Bunter Sandstone, an existing 44-km × 22-km sector model was selected. Numerical simulations of both geological models were constructed and similar suites of CO_2 injection cases were tested in both simulations. These simulation suites each included a drilling sensitivity study to estimate a reasonable maximum number of wells that could be effectively utilized for injection within the simulation area and a series of cases to show how 50-year storage efficiency changes as the number of wells increases. A series of alternative scenarios were also executed for both areas to test their sensitivity to different reservoir conditions and different storage development premises. The Stage 1 study showed that the estimation of the amount of injected CO_2 dissolved in formation brine may be influenced by the size of the simulation grid cells. Therefore, an additional sensitivity study was performed using the Minnelusa simulation to systematically investigate this question.

The modelling and simulation efforts of Stage 2 were more geographically focused in comparison to the Stage 1 investigation. An area 50-km wide by 25-km long (1250 km^2) near the eastern margin of the Powder River Basin (Figure 1) of the aforementioned model was selected for use in Stage 2 investigations based upon the presence of desirable petrophysical properties (porosity and permeability). The modelled area exhibited a porosity ranging from 0% to 22% with an average value of 6.9% and permeability ranging from 0.01 mD to 385 mD with a pore volume weighted average of 17.6 mD. This modelled area was designed to investigate the effect of changing grid resolution (cell size) on simulated dissolved CO_2 and to obtain different CO_2 injection simulations (injected volumes, storage efficiency). The designated model area was also used to estimate cost–benefit ratios with differing injection well number/density) over a realistic temporal context of 50 years.

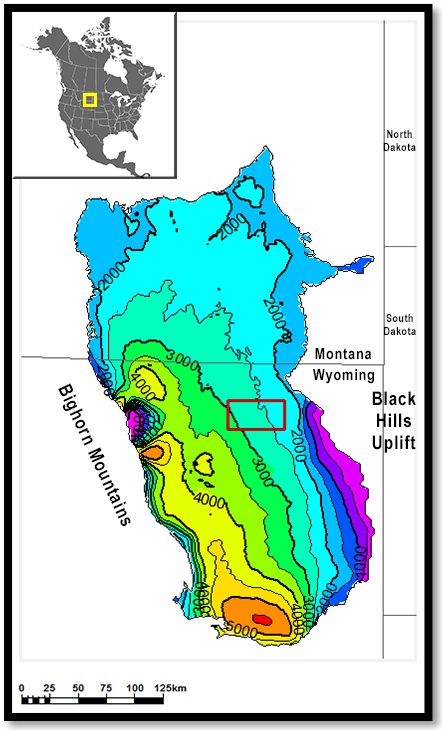

Figure 1. Minnelusa Formation measured depth (m) map within the Powder River Basin of Montana and Wyoming. The Minnelusa model extent is overlain (red rectangle). Contour interval is 500m.

A series of grids were created, all with equal extents (50 km × 25 km) and 50 proportional layers of approximately 1.5 m in thickness. Cell sizes were calculated by applying divisors of 9, 5, 3, and 1 to the original cells 1250 m in length and width. The resulting cells were 139 × 139 m, 250 × 250 m, 417 × 417 m, and 1250 m in length and width, respectively. To explore injection sensitivities to lithofacies distribution, the base case model was altered by varying the amount of sandstone lithofacies within the model. The sandstone lithofacies proportions were varied ±10%, resulting in low, mid, and high cases having 51%, 61%, and 71% sandstone proportions, respectively. Modelled properties were distributed in the fine-scale 139-m × 139-m cell grid area and upscaled into the coarser grids. This approach resulted in averaged properties for the grids containing larger cells but similar pore volumes across each. The low, mid, and high cases, in terms of facies distributions, were a topic of in-depth internal discussion at the EERC. Without having proper statistical support for 'P10/P50/P90' nomenclature for the Minnelusa Formation, a decision was taken to implement the less precise 'low/mid/high' descriptors.

The Bunter Formation comprises a series of medium- to coarse-grained red sandstones interbedded with very coarse sandstones and meter-scale conglomerate layers. The Bunter Sandstone represents a single flow unit and has been previously studied as a desirable target for CO_2 storage (Williams et al, 2013[2], Noy et al, 2012[3]; Brook et al, 2003[4]) because it has reservoir characteristics amenable to injection activities, has numerous dome structures (structural expressions of underlying salt diapirs) which act as natural structural traps, and is well sealed above and below by the evaporites and mudstones of the Upper Triassic Haisborough Group and the Bunter Shale Formation, respectively.

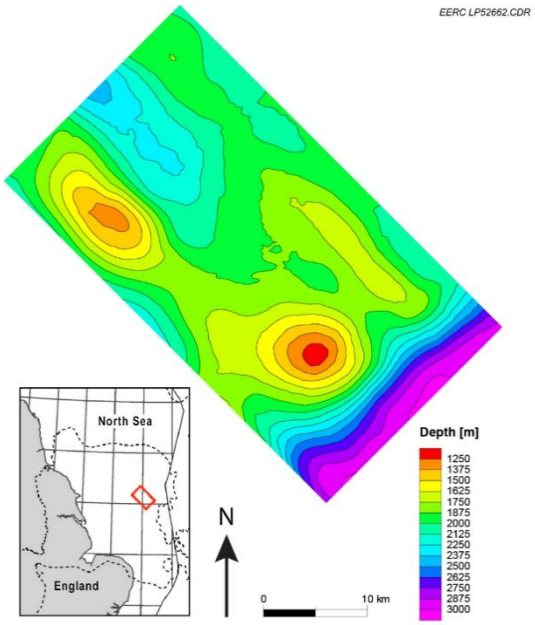

Figure 2. Depth to the top of the Bunter Sandstone, which serves as the upper limit of the geological model. Inset map, adapted from Williams et al (2013), depicts the location of the model (red rectangle) within the North Sea and extent of the Bunter Sandstone (dotted line) in relation to the east coast of England.

[2] Williams, J.D.O., Jin, M., Bentham, M., Pickup, G.E., Hannis, S.D., and Mackay, E.J., 2013, Modelling carbon dioxide storage within closed structures in the UK Bunter Sandstone Formation: International Journal of Greenhouse Gas Control, v. 18, p. 38–50, Copyright 2013, modifications with permission from Elsevier.

[3] Noy, D.J., Holloway, S., Chadwick, R.A., Williams, J.D.O., Hannis, S.A., and Lahann, R.W., 2012, Modelling large-scale carbon dioxide injection into the Bunter Sandstone in the UK Southern North Sea: International Journal of Greenhouse Gas Control, v. 9, p. 220–233.

[4] Brook, M., Shaw, K., Vincent, C., and Holloway, S., 2003, GESTCO Case Study 2a-1—storage potential of the Bunter Sandstone in the UK sector of the southern North Sea and the adjacent onshore area of eastern England: Nottingham, UK, British Geological Survey, 44 p. (CR/03/154N).

An existing model of the Bunter Sandstone, was developed in similar studies of CO_2 storage by the UK's Energy Technologies Institute (ETI) (Energy Technologies Institute, 2016a; Williams et al, 2013). This model was adapted by EERC to obtain CO_2 storage simulations over a realistic timespan of 50 years. The model encompassed the Bunter Sandstone in the study area (using the top of the Bunter Sandstone as the upper limit and the top of the Bunter Shale as the bottom) and gridded with 200-m × 200-m cells. The model ranged in thickness from 135 to 375 m with an average thickness of 235 m. The reservoir was divided into five intervals according to geophysical log analysis performed by Williams et al (2013).

Porosity logs, calculated by Williams et al (2013) through lithologic, petrophysical, and geophysical analyses, served as the basis for geostatistical distributions. The resulting porosities ranged generally from 10% to nearly 30% throughout the reservoir. Permeability of the Bunter Sandstone was calculated using the Kozeny–Carman equation resulting in permeabilities ranging from 0.6 to 106 mD with a pore volume weighted average of 40 mD.

Findings of the Study

Minnelusa Formation Dynamic Simulation Results

Following a calculation of the effective volumetric CO_2 storage resource potential and efficiency, a series of simulations were performed to determine the effective dynamic CO_2 storage resource potential and efficiency. The dynamic simulation workflow was conducted by importing the Minnelusa geologic model sampled for 250-m × 250-m grid cells into Computer Modelling Group's (CMG's) GEM software, a fully compositional simulator. Fifty layers with an average thickness of 1.5 meters were used in the creation of the model. After initial construction of the simulation, determinations were made for injection simulation design, boundary conditions, and variations in structural setting. The injection simulation results are reported for a 50-year injection period, although most cases were executed for 100 years to aid in the interpretation of the results. Effective dynamic CO_2 storage resource potential and efficiency were determined and, where appropriate, compared to the estimated static values.

Figure 3 represents the summation of the CO_2 areal plume distributions of the base case. It is evident from this figure that wells on the perimeter of the selected area maintain higher injectivity than wells in the centre of the pattern, regardless of the well kh (vertical permeability). Figure 4 shows the plume distribution in cross section, which also demonstrates the lesser quantity of CO_2 injected in the interior parts of the model area.

Figure 5 represents the dynamic CO_2 storage efficiency factor vs. the number of wells of the Minnelusa Formation. Compared to the static CO_2 storage efficiency factor which is calculated by the volumetric method, none of the seven cases reached the volumetric storage efficiency within 50 years. This is primarily because of the strong dynamic effect caused by pressure build-up and interference between wells. It also shows that the rate of increase for the dynamic storage efficiency decreases rapidly after the number of wells exceeds 90, which is equivalent to an average well spacing of 13.9 km^2 per well for this model.

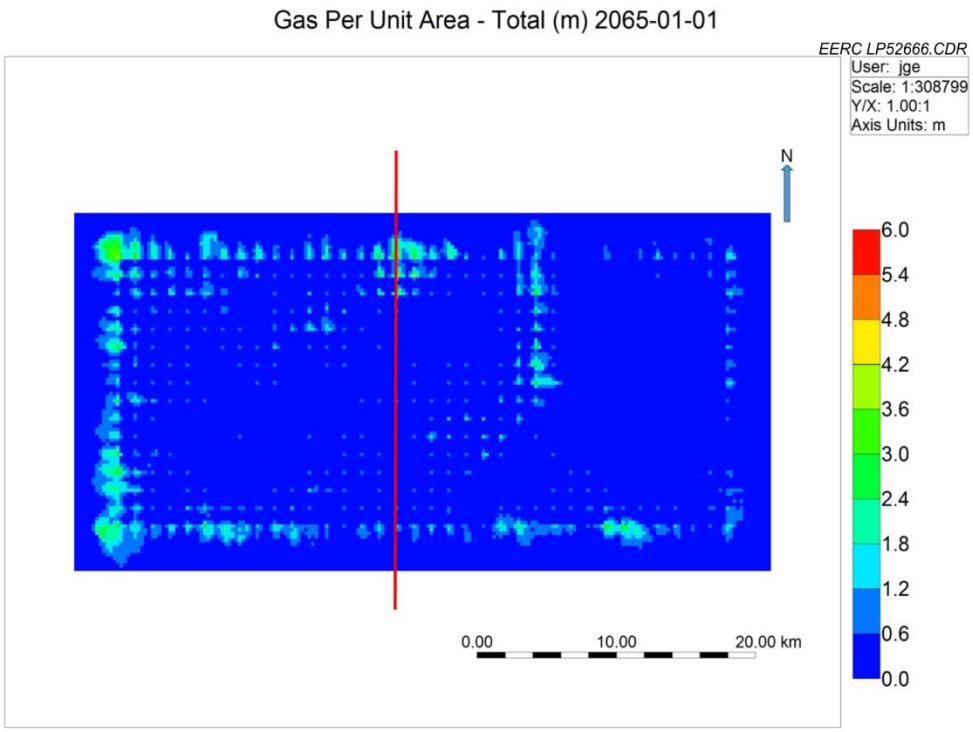

Figure 3. Well placement and injection sensitivity investigation in the Minnelusa Formation: CO_2 footprint (total gas per unit area in meters) after 50 years of injection in the D2 base case.

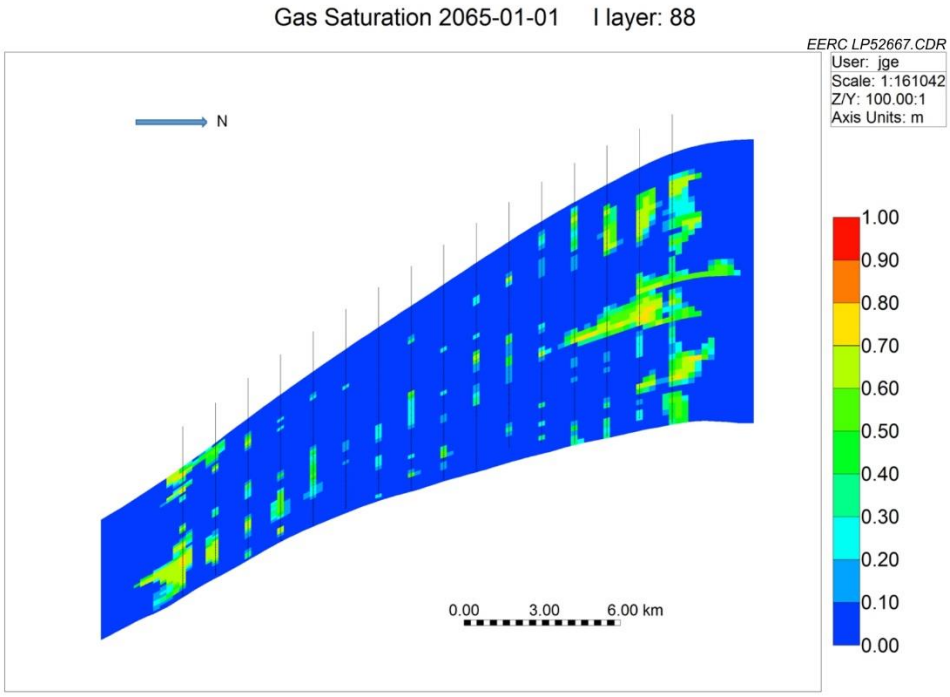

Figure4. Well placement and injection sensitivity investigation in the Minnelusa Formation: CO_2 plume in the D2 base.

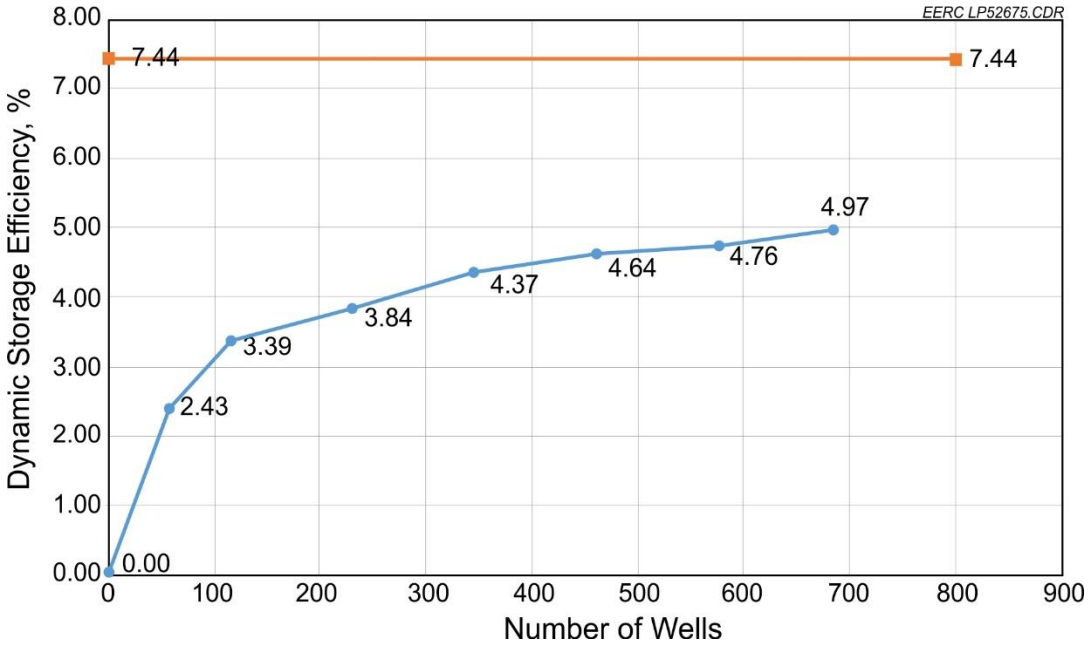

Figure 5. Well placement and injection sensitivity investigation: dynamic CO_2 storage efficiency vs. number of wells for the Minnelusa Formation. Volumetric effective efficiency of 7.44%, for the base case lithology description is also shown.

The effect of different formation conditions, in terms of permeability and dynamic behavior were modelled for comparison. The effective CO_2 storage efficiency, optimistic (E 5.36%), base (E 4.75%), and conservative (E 4.4%) lithology distribution cases for the Minnelusa model are represented in Figure 6. These variations were created by increasing and decreasing the reservoir sand fraction in the geological model, resulting in changes to the percentage of bulk rock volume amenable to storage. These cases resulted in variation of the practical efficiency from 4.04% (conservative case) to 5.36% (optimistic case), as shown in Figure 6. This illustrates that heterogeneity and different model realizations can substantially influence the quantity of injected CO_2. If brine extraction is allowed, capacity can be increased especially over a time span of more than 50 years (E 5.94%).

The water flux across the boundary is estimated by using the Carter–Tracy approximation, and saline formation water is allowed to flow from the reservoir into the connecting aquifer cells where the pressure of a cell exceeds the adjacent aquifer pressure. A closed boundary case is represented in the model where there is no aquifer hydraulic communication across the model boundary. The system effectively acts as a closed system with a low E factor of 1.25%.

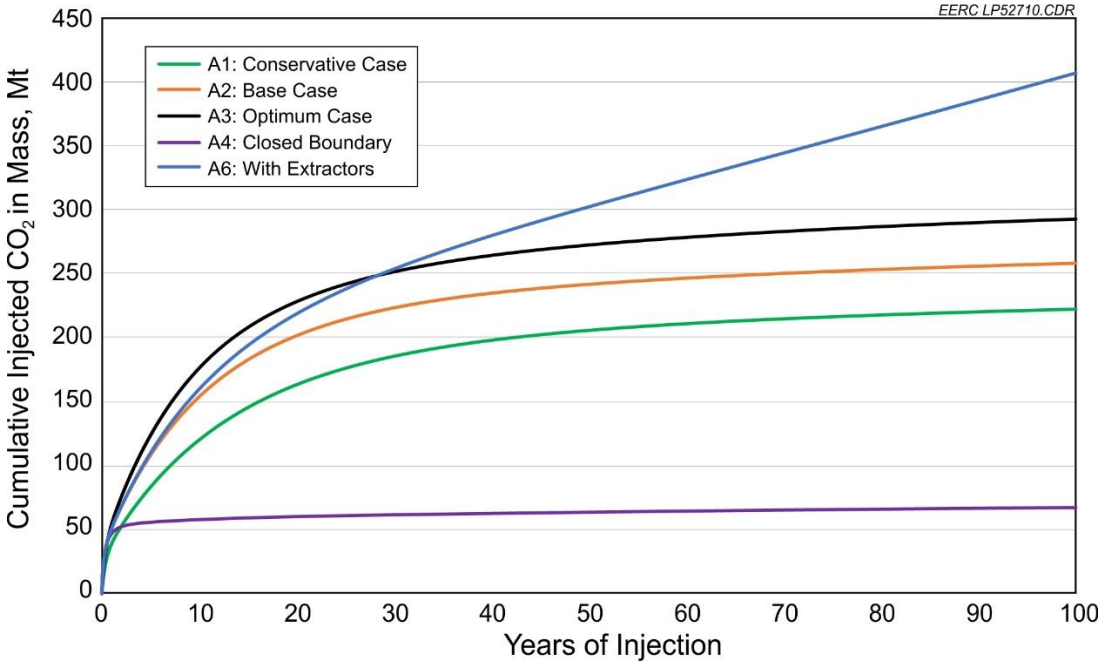

Figure 6. Comparison of the effects of lithology distribution and boundary conditions in the Minnelusa Formation on CO_2 storage.

The predicted injection rate and cumulative injection can vary considerably with grid cell size, even when using the same static model and well locations which is evident from the values presented in Table 1. Larger grid cells result in lower injection rates. It should be stressed that this is an artefact of the model.

Table 1. Minnelusa Simulation Results: Solubility Sensitivity Investigation

Case ID	Cell Width, m	Salinity, ppm	Temperature, °C, av	Injected CO_2, million tonnes at 50 years	Efficiency, %
S1	1250	20,000	75.7	82.7	1.53
S2	417	20,000	75.7	97.4	1.80
S3	250	20,000	75.7	101.9	1.88
S4	139	20,000	75.7	102.1	1.89

Bunter Sandstone Dynamic Simulation Results

The dynamic efficiency factors with 50 years of injection were evaluated for four preliminary cases for the Bunter in order to estimate a reasonable 100% well placement base case for further sensitivity investigations. All of these cases were executed by placing an even pattern of wells across the entire simulation area. The incremental efficiency factor is very small when the number of wells exceeds 91, as shown in Figure 7 which serves as the base case for well placement in the injection sensitivity investigation.

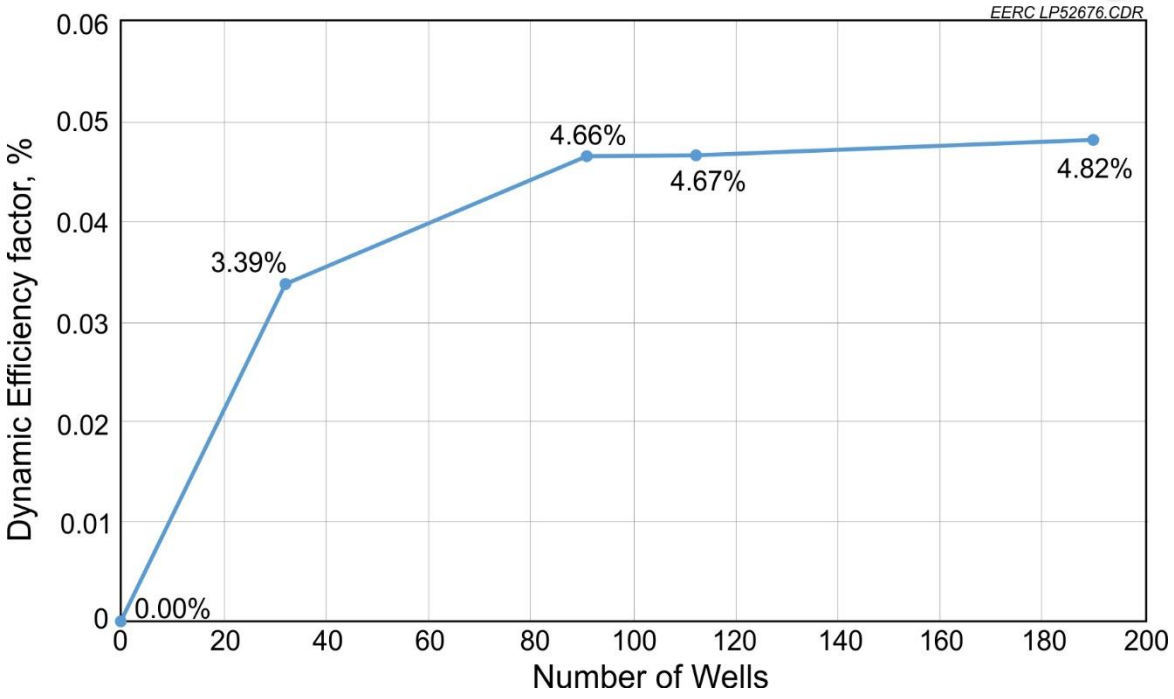

Figure 7. Dynamic efficiency factor vs. number of wells for Bunter Sandstone model area. Volumetric efficiency factor assumed suitable for the Bunter is 14%.

A comparison between an open boundary and a closed boundary for the Bunter shows that there is a marked difference in storage efficiency (see Figure 8 and Table 2) for the same number of injector wells (91). Structural influences in the form of a monocline make only a marginal difference by comparison.

Table 2. Summary of Alternative Simulation Scenarios and Dynamic Efficiency Factor for Each Case in the Bunter Formation

Bunter Case ID	No. of wells	Boundary	Structure	CO_2 mass injected, Mt	Efficiency, %
B-A2	91	Open	Actual	1770	4.66
B-A4	91	Closed	Actual	426	0.98*
B-A7	91	Actual	Flat	1613	4.25
B-A8	91	Actual	Monocline	1647	4.34

* Value revised down from 1.14% to 0.98% following review because the pore pressure was found to be too high at the shallowest point in the Bunter structure. Consequently the E value had to be revised down to maintain reservoir integrity

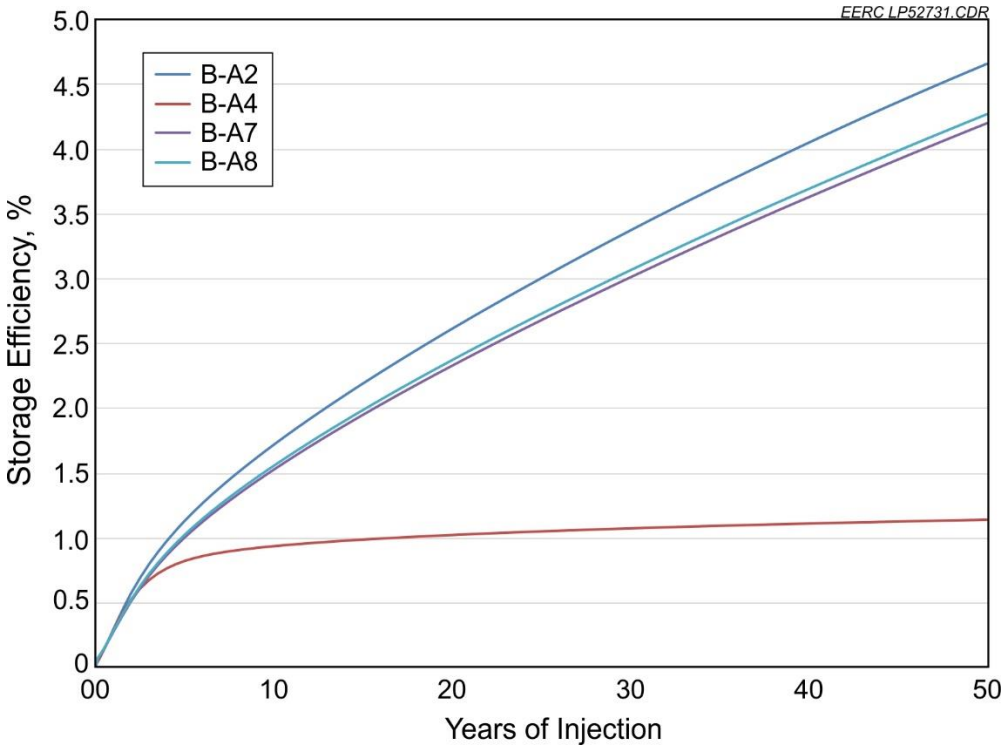

Figure 8. Bunter storage efficiency over time for open, closed (actual with extractor boundary) conditions, and flat and monocline structural.

The impact of water extraction was profound, increasing the storage efficiency from 4.66% to 7.39%. Average CO_2 injection per well, including the total number of extraction wells, would be about 24 million tonnes over the course of 50 years of injection. This is over 5 million tonnes more per well than the A2 base case.

Model simulations have also revealed that different structural settings, and the relative proximity and distribution of wells, can have a significant impact on storage efficiency. Collectively the structure of the reservoir formation, and well pattern, influence pressure constraints and fluid flow behavior because of buoyancy effects. The trap structural setting represents the actual Bunter structure in this instance. In addition to three different structural settings, two different well configurations were also modelled: one where the wells were concentrated; and the other where they were dispersed, as depicted in Figure 9.

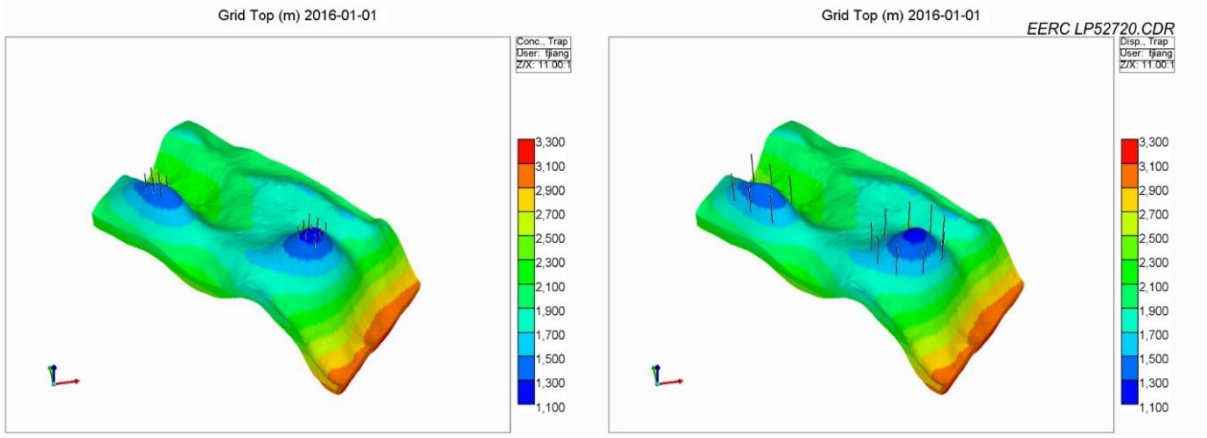

Figure 9. Concentrated well placement (left) and dispersed (right).

The influence of well placement and the structural configuration of the reservoir and caprock for the Bunter Formation are evident from the simulation results in Table 3 and Figure 10. Dispersed wells clearly show the greatest mass per well. This approach highlights how simulations could be useful for designing field development and the associated cost-benefits.

Table 3. Bunter Storage Efficiency, Total CO_2 Mass Injected, CO_2 Mass in Solution, and Mass per Well for Plume Design Cases

Bunter Case ID	Structure	Plume Design	Mass CO_2 Injected, Mt	Efficiency, %	CO_2 in Solution, Mt	Mass per Well, Mt
B-7D	Flat	Dispersed	818	2.12	87	55
B-8D	Monocline	Dispersed	783	2.08	83	52
B-9D	Trap	Dispersed	675	1.80	73	45
B-10C	Flat	Concentrated	611	1.57	63	41
B-11C	Monocline	Concentrated	591	1.56	61	39
B-12C	Trap	Concentrated	386	1.02	40	26

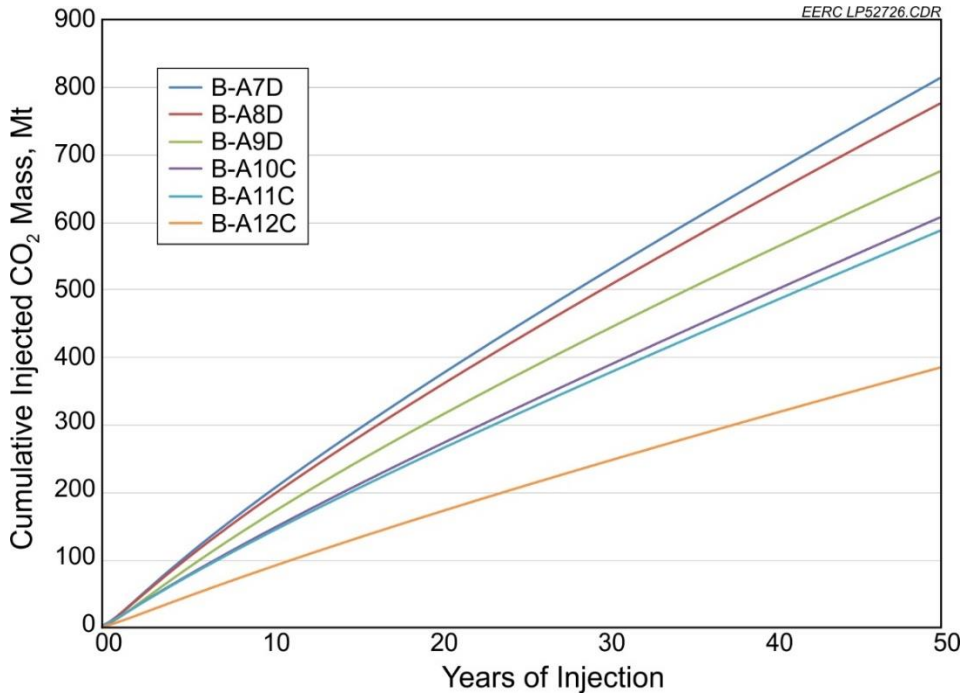

Figure 10. Comparison of the effects of well distribution and structure in the Bunter Formation on CO_2 storage.

Cost-Benefit Analysis

The objective of this cost-benefit analysis was to conduct a comparison of storage cost relative to the quantity of CO_2 stored especially in situations where longer-term (50+ years) of storage has taken place over a large area. The analysis can be used to identify an optimum quantity of CO_2 that can be stored relative to overall cost and therefore the optimum CO_2 storage value for a specified area. A three stage approach was adopted:

- Determination of an approximate generic cost of storing CO_2 in DSFs in on and offshore scenarios for each phase of a storage project from initial screening through design, construction to injection. Then estimate the storage cost from simulations for each formation from the amount of CO_2 stored.
- Representative costs were used to develop a cost per tonne estimate for each of the simulated scenarios.
- The relationship of storage to cost by comparison of cost per tonne to total CO_2 stored was then analysed.

The Minnelusa formation storage cost was based on a cost model developed by the US DOE National Energy Technology Laboratory (NETL). This spreadsheet based model was used to create an estimate of CO_2 storage in onshore DSFs. The Bunter costs were based on one of five ETI cost models for different offshore DSFs.

For the Minnelusa Formation an arbitrary base case was used assuming 576 wells. The wells were ranked according to their permeability thickness (kh). The well depth used in the cost model was set to 8,700 feet (2,652.5 m). A 100-mile pipeline (~161 km) was included in the model. The ETI cost model assumed 40 years of CO_2 injection, 160 km pipeline and 12 injection wells per platform.

The results of the cost analysis for the Minnelusa Formation are presented in Figure 11. The cost-factor is a unitless cost factor normalised to 2015 US$ to enable comparison between two different currencies and avoids an escalation factor. This comparison is meant to provide a high-level relationship between the cost of transport and storage and total CO_2 storage.

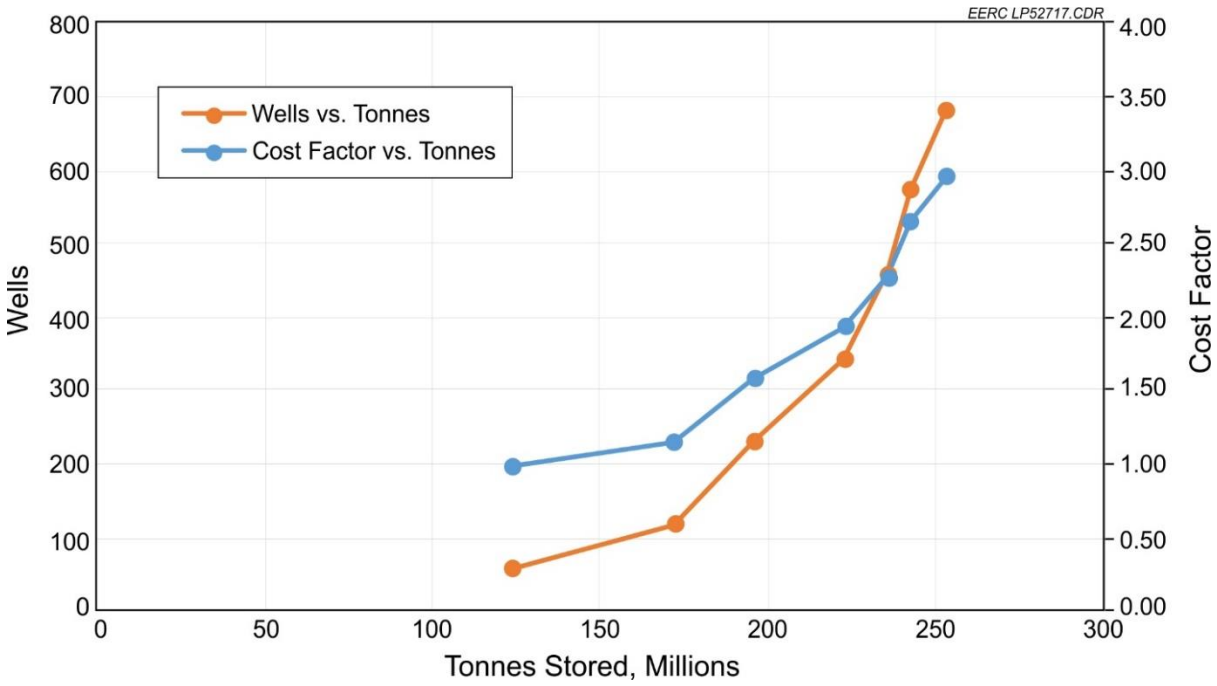

Figure 11. Relationship between number of wells, total tonnes stored, and cost factor for the Minnelusa simulation scenarios.

What is evident from this analysis is that there is a large increase in total storage between 58 and 115 wells followed by smaller gains until a point where 345 wells is reached. Increasing

the number of wells beyond this point results in only incremental gains even after adding nearly six times the number of wells. This observation has been previously observed and shows that the majority of injected CO_2 comes from a small number of wells. This is attributed to the nature of the storage formation and pressure interference between wells. There is also a comparatively small increase in cost factor observed between 58 and 115 wells. There is a moderate increase above the 115 well point until the 345 point is reached when there is a dramatic increase in the cost factor.

The results of the cost benefit analysis for the Bunter Formation are depicted in Figure 12. There is some similarity with the Minnelusa Formation cost analysis although there is a more gradual transition from 9 to 36 wells which is attributed to the more uniform distribution of good reservoir properties within the Bunter. With an increasing number of wells above 36 there is a decline in the cost-benefit relative to the quantity of CO_2 stored. In both cases 20% of all the wells in the cost model were able to deliver more than 60% of the total CO_2 injected (68% for the Minnelusa and 63% for the Bunter). In both modelled formations the number of wells was the primary variable in determining the cost factor. It is possible that large-scale development over a number of years might be able to achieve some economies of scale to counter balance the decrease in cost-benefit with increased injection.

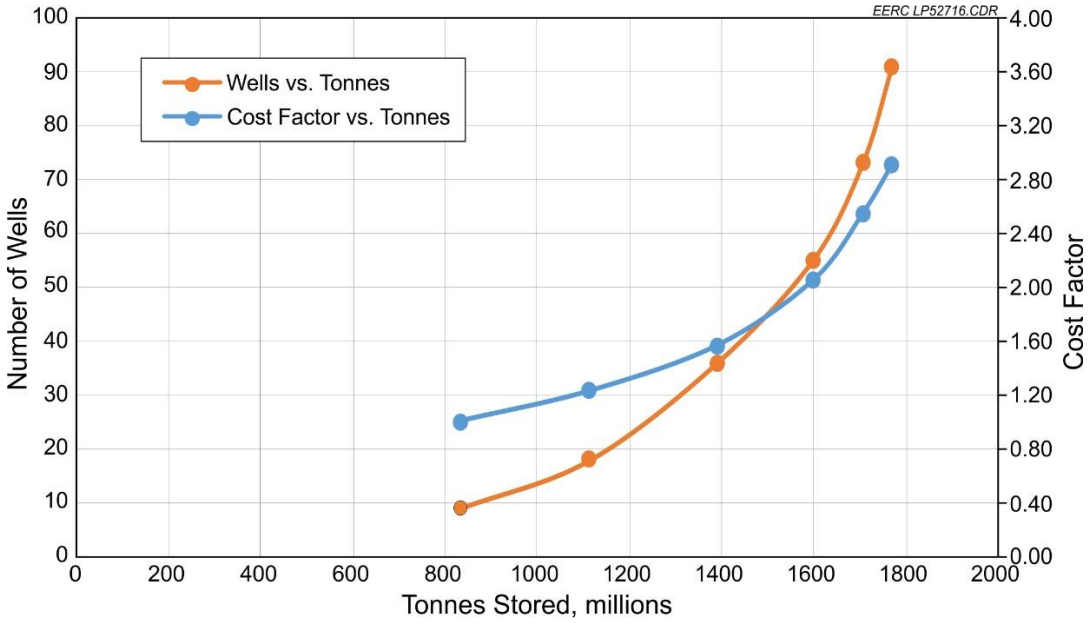

Figure 12. Relationship between number of wells, total tonnes stored, and cost factor for the Bunter Formation simulation scenarios.

Comparison with Stage 1 Minnelusa Formation Dynamic Modelling Results

Comparisons between dynamic modelling of the Minnelusa Formation in the Stage 1 study and Stage 2 studies need to be treated with caution. In the first instance the Stage 1 model area covered 58,632 km^2 are was based on a 1250 x 1250 m grid. For most cases this equated to a well density of 0.008wells/km^2. Stage 2 was deliberately set up over a much smaller area (1,250 km^2) and incorporated models over different grid cell dimensions. Well densities are significantly more concentrated and range from 0.0464 to 0.4608 well/km^2. Consequently, direct comparisons can only be very general. All the comparisons from both studies assume a 50 year horizon.

Table 4 A very general comparison of the Minnelusa Formation between Stage 1 and Stage 2

Condition	Stage 1		Stage 2	
	Mt CO_2 injected	E factor %	Mt CO_2 injected	E factor %
P50 Base Case - Open	1,725	1.28	242	4.75
P50 Base Case - Closed	1,613	1.20	64	1.25
P50 Vert & Ext	3,238	2.41	302	5.94
Model Area km^2	58,632		1,250	
Grid m	1,250		250	
Well density wells/km^2	0.008		0.0464 - 0.0728	

The dynamic modelling applied in both studies was used to estimate CO_2 storage capacity under different scenarios. These scenarios also generated different efficiency (E) factors that are indicative of formation storage capacity based on different assumptions. What is evident from both studies is that one of the biggest single factors that influences capacity is the impact of brine extraction. One model output for the Minnelusa from the Stage 1, assuming a P50 condition, resulted in an E value of 1.28% (1,725 Mt) for an open condition and an E value of 1.24% for a closed condition. Under the same conditions (P50), and assuming vertical wells with extraction, the E factor increases to 2.41% (3,238 Mt CO2 injected). A model realization from Stage 2 revealed the same trend. In this instance a base case with 576 wells, resulted in an E value of 4.75% for an open condition and E 1.25% for a closed condition. With extractors the E value rose to 5.94% but this case was run with a 250 x 250m grid which suggests grid dimension may be the biggest single influence on the E factor. There is an example from the Stage 2 study which highlights this factor. A solubility sensitivity example that assumed the same salinity and reservoir temperature conditions, but run at different grid scales, shows that for a larger grid of 1250 x 1250 E was 1.53% compared with E 2.20% for a finer 250 x 250 m grid. The Stage 2 report does state that larger grid cells result in lower injection rates and therefore lower E values.

Expert Review Comments

There were nine reviewers who provided a number of detailed comments

The amount of CO_2 in solution, and its dependency on grid-cell size, is a key issue. One reviewer noted that the variation in dissolution due to temperature and salinity differences is well known. The range in dissolved CO_2 values are presented only to demonstrate that grid cell size can have a larger impact on calculated dissolved CO_2 quantity than reasonable uncertainty in simulation input values of salinity and temperature.

Another reviewer commented that the cumulative CO_2 mass injected should be compared to the full volume of the aquifer and not to the aquifer volume of the domain. This objective was not the goal of the study it was deliberately kept to a more local scale.

The assertion that the E factor calculated cannot apply to the full aquifer was acknowledged by the authors. The E factor was only ever intended to apply to an area of commercial development size and time scale. Indeed, if CO_2 storage was to be applied to other similar domains filling the full aquifer, then pressure in all domains would rise, and they would no longer benefit from nearby hydrostatic aquifers that would otherwise dissipate pressure. The results of previous closed aquifer system studies would apply.

Central wells in the modelled area show a significant lower CO_2 plume which one reviewer interpreted as a modelling artefact related to the domain size. The authors of the study countered this view and offered an alternative explanation. The constrained plume is a result of pressure interference between the central wells. This demonstrates that even at a practical-to-large scale of a single development project the interference effects inhibiting injection in the interior of the injection pattern are significant (see Figure 13).

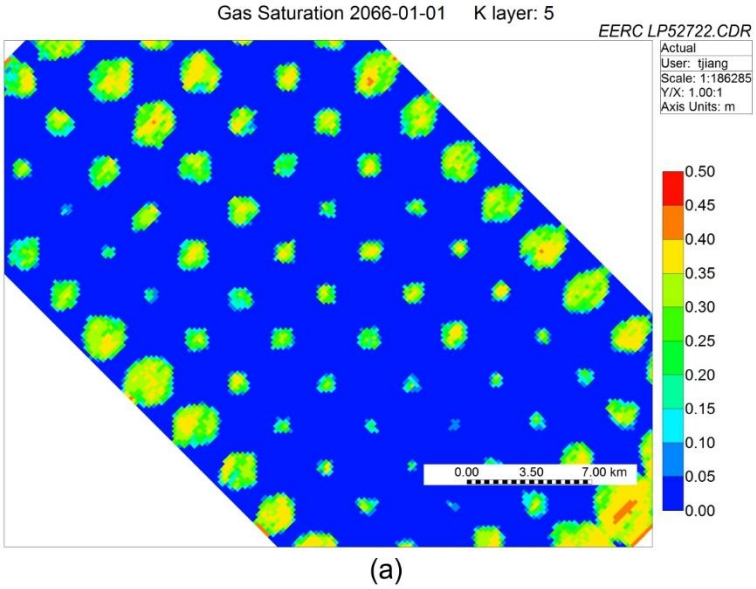

Figure 13 CO_2 plume difference for the Bunter Case B-A2, with no extractor wells.

The injection rates of the wells are together a critical factor that impacts both the pressure increase in the aquifer and the cumulative amount of CO_2 injection. One reviewer observed that the authors do not indicate anywhere in the manuscript how the injection rates are controlled during the dynamic simulations. The authors explained that for the Minnelusa the well control constraints are the same as stated in the Stage 1 report. More specifically, those constraints are 2 Mt/y per well unless bottom-hole injection pressure (BHP) reaches the level of 13.6 kPa/m (0.6 psi/ft) multiplied by the top perforation depth, which is a very common type of constraint set used in numerical simulations. Even the best injection wells in the Minnelusa study area cannot sustain a rate of 2 Mt/y for long and reach their maximum allowable BHP. Consequently, their injection rate slowly declines, giving the concave shape to the profiles as noticed by the reviewer. In the case of the Bunter the authors used constraints of 2.9 Mt/y per well and 16.05 kPa/m, approximately 10% lower than the fracture pressure gradient that was assumed in a previous study (Williams et al, 2013).

The authors agreed with the reviewer to the degree that when designing an optimized injection plan for a specific project the annual injection rate profile is a critical parameter and that it is most commonly (near) constant. The objective in Stage 2 was somewhat different in that the critical parameter was a realistic injection period for a CO_2 storage project (i.e. 50 years). An attempt was made to find a practical limit to cumulative injection within that time frame and within the model domain. To additionally maintain a constant injection rate would require a degree of optimisation that was beyond the objectives of the project.

The draft report did not include key information on how the pressure constraint was defined. The authors explained that different gradients were used for the two study areas. No assumption of equivalence was made between the two on this basis. The Minnelusa used 13.6

kPa/m, as referenced in Table B-1 of the Stage 1 work. The source reference is included in the report (Barati, 2011[5]). The Bunter uses a gradient of 16.05 kPa/m referenced from Williams, et al, (2013).

The E factor for the Bunter had to be revised down for the Bunter for the most conservative case from 1.14% to 0.98% because the pore pressure was too high. Storage capacity also needs to be revised down and will be constrained by the minimum caprock pressure threshold.

The same reviewer also observed that the draft report did not specify if other locations away from the wells are also monitored for pressure build-up beyond the allowable reservoir pressure. The authors responded by stating that they would include a better description of the application of pressure gradient to injection pressure control. In open systems such as those modelled in this study, general pressure dissipation is experienced over time. Certainly in the case of a detailed project design this effect would be carefully considered; however, in that instance the fracture gradient would be more precisely known (through well drilling, core testing, etc.). In lieu of site-specific data, reasonable values based on literature were used in this study and in the Stage 1 study.

In response to the influence of well density on pressure interference the authors stressed that as the number of injection wells increases in a system, it appears that a steadily larger fraction of the total are influenced by pressure interference from their neighbours. Thus, the closer a DSF approaches full development, the more its efficiency would approach that of a closed system, even if it has open boundaries. Careful basin-wide, long-term planning would be needed to mitigate this effect; however, this study is essentially considering "early adopter" cases, which would not suffer the worst of pressure build-up interference.

One key conclusion that can be drawn from this work is that the differences between open and close boundaries clearly signifies the importance of defining or conducting a careful preliminary assessment of boundary conditions.

One reviewer commented that a $\pm$ 10% variation in lithofacies seems to be a narrow span to define low, mid and high cases. The authors explained that without having proper statistical support for 'P10/P50/P90' nomenclature, it was decided to implement the less precise 'low/mid/high' descriptors instead. 61% was deemed the mid case for the Stage 2 Minnelusa effort, in turn providing some continuity to the previous Stage 1 work. Variation of ±10 percent reservoir sand was an arbitrary, yet symmetrical, amount chosen to represent low and high cases. Heterogeneity is inevitable for a formation over 1,250 km^2 area.

One reviewer commented that it would be useful to give more information on how the Bunter Sandstone model was constructed. The authors explained that an existing geological model of the Bunter Sandstone, was developed from similar studies of CO_2 storage by Williams et al (2013). An adapted version of this model was also used in studies by the ETI (Energy Technologies Institute, 2016a)[6]. For the purposes of this study, the geological structural surfaces, reservoir intervals, and porosity logs used in both the ETI and Williams et al (2013) studies were used to create the structural model and the porosity logs served as the basis for creating petrophysical property distributions. The Bunter model was created with the same

[5] Barati, R., 2011, EORI collaboration in solving the challenges of Minnelusa: Presented at the EOR Commission and Technical Advisory Board Meeting, Laramie, Wyoming, www.uwyo.edu/eori/_files/eroctab_july_2011/reza%20-minelusapres%2007-19-2011%20tab_reza.pdf (accessed November 2016).

[6] Energy Technologies Institute, 2016a, D10: WP5A—Bunter storage development plan: Report of DECC Strategic UK CCS Storage Appraisal Project, commissioned by the Energy Technologies Institute and funded by the Department of Energy and Climate Change, prepared by Pale Blue Dot Energy and Axis Well Technology, United Kingdom, 10113ETIS-Rep-13-03, March.

Minnelusa simulation goals to obtain CO_2 storage simulation outcomes over a realistic temporal span of 50 years; however, no CO_2 dissolution sensitivity investigations were undertaken for the Bunter.

It was suggested that large scale deployment of CCS will require some degree of water extraction. Although this is widely acknowledged, the incorporation of water extraction into the cost analysis would require multiple additional assumptions to be made that are beyond the scope of this study.

Conclusions

- Brine extraction can have a significant impact on storage capacity if injection is permitted beyond 50 years in the case of the Minnelusa. The impact of water extraction on the Bunter was profound raising storage efficiency from 4.7% to 7.4%
- The biggest influence on capacity is the extent to which a system is open or closed at the model boundary.
- The injection rate and cumulative injection can vary considerably with grid size assuming salinity and temperature levels remain constant. Larger grid cells result in lower injection rates. This is a function of the model's structure rather than a physical property of the formation.
- The incremental efficiency factor increase is very small when the number of wells exceeds 90 in both cases.
- The model showed that well configuration can also influence storage efficiency. There is a notable decline in storage efficiency in the Bunter where wells are concentrated.
- The differences between open and close boundaries clearly signifies the importance of defining or conducting a careful preliminary assessment of boundary conditions.
- The cost-benefit analysis shows that in both formations there is a dramatic fall off in cost-benefit relative to the amount of injected CO_2 above 60% of the total number of wells in the model. Over 60% of the CO_2 can be delivered by 20% of the wells used in each model.
- The storage capacity and the efficiency factor will ultimately be constrained by the caprock threshold.

Recommendations

- CO_2 storage capacity and stated E factors for a formation need to be supported by values for key parameters that influence them: i.e. grid cell size, domain dimensions, formation boundary conditions, especially whether hydraulic communication occurs beyond the model domain, salinity and temperature.
- Capacity estimates and E Factor should state whether they are based on measured or estimated caprock pressure thresholds.
- E factors and capacity should be expressed as a range from conservative to base case and optimistic.
- Dynamic storage values should state the length of the injection period that the capacity estimate is based on and the injection rate.
- The number and distribution of wells should be stated.
- There needs to be a comparison of storage estimates based on different dynamic models for prospective DSFs and a critique of the merits of different models.

CO_2 STORAGE EFFICIENCY IN DEEP SALINE FORMATIONS – STAGE 2

Revised Final Report

(for the period of May 1, 2016, through April 30, 2017)

Prepared for:

James Craig

IEA Greenhouse Gas R&D Programme
Cheltenham Office Park
Hatherley Lane
CHELTENHAM, Gloucestershire, GL51 6SH
UNITED KINGDOM

Agreement No. IEA/CON/16/234

Submitted by:

Lawrence J. Pekot
Scott C. Ayash
Nicholas W. Bosshart
Neil W. Dotzenrod
Jun Ge
Tao Jiang
Lonny L. Jacobson
Heidi M. Vettleson
Wesley D. Peck
Charles D. Gorecki

Energy & Environmental Research Center
University of North Dakota
15 North 23rd Street, Stop 9018
Grand Forks, ND 58202-9018

2017-EERC-08-11 August 2017

EERC DISCLAIMER

LEGAL NOTICE This research report was prepared by the Energy & Environmental Research Center (EERC), an agency of the University of North Dakota, as an account of work sponsored by IEA Greenhouse Gas R&D Programme (IEAGHG) and the U.S. Department of Energy (DOE). Because of the research nature of the work performed, neither the EERC nor any of its employees makes any warranty, express or implied, or assumes any legal liability or responsibility for the accuracy, completeness, or usefulness of any information, apparatus, product, or process disclosed or represents that its use would not infringe privately owned rights. Reference herein to any specific commercial product, process, or service by trade name, trademark, manufacturer, or otherwise does not necessarily constitute or imply its endorsement or recommendation by the EERC.

DISCLAIMER

This report was prepared as an account of work sponsored by an agency of the United States Government. Neither the United States Government, nor any agency thereof, nor any of their employees, makes any warranty, express or implied, or assumes any legal liability or responsibility for the accuracy, completeness, or usefulness of any information, apparatus, product, or process disclosed, or represents that its use would not infringe privately owned rights. Reference herein to any specific commercial product, process, or service by trade name, trademark, manufacturer, or otherwise does not necessarily constitute or imply its endorsement, recommendation, or favoring by the United States Government or any agency thereof. The views and opinions of authors expressed herein do not necessarily state or reflect those of the United States Government or any agency thereof.

ACKNOWLEDGMENTS

This report was prepared with support of IEAGHG and DOE National Energy Technology Laboratory Cooperative Agreement No. DE-FE0024233. However, any opinions, findings, conclusions, or recommendations expressed herein are those of the author(s) and do not necessarily reflect the views of IEAGHG and DOE.

The authors acknowledge Energy Technologies Institute (ETI) and Pale Blue Dot for their generous assistance in providing data and interpretations used by the project. We thank Schlumberger and the Computer Modelling Group for the use of their software packages in the development and execution of the modeling and simulation portions of this project. The authors thank the staff of the EERC for their hard work helping to prepare this report. We also acknowledge the Plains CO_2 Reduction (PCOR) Partnership, under which many of the ideas and philosophy used in this report were first formulated.

TABLE OF CONTENTS

LIST OF FIGURES iii

LIST OF TABLES vi

EXECUTIVE SUMMARY viii

INTRODUCTION 1

PREVIOUS WORK 2

APPROACH 3

MODEL CONSTRUCTION 4
- Minnelusa Model 4
- Bunter Model 8

NUMERICAL SIMULATION 11
- Static Volumetric Storage Efficiency Factor for the Saline Formations 11
- Minnelusa Simulation Work Plan 12
  - Dynamic Simulation 12
  - Well Placement and Injection Sensitivity Cases 13
  - Alternative Simulation Scenarios 14
- Minnelusa Formation Dynamic Simulation Results 15
  - Well Placement and Injection Sensitivity Investigation 15
  - Alternative Simulation Scenario Investigation 19
- Bunter Simulation Work Plan 24
  - Dynamic Simulation 24
  - Well Placement and Injection Sensitivity Cases 25
  - Alternative Simulation Scenarios 26
- Bunter Sandstone Dynamic Simulation Results 27
  - Preliminary Sensitivity Investigation 27
  - Well Placement and Injection Sensitivity Investigation 28
  - Alternative Simulation Scenarios 30

SOLUBILITY SENSITIVITY INVESTIGATION 43

COST–BENEFIT ANALYSIS 47
- Objectives 47
- Approach 48
- Challenges 48

Continued . . .

TABLE OF CONTENTS (continued)

Method 49
Analysis 50
Minnelusa Formation 50
Selection of Formation 50
Number and Depth of Wells 50
3-D Seismic Area and Collection Interval 51
Other Assumptions 51
Bunter Sandstone Formation 52
Number of Wells 52
Other Assumptions 53
Results 54
Minnelusa Formation 54
Bunter Formation 55
Original Scenarios 56
Alternate Scenarios 56
Comparison of Minnelusa and Bunter 57
Conclusions 59

RESULTS AND DISCUSSION 60
Comparison to the Stage 1 Report 60
Other Results and Discussion Items 61

FUTURE WORK 64

CONCLUSION 65

REFERENCES 66

ADDITIONAL FIGURES FOR THE MINNELUSA SIMULATIONS ..... Appendix A

ADDITIONAL FIGURES FOR THE BUNTER SIMULATIONS ..... Appendix B

LIST OF FIGURES

1 Storage resource/capacity classification system 2

2 Stratigraphy of the Minnelusa Formation, Powder River Basin 5

3 Minnelusa Formation measured depth (m) map within the Powder River Basin of Montana and Wyoming 6

4 Depiction of the various grid cell sizes used to investigate the sensitivity of simulated dissolved CO_2 7

5 Stratigraphy of the study area 8

6 Depth to the top of the Bunter Sandstone, which serves as the upper limit of the geologic model 9

7 Correlation of reservoir zones 10

8 Distributed effective porosity of the Bunter Sandstone geologic model 11

9 Well placement and injection sensitivity investigation: cumulative CO_2 (mass) with differing well numbers 17

10 Well placement and injection sensitivity investigation: CO_2 footprint (total gas per unit area in meters) after 50 years of injection in the D2 base case 17

11 Well placement and injection sensitivity investigation: CO_2 plume in the D2 base case 18

12 Well placement and injection sensitivity investigation: pore pressure distribution in the D2 base case at the end of injection 18

13 Well placement and injection sensitivity investigation: dynamic CO_2 storage efficiency vs. number of wells for the Minnelusa Formation 19

14 Comparison of the effects of lithology distribution and boundary conditions on CO_2 storage 21

15 Comparison of the effects of structural setting and well concentration on CO_2 storage 22

Continued . . .

LIST OF FIGURES (continued)

16 Comparison of the effects of well concentration on CO_2 storage 23

17 Depth to the top of the Bunter Sandstone, which serves as the upper limit of the geologic model 25

18 Dynamic efficiency factor vs. number of wells for Bunter Sandstone model area 28

19 Bunter well placement and injection sensitivity investigation: cumulative CO_2 (mass) with differing numbers of wells 29

20 Dynamic efficiency factor vs. number of wells for different performance-ranking methods 30

21 Well placement for different performance-ranking methods (40% of wells): a) cumulative injection ranking and b) average kh ranking 31

22 Bunter storage efficiency over time for actual, open, closed, actual with extractor boundary conditions, and flat and monocline structural 33

23 Cross-sectional view of CO_2 saturation profiles at 50 years for a) actual structural, b) flat structural, and c) monocline structural tilt upward 34

24 Cross-sectional view of CO_2 pressure profiles at 50 years for a) actual structural, b) flat structural, and c) monocline structural tilt upward 35

25 Dip angle difference of Case B-A8 and Case B-A8-2. Case B-A8-2 has reversed dip angle and the same average depth 36

26 Effects of formation depth and dip angle on flat and monocline structural cases 37

27 Concentrated well placement (left) and dispersed (right) 38

28 Storage efficiency vs. years of injection 39

29 Total CO_2 mass injected vs. years of injection 39

30 Schematic view of the model with additional extractors located in the middle of the sector model 41

Continued . . .

LIST OF FIGURES (continued)

31 CO_2 plume difference for the cases: a) Case B-A2, no extractor wells and b) Case B-A1 with 24 extractor wells 42

32 Cumulative dissolved CO_2 mass with time for different gridding systems 44

33 Cumulative dissolved CO_2 vs. cumulative injected CO_2 mass 45

34 Effect of grid cell size on the simulated dissolved CO_2 in the Minnelusa Formation for 50 Mt injected 45

35 Effect of salinity and temperature on the simulated dissolved CO_2 47

36 Relationship between number of wells, total tonnes stored, and cost factor for the Minnelusa simulation scenarios 54

37 Relationship between number of wells, total tonnes stored, and cost factor for the Bunter Formation simulation scenarios 56

38 Relationship between number of wells, total tonnes stored, and cost factor for the alternate Bunter Formation scenarios 57

39 Comparison of the relationship between cost factor and total tonnes stored in both Minnelusa and original Bunter Formation scenarios 58

40 Comparison of the relationship between total number of wells plotted and total tonnes stored in both Minnelusa and original Bunter Formation scenarios 58

LIST OF TABLES

1 Saline Formation Displacement Efficiency Terms 12

2 Properties Used in the Base Case Simulation Model of the Minnelusa Formation 13

3 Well Placement and Injection Sensitivity Investigation: Minnelusa Model 14

4 Alternative Modeling Scenarios: Minnelusa Model 15

5 Minnelusa Simulation Results: Well Placement and Injection Sensitivity Investigations 16

6 Minnelusa Simulation Results: Alternative Modeling Scenarios with 50 years of Injection 20

7 Properties Used in the Base Case Simulation Model of the Bunter Formation 24

8 Well Placement and Injection Sensitivity Investigation: Bunter Model 26

9 Alternative Modeling Scenarios: Bunter Model 27

10 Summary of Preliminary Case Results for Differing Numbers of Wells and Well Placement: Bunter Model 27

11 Bunter Simulation Results: Well Placement and Injection Sensitivity Investigations 29

12 Summary of Alternative Simulation Scenarios and Dynamic Efficiency Factor for Each Case: Bunter Model 32

13 Summary of Cases for Different Depths and Reversed Dip Angle: Bunter Model 37

14 Storage Efficiency, Total CO_2 Mass Injected, and Mass per Well for Plume Design Cases: Bunter Model 38

15 Comparison of Cases with Different Perforation Intervals for Extraction Wells: Bunter Model 42

16 Minnelusa Simulation Results: Solubility Sensitivity Grid Cell Investigation 43

17 Minnelusa Simulation Results: Solubility Sensitivity Comparison Cases 46

Continued . . .

LIST OF TABLES (continued)

18 Minnelusa Formation Simulation Cases Used for the Cost–Benefit Assessment 51

19 Unit Costs Developed Based on the ETI Work 52

20 Bunter Formation Simulation Cases Used for the Cost–Benefit Assessment 53

21 Bunter Formation Alternate Scenarios Optimized for 12 Wells per Platform 53

22 Comparison of Stage 1 and Stage 2 Simulation Premises and Results 59

23 Minnelusa and Bunter Selected Simulation and Economic Results 62

CO_2 STORAGE EFFICIENCY IN DEEP SALINE FORMATIONS – STAGE 2

EXECUTIVE SUMMARY

The Energy & Environmental Research Center (EERC) has prepared this evaluation for the IEA Greenhouse Gas R&D Programme (IEAGHG) and the U.S. Department of Energy (DOE). This follow-up report, or Stage 2 evaluation, builds upon an IEAGHG Stage 1 report, also prepared by the EERC, "CO_2 Storage Efficiency in Deep Saline Formations: A Comparison of Volumetric and Dynamic Storage Resource Estimation Methods." The Stage 1 report used numerical reservoir simulation techniques to estimate dynamic carbon dioxide (CO_2) storage resources for basin-scale storage formation units as a point of comparison to volumetric resource calculations. However, these simulations employed hundreds of injection wells operating over hundreds to thousands of years. These results were useful for their intended purpose but did not address the practical limitations faced by actual CO_2 storage project design criteria. This Stage 2 evaluation was intended as a step toward applying such limitations to specific areas of deep saline formations (DSFs) that have been previously studied in order to estimate practical storage efficiency factors.

Two DSFs were investigated: the Minnelusa Formation of the Powder River Basin in the Rocky Mountain region of the United States and the Bunter Sandstone in the southern North Sea Basin of the United Kingdom Continental Shelf. The Minnelusa was studied in the Stage 1 work. The Bunter has been previously studied by others (Noy and others, 2012) and was chosen as the second reservoir to study, based on this previous work and its familiarity to many readers. Also, it is an offshore environment that was expected to provide contrast to the onshore Minnelusa. For each area, reservoir simulation sector models were created: 1250 km^2 for the Minnelusa and 1056 km^2 for the Bunter. Drilling scenarios were executed to determine the number of wells needed to approach a reasonable maximum CO_2 storage efficiency that could be achieved during a premised 50-year injection period. For the Minnelusa, that efficiency factor was 4.75%, and the equivalent factor for the Bunter was 4.66%. A series of cases with differing numbers of wells were also created to yield differing efficiency factors in order to determine how storage efficiency improved with increasing development intensity.

Several alternative scenarios were tested for each DSF, including conservative and optimistic reservoir quality, open- and closed-boundary conditions, use of water extraction wells, variations in geologic structure, and concentrated well placement vs. dispersed pattern drilling. As expected, the closed-boundary conditions performed poorly and the extraction well cases performed the best. For the Minnelusa, closed-boundary efficiency was 1.25% while the extraction well case reached 5.94%. A conservative geologic model allowed an efficiency of 4.04% whereas an optimistic geologic model yielded 5.36%. For the Bunter, closed-boundary efficiency was 1.14% while the extraction well case reached 7.39%. A case that used a limited number of wells located near the top of structural closures allowed an efficiency of only 1.02%, slightly less than the closed-boundary case. The majority of the simulated Bunter is located in off-structure areas.

Also, CO_2 storage development cost information and cost estimation methodologies were assembled to make first-order cost estimates for the simulated development cases. This work allowed the creation of unit cost indices for each study area that showed how unit costs increased

as development intensity increased. For both the Minnelusa and the Bunter, an optimal unit cost index value was reached when drilling development was only 20% of the maximum well density. The practical storage efficiency for these optimal unit cost cases was similar for both the Minnelusa and the Bunter, 3.4% and 2.9%, respectively. These levels of efficiency are considerably higher than those achieved for the 50-year simulation results presented in the Stage 1 study, but lower than those achieved for the 2000-year open reservoir boundary simulation cases presented in that report.

An additional investigation was performed using the Minnelusa study area. The calculated quantity of CO_2 dissolved in the formation brine of a simulated area varies with the size of the simulation grid cells, and this effect was explored by a series of grid cell sensitivity cases. For the four cases executed, it is shown that dissolved CO_2 increased linearly with cell size. For 1250-m × 1250-m grid cells, 20.7% of the CO_2 was calculated as dissolved in the formation brine. For 139-m × 139-m grid cells, only 8.8% of the CO_2 was calculated as dissolved in the formation brine. Extrapolation of the linear trend down to a hypothetical cell size of zero yielded a dissolved fraction of only 7.5%, a major difference from the estimate arrived at when using coarse grid cells.

This project was cofunded through the EERC–DOE Joint Program on Research and Development for Fossil Energy-Related Resources Cooperative Agreement No. DE-FE0024233. Nonfederal funding was provided by IEAGHG.

References

Noy, D.J., Holloway, S., Chadwick, R.A., Williams, J.D.O., Hannis, S.A., and Lahann, R.W., 2012, Modelling large-scale carbon dioxide injection into the Bunter Sandstone in the UK southern North Sea: International Journal of Greenhouse Gas Control, v. 9, p. 220–233.

CO_2 STORAGE EFFICIENCY IN DEEP SALINE FORMATIONS – STAGE 2

INTRODUCTION

In an effort to mitigate the increase in atmospheric concentrations of anthropogenic carbon dioxide (CO_2) that is caused by emissions from large stationary sources, governmental/regulatory entities are pursuing geologic storage of CO_2 as one approach in a portfolio of greenhouse gas reduction strategies. Over the past 7 years, studies have developed CO_2 storage resource estimation methodologies for deep saline formations (DSFs) (generally deeper than 800 m and with salinity greater than 10,000 mg/L), with the goal of providing reliable estimates of the potential CO_2 storage in these formations. Previously developed methodologies have focused on providing ultimate storage estimates classified by a generic aquifer lithology (clastics [sandstone], limestone, and dolomite [dolostone]) and an assumption of boundary conditions (i.e., open or closed hydrogeologic systems) (IEA Greenhouse Gas R&D Programme, 2009; U.S. Department of Energy National Energy Technology Laboratory, 2012; Peck and others, 2014). Recent investigations have focused on comparative analyses of static volumetric and numerical simulation estimates of CO_2 storage and efficiency (IEA Greenhouse Gas R&D Programme, 2014). Numerical simulations have shown relatively good agreement with static volumetric estimates; however, the numerical simulations indicate that it may take hundreds to thousands of years to reach the volumetrically calculated ultimate storage capacity for basin-scale storage operations, which is beyond the practical time frame of interest for mitigating climate change in the next century (Bachu, 2015).

The aim of this study by the Energy & Environmental Research Center (EERC) was to build upon and expand the work of the Stage 1 study (IEA Greenhouse Gas R&D Programme, 2014). This Stage 2 study investigates the range of storage efficiency that is practically achievable within a more urgent time frame (50-year injection period) and within a limited area that may be suitable for a large commercial injection project. This study assesses key factors that may influence the effectiveness of CO_2 storage within that shorter time frame and limited area. In that regard, this study represents a step toward defining the practical storage capacity, as indicated in Figure 1, for the study areas.

To accomplish this project, two contrasting, but comparable, DSF reservoirs previously considered for CO_2 storage were further investigated. The Minnelusa Formation in the Powder River Basin, United States, which was investigated in the Stage 1 study is reexamined on a sector model scale to provide continuity with the previous work to allow for direct comparison of the new work with previous efforts. This Stage 2 study also investigated a sector of the Bunter Sandstone located in the United Kingdom's sector of the southern North Sea Basin to provide an offshore and European counterpoint to the continental setting of the Minnelusa. Additionally, cost estimate data have been collected, and cost estimate methods have been investigated. This work provides guidance for CO_2 storage development costs and how they may vary with the intensity and infrastructure footprint needed to approach the volumetrically calculated ultimate storage capacity for large-scale storage areas. The cost evaluation has incorporated results of the modeling exercises to produce cost–benefit indices for onshore and offshore storage development.

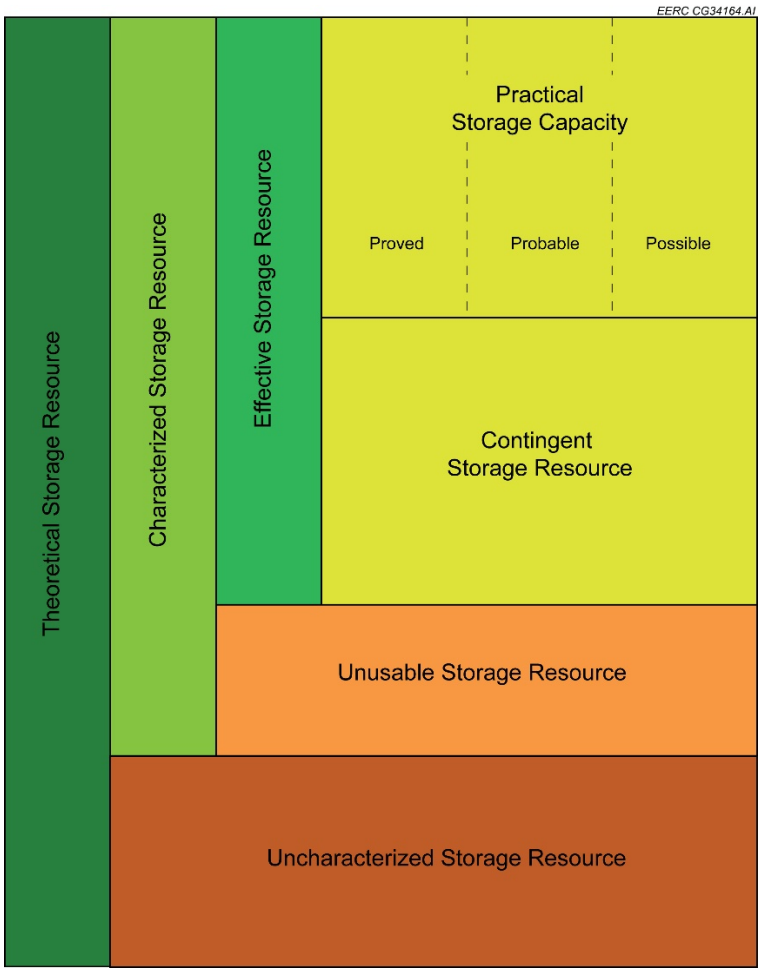

Figure 1. Storage resource/capacity classification system (IEA Greenhouse Gas R&D Programme, 2009).

This study represents a step in the direction of determining how the terms “practical storage capacity” and a corresponding “practical storage efficiency” may be applied by placing initial general economic and time constraints on the ability to achieve CO_2 storage. In this work, efficiency is a value derived from calculated cumulative injection (capacity), and it is this capacity that may be considered the practical storage capacity, indicated in Figure 1. However, accepted economic or engineering rules to apply to the definition of practical storage capacity have not yet been developed, and as such, further subdivision among “proved,” “probable,” and “possible” categories remains for future work as an economical CO_2 storage business develops.

PREVIOUS WORK

The topic of CO_2 storage resource and storage efficiency factors of DSFs has been extensively studied. The two complementary approaches to this work are volumetric calculations and dynamic calculations.

Volumetric calculations rely on a geologic description of the study area to determine the pore volume for the area, or fraction thereof, that can be filled with CO_2 at the specified reservoir pressure and temperature and then calculate the storage capacity. Several methods have been developed to estimate the CO_2 storage capacity of DSFs, including methods developed by the U.S. Department of Energy (DOE) (2007, 2008, 2010; Litynski and others, 2010), the Carbon Sequestration Leadership Forum (CSLF) (2005, 2007, 2008; Bachu and others, 2007; Bradshaw and others, 2007), the IEA Greenhouse Gas R&D Programme (IEAGHG) (2009), the U.S. Geological Survey (USGS) (Brennan and others, 2010; Blondes and others, 2013), CO_2 GeoCapacity (Vangkilde-Pedersen and others, 2009; Zhou and others, 2008; Szulczewski and others, 2012).

Dynamic calculations using reservoir simulation software also rely on a geologic description of the study area but then apply a set of time-dependent operating premises to inject CO_2 into the pore space. These methods generally provide somewhat lower estimates of storage capacity because the software can account for the limitations that geologic conditions place on the ability of injection wells to displace the saline pore water, such as pressure interference between storage sites, model boundary conditions, general pressure buildup in the reservoir, or pressure relief mechanisms (Zhou and Birkholzer, 2011; Birkholzer and Zhou, 2009; IEA Greenhouse Gas R&D Programme, 2010; Nicot, 2008).

In an attempt to make more direct comparisons between volumetric storage resource estimates and dynamic estimates, the previously completed Stage 1 study designed simulation exercises intended to approach the volumetric resources calculated for two basin-scale geologic systems: the Minnelusa Formation in the Powder River Basin of the United States and the Qingshankou–Yaojia system of the Songliao Basin of China (IEA Greenhouse Gas R&D Programme, 2014). In the Stage 1 study, simulation cases employing injection periods of up to 2000 years and 820 injection wells distributed across the Minnelusa and dynamic resource estimates obtained were comparable to volumetric estimates. As noted in the Introduction, IEAGHG (2014) is referred to as the Stage 1 study since it forms the basis and starting point for this study.

However, the numerical simulations of the type in the Stage 1 study, while enlightening, were not intended to address the practicalities of actual CO_2 storage development projects. It is the practical constraints of such projects that will determine the practical storage capacity and practical storage efficiency of a specific area of a DSF. This Stage 2 study begins to address these practicalities.

APPROACH

This study uses previous work as its starting point to make progress toward the objective of estimating practical storage efficiency that might be achieved in DSFs when constrained by project development factors such as a 50-year injection period and increasing unit storage costs as development intensity increases. Existing geologic models were used for the two areas that were studied. For the Minnelusa Formation, a 50-km × 25-km sector was selected from a basin-scale model of the formation. For the Bunter Sandstone, an existing 44-km × 24-km sector model was selected.

Numerical simulations of both geologic models were constructed, and similar suites of CO_2 injection cases were tested in both simulations. These simulation suites each included a drilling sensitivity study to estimate a reasonable maximum number of wells that could be effectively utilized for injection within the simulation area and a series of cases to show how 50-year storage efficiency increases as the number of wells increases.

A series of alternative scenarios were also executed for both areas to test their sensitivity to different reservoir conditions and different storage development premises.

The Stage 1 study highlighted that the amount of injected CO_2 dissolved in formation brine may be influenced by the size of the simulation grid cells. Therefore, an additional sensitivity study was performed using the Minnelusa simulation to systematically investigate the question.

Finally, a generalized economic evaluation was performed for the two study areas. CO_2 storage development cost data were collected, and two existing costing methods were discovered and applied to the drilling sensitivity results to create relative storage cost indices for progressively more intense development within the study areas. These indices are useful to suggest how much CO_2 storage development, and its associated practical storage efficiency, can be attempted before average unit cost for storage becomes cost prohibitive or results in diminishing returns.

MODEL CONSTRUCTION

The Minnelusa Formation within the Powder River Basin, United States, a focus of the CO_2 Storage Efficiency in Saline Formations – Stage 1 work (IEA Greenhouse Gas R&D Programme, 2014), hereafter referred to as "Stage 1," was selected for further investigative analyses in this study (hereafter referred to as "Stage 2"). A subregion of the model used in the Stage 1 work was selected in order to provide continuity to, and build upon, these previous efforts. Additionally, to provide an offshore case study counterpart, the Bunter Formation of the United Kingdom's North Sea was selected for the purposes of Stage 2. The modeling construction and preparation of these two units are discussed in the following sections.

Minnelusa Model

The Pennsylvanian/Lower Permian Minnelusa Formation of the Powder River Basin, United States, is divided into three members bounded by unconformities (Figure 2). The upper member of the Minnelusa Formation represents a single flow unit characterized by a complex succession of eolian sands and carbonates deposited in an intracratonic basin during the early Permian (Anna, 2009).

The Stage 1 work found the Minnelusa Formation had "fair storage properties" and "act[ed] more as an open system," with areas of discharge to the east in the Black Hills and recharge from the west in the Bighorn Mountains (IEA Greenhouse Gas R&D Programme, 2014).

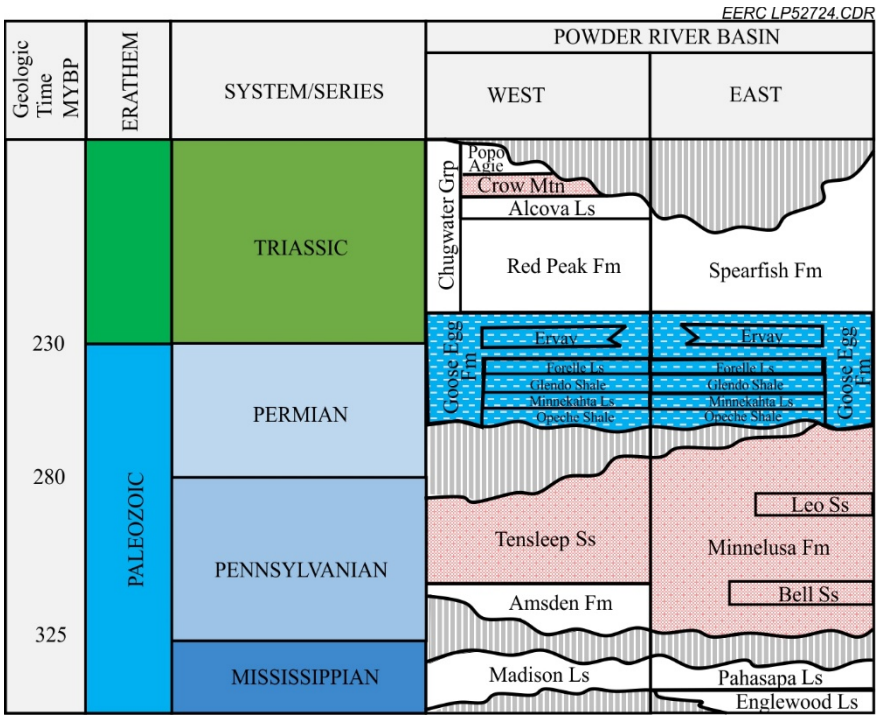

Figure 2. Stratigraphy of the Minnelusa Formation, Powder River Basin (Anna, 2009). It should be noted that in the two far right columns, the red color indicates reservoir/aquifer units; the blue color indicates seals/aquitards.

The Stage 1 simulation efforts were conducted using a formation-scale (full extent of the Powder River Basin) "Minnelusa" model with 1250-m × 1250-m grid cell (X and Y dimensions). This Minnelusa model, constructed in the Stage 1 work and modified for Stage 2, was not designed to be representative of the actual Minnelusa Formation, rather a generic "Minnelusa-like" eolian sandstone model adhering to the actual Minnelusa Formation. Details of the Stage 1 Minnelusa model construction are described in IEAGHG (2014).

The modeling and simulation efforts of Stage 2 were more geographically focused in comparison to the Stage 1 investigation. An area 50 km wide by 25 km long (1250 km^2) near the eastern margin of the Powder River Basin (Figure 3) of the aforementioned model was selected for use in Stage 2 investigations based upon the presence of desirable petrophysical properties (porosity and permeability). The modeled area exhibited a porosity ranging from 0% to 22%, with an average value of 6.9%, and permeability ranging from 0.01 to 385 mD, with a pore volume weighted average of 17.6 mD. This modeled area, exhibiting monoclinic structural dip to the west, served as the basis for CO_2 storage simulations designed to investigate the effect of changing grid resolution (cell size) on simulated dissolved CO_2 and to obtain CO_2 injection simulation outcomes (injected volumes, storage efficiency, and cost–benefit ratios with differing injection well number/density) over a realistic temporal context of 50 years.

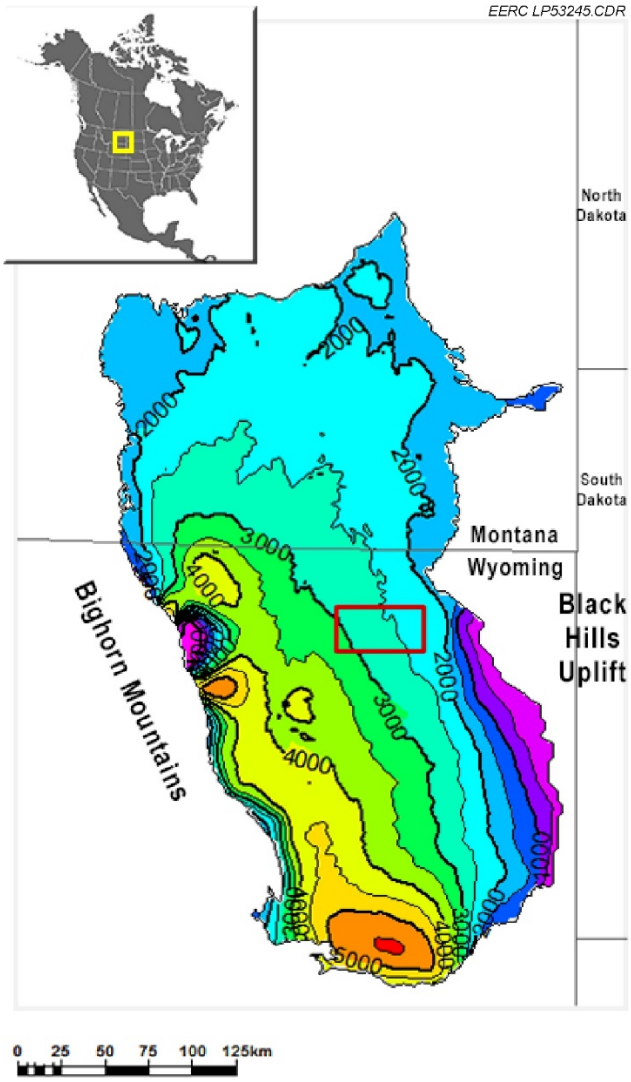

Figure 3. Minnelusa Formation measured depth (m) map within the Powder River Basin of Montana and Wyoming. The Minnelusa model extent is overlain (red rectangle). Contour interval is 500 m.

Because the geographical extent of the efforts discussed here (Stage 2) were substantially reduced in comparison to the Stage 1 work, computational efficiency allowed for a similar reduction in cell size. An aspect noted by the Stage 1 work needing further investigation was the sensitivity of dissolved CO_2 during simulated injection to varying grid cell size. It was believed that the larger cell sizes used in the Stage 1 efforts may have led to overestimation of dissolved CO_2, as the large cells could not accurately capture the injected CO_2 plume extents. Thus a series of grids were created, all with equal extents (50 km × 25 km) and 50 proportional layers of approximately 1.5 m in thickness. Cell sizes were calculated by applying divisors of 9, 5, 3, and 1 to the original cells 1250 m in length and width. The resulting cells were 139 m × 139 m, 250 m × 250 m, 417 m × 417 m, and 1250 m in length and width, respectively (Figure 4). While

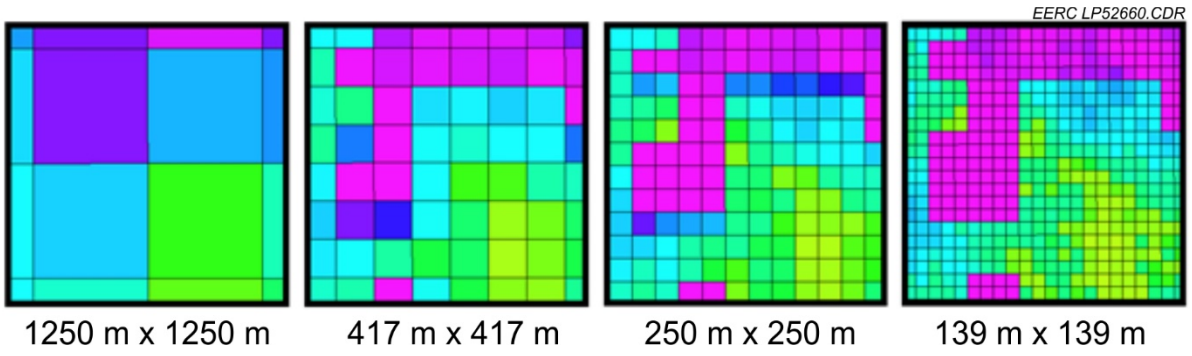

Figure 4. Depiction of the various grid cell sizes used to investigate the sensitivity of simulated dissolved CO_2.

these grids all served in the CO_2 dissolution sensitivity study discussed in the following sections of this report, the grid composed of 250-m × 250-m cells was chosen to serve as the base case for subsequent simulations of CO_2 injection with varying well densities.

To explore injection sensitivities to lithofacies distribution, the base case model was altered by varying the amount of sandstone lithofacies within the model. The sandstone lithofacies proportions were varied ±10%, resulting in low, mid, and high cases having 51%, 61%, and 71% sandstone proportions, respectively. Modeled properties were distributed in the fine-scale 139-m × 139-m cell grid area and upscaled into the coarser grids. This resulted in averaged properties for the grids containing larger cells but similar pore volumes across each. Initial property distributions occurred in the finest grid resolution (139-m × 139-m cells). This property distribution was upscaled into the successively coarser grids (250-m × 250-m cells, 417-m × 417-m cells, and 1250-m × 1250-m cells). Porosity upscaling occurred through simple averaging (arithmetic) of the finer cells intersecting the coarser cells to keep pore volume similar between the cases. Permeability upscaling occurred through geometric averaging (geomean) of the finer cells intersecting the coarser cells, as is most appropriate for variables having logarithmic distribution.

The low, mid, and high cases, in terms of facies distributions, were a topic of in-depth internal discussion at the EERC. It was initially thought that efforts would focus on determining P10, P50, and P90 facies distributions. A proper justification for such distributions would have been achieved by 1) modeling a suite of different eolian sandstone units, 2) assessing (vertical) facies associations from well logs for each, 3) upscaling these facies associations into grids with cell sizes similar to what was intended to be used in this study, 4) ranking the resulting upscaled facies proportions, and 5) from the ranked facies proportions determine the 10th, 50th, and 90th percentiles. This effort, however, would not have been temporally efficient and conflicted with the project's overall time frame. Without having proper statistical support for "P10/P50/P90" nomenclature, the less precise "low/mid/high" descriptors were implemented.

With regard to the 61% ± 10% reservoir sand variation, this was also a topic of rigorous discussion. The upscaled Minnelusa facies percentages from the Stage 1 work were 61% reservoir sand and 39% nonreservoir carbonate. Reverting to general geologic discussion, most sandstone units in intracratonic basins (regardless of depositional environment) contain substantial heterogeneity and

some nonreservoir component. Thus 100% (and even 90%) reservoir sand content is not a likely scenario in any given location (certainly not over a 1250-km area), thus too high to be considered. On the other end of that argument, a unit containing less than 50% sand is 1) less likely to be considered a sandstone, rather a (perhaps sandy) siltstone/shale/carbonate or something else other than a sandstone, and 2) less likely to be the primary target of CO_2 storage activities (at least until other potential targets' storage resource have been exploited or deemed otherwise unsuitable). Thus 61% was deemed the mid case for the Stage 2 Minnelusa effort, in turn providing some continuity to the previous Stage 1 work. Variation of ±10% reservoir sand was an arbitrary, yet symmetrical, amount chosen to represent low and high cases.

Bunter Model

The Triassic Bunter Sandstone is a formation within the Bacton Group of the southern North Sea Basin (Figures 5 and 6). The Bacton Group represents a phase of clastic deposition in a nonmarine environment when the Zechstein Sea (Permian) withdrew. The Bacton Group consists largely of nonmarine red mudstones, shales, and sandstones.

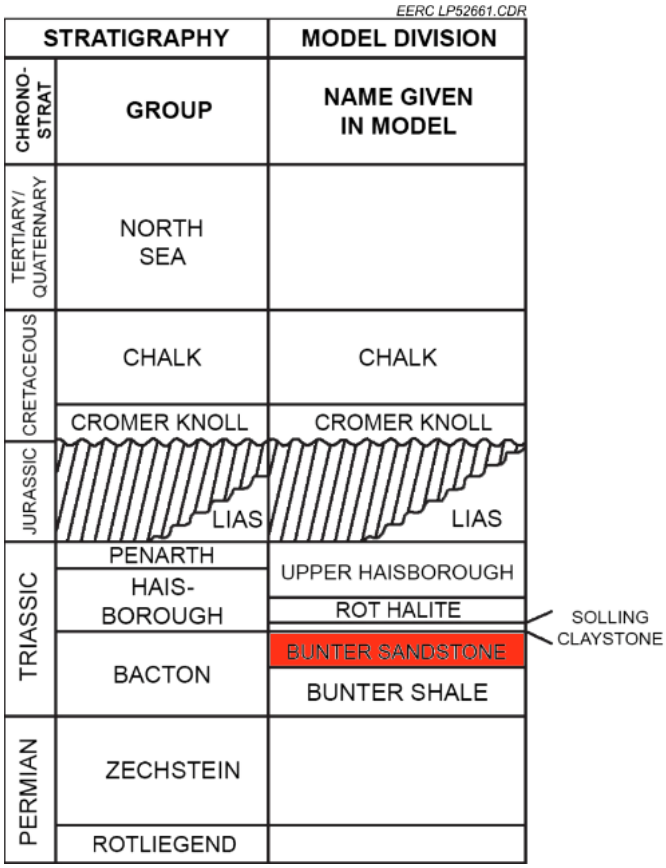

Figure 5. Stratigraphy of the study area (modified from Williams and others, 2013, with permission from Elsevier).

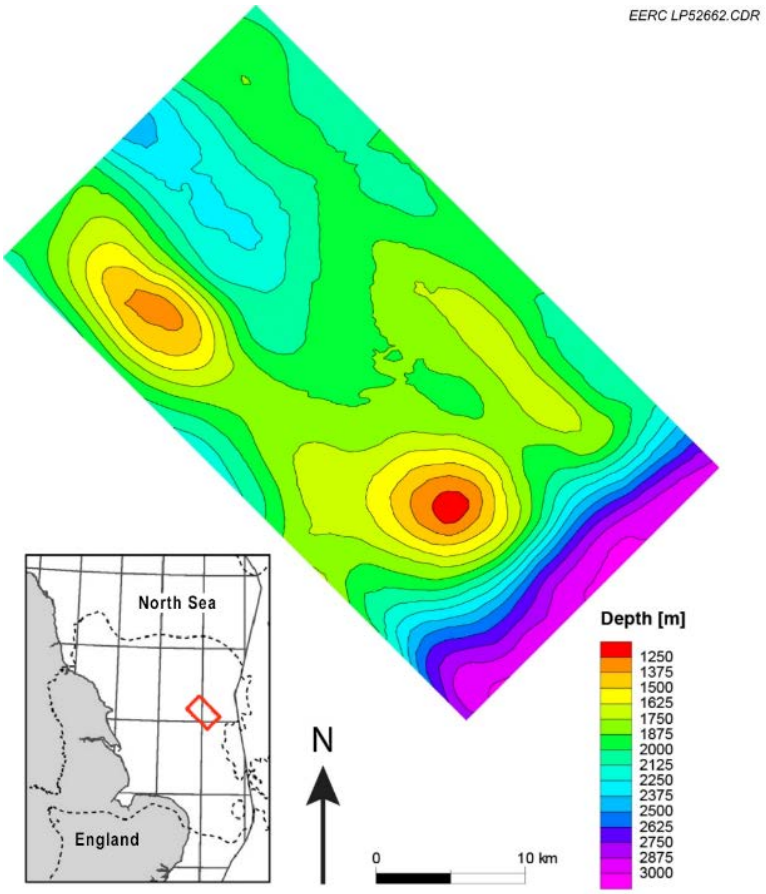

Figure 6. Depth to the top of the Bunter Sandstone, which serves as the upper limit of the geologic model. Inset map (modified from Williams and others, 2013, with permission from Elsevier) depicts the location of the model (red rectangle) within the North Sea and extent of the Bunter Sandstone (dotted line) in relation to the east coast of England.

The Bunter Formation comprises a series of medium- to coarse-grained red sandstones interbedded with very coarse sandstones and meter-scale conglomerate layers. Brook and others (2003) indicated that strata near the basin margins probably formed as a series of alluvial fans which were dissected by braided river channels and deposited in a semiarid/arid climate. Toward the center of the basin, there are far fewer conglomerates, and the sandstones present were mostly deposited by sheet floods on a large, flat plain. The Bunter Sandstone represents a single flow unit and has been previously studied as a desirable target for CO_2 storage (Williams and others, 2013, Noy and others, 2012; Brook and others, 2003) because it has reservoir characteristics amenable to injection activities, has numerous dome structures (structural expressions of underlying salt diapirs) which act as natural structural traps, and is well sealed above and below by the evaporites and mudstones of the Upper Triassic Haisborough Group and the Bunter Shale Formation, respectively.

An existing geologic model of the Bunter Sandstone, developed in similar studies of CO_2 storage by Williams and others (2013), was obtained to expedite the proposed efforts. An adapted version of this model was also used in studies by the Energy Technologies Institute (ETI) (Energy

Technologies Institute, 2016a). For the purposes of this study, the geologic structural surfaces, reservoir intervals, and porosity logs used in both the Energy Technologies Institute and Williams and others (2013) studies were used to create the structural model, and the porosity logs served as the basis for creating petrophysical property distributions. Similar to the Minnelusa simulation goals above, the Bunter model was created to obtain CO_2 storage simulation outcomes over a realistic temporal context of 50 years; however, no CO_2 dissolution sensitivity investigations were undertaken for the Bunter. Thus the model modifications for this study were more straightforward. The model encompassed the Bunter Sandstone in the study area (using the top of the Bunter Sandstone as the upper limit and the top of the Bunter Shale as the bottom) and gridded with 200-m × 200-m cells. The model ranged in thickness from 135 to 375 m, with an average thickness of 235 m. The reservoir was divided into five intervals according to geophysical log analysis performed by Williams and others (2013) (Figure 7).

Porosity logs, calculated by Williams and others (2013) through lithologic, petrophysical, and geophysical analyses, served as the basis for geostatistical distributions. The resulting porosities ranged generally from 10% to nearly 30% throughout the reservoir (Figure 8). Permeability of the Bunter Sandstone was calculated using the Kozeny–Carman equation (Carman, 1956), resulting in permeabilities ranging from 0.6 to 106 mD, with a pore volume weighted average of 40 mD.

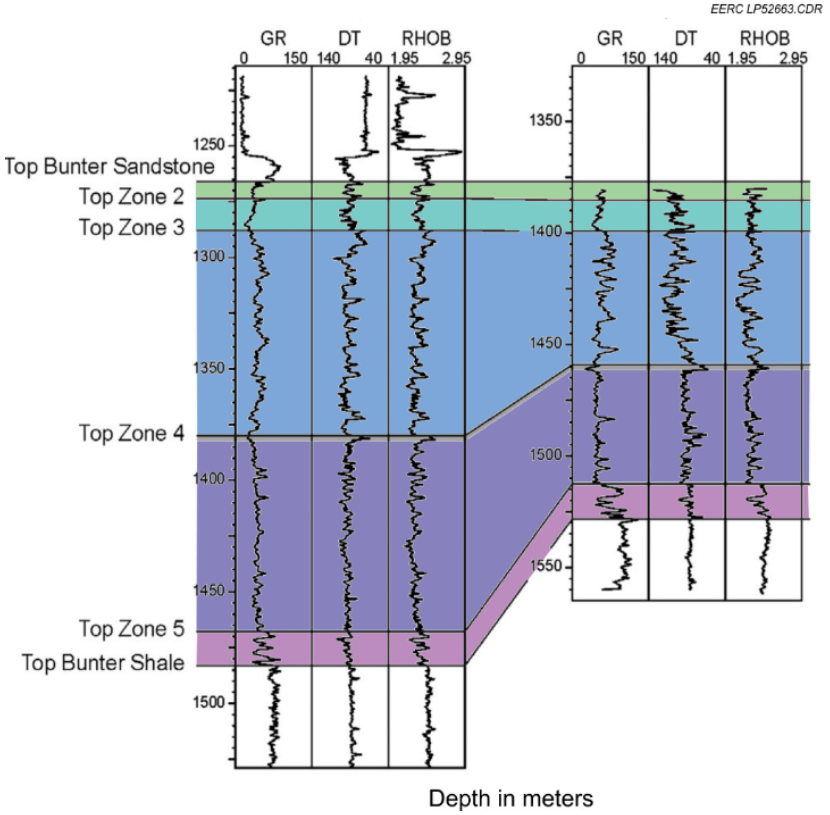

Figure 7. Correlation of reservoir zones (modified from Williams and others, 2013; with permission from Elsevier).

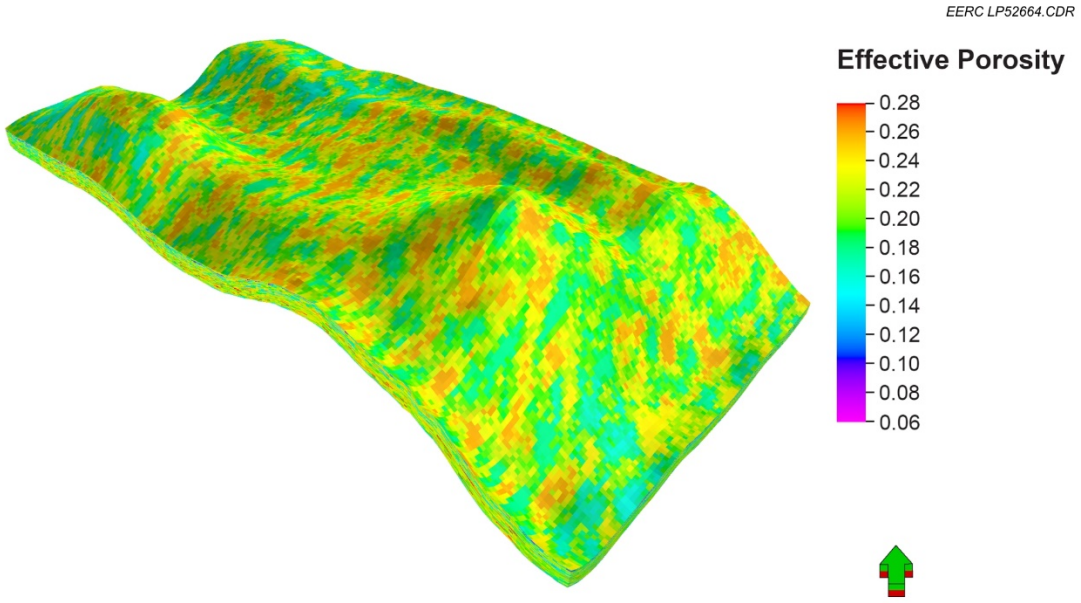

Figure 8. Distributed effective porosity of the Bunter Sandstone geologic model (5× vertical exaggeration).

NUMERICAL SIMULATION

Static Volumetric Storage Efficiency Factor for the Saline Formations

According to DOE methodology, published in the 3rd edition of the Carbon Sequestration Atlas of the United States and Canada (U.S. Department of Energy, 2010), the following equations were used to evaluate the effective static volumetric storage efficiency:

$$E_{geol} = E_{An/At} * E_{hn/hg} * E_{\varphi eff/\varphi tot} \quad \text{[Eq.1]}$$

$$E_D = E_{vol} * E_d \quad \text{[Eq. 2]}$$

$$E_E = E_{geol} * E_D \quad \text{[Eq. 3]}$$

where E_{geol} is the effective-to-total pore volume ratio and defined as the area where there is sufficient formation at a depth where CO_2 will remain in the supercritical state. $E_{An/At}$ is the effective net-to-total areal ratio, $E_{hn/hg}$ is net-to-gross thickness, and $E_{\varphi eff/\varphi tot}$ is the effective-to-total porosity. E_D is the displacement efficiency and split into the E_{vol}, the volumetric displacement efficiency, and the E_d, the microscopic displacement efficiency. These terms are the same as those used in the Stage 1 study (Craig and others, 2014; IEA Greenhouse Gas R&D Programme, 2014).

The sector geologic models of the Minnelusa Formation and Bunter Sandstone were used to estimate their respective volumetric storage efficiency factors. The sector models were clipped from larger-scale models and contain only the reservoir portions of the model. Thus $E_{An/At}$, $E_{hn/hg}$, and $E_{\varphi eff/\varphi tot}$ are all known to be 100% for all of those terms, and the E_{geol} would, therefore, be

100%. The volumetric efficiency calculation would then be determined by the formation displacement efficiency factor, E_D. The E_D ranges from 7.4% to 26% for different lithology and geologic realizations (Table 1). In the Stage 1 study, the base case value for E_E in the Minnelusa basin-scale model was 6.3%. In this study, a sector area of the Minnelusa with relatively better than average reservoir properties was chosen for simulation, and the resulting value of E_E for that area was determined to be 7.44%. The low and high reservoir sand proportion values for the Minnelusa are 5.84% and 9.11%, respectively. The corresponding values for E_E in the Bunter Sandstone are 7.4%, 14%, and 24% for the low, medium, and high scenarios, calculated directly from Eq. 3 and Table 1.

Table 1. Saline Formation Displacement Efficiency Terms, E_D (U.S. Department of Energy, 2010)

Lithology	P_{10}	P_{50}	P_{90}
Clastics	7.4%	14%	24%
Dolomites	16%	21%	26%
Limestones	10%	15%	21%

The Minnelusa model E_E values were calculated as a product of effective-to-total pore volume ratio (E_{geol}) and displacement efficiency (E_D). E_{geol} was calculated from specific model characteristics, including net-to-gross area (A_N/A_T), net-to-gross thickness (H_N/H_G), and effective-to-total porosity ($E_{\varphi eff/\varphi tot}$). Because no parts of the Minnelusa were eliminated from the modeled area or thickness (the whole of the model was at depths/conditions suitable for CO_2 storage), A_N/A_T and H_N/H_G were 100%. Thus E_{geol} was simplified to $E_{\varphi eff/\varphi tot}$. This was calculated for each Minnelusa case (low/mid/high) by comparing the reservoir sand facies pore volume to the models' overall pore volume (reservoir and nonreservoir facies' pore volumes together). For the reported E_E values for both the Minnelusa and Bunter cases, E_D was assumed as the P50 clastic formation displacement efficiency (E_D) published in U.S. Department of Energy (2010), with a value of 0.14.

The Minnelusa E_E values used the Clastic P50 E_D value (0.14) from U.S. Department of Energy (2010) and changing E_{geol} from low/mid/high case models, whereas the Bunter E_E P10/P50/P90 values differed by using the range of E_D values from U.S. Department of Energy (2010) against a static E_{geol} value calculated from the model. As such, the two cases are not directly comparable.

By applying these efficiency factors to the simulated reservoir volumes, the calculated volumetric CO_2 storage resource for the Minnelusa area is 5086 Mt. For the Bunter, the corresponding CO_2 storage resource is 4571 Mt.

Minnelusa Simulation Work Plan

Dynamic Simulation

Following a calculation of the effective volumetric CO_2 storage resource potential and efficiency, simulation is performed to determine the effective dynamic CO_2 storage resource potential and

efficiency. The dynamic simulation workflow was conducted by importing the Minnelusa geologic model sampled for 250-m × 250-m grid cells into Computer Modelling Group's (CMG's) GEM software, a fully compositional simulator. Fifty layers with an average thickness of 1.5 m were used in the creation of the model. Key parameters for the simulation are given in Table 2. Additional information about the simulation and figures showing results of the cases are presented in Appendix A. After initial construction of the simulation, determinations were made for injection simulation design, boundary conditions, and variations in structural setting. The well injection rates were limited by injecting at maximum bottomhole pressure (BHP) constraint. The BHP limit to be applied used the same methodology as for the Stage 1 study and is based on the perforation depth and a pressure gradient of 13.6 kPa/m, approximately 10% lower than the fracture pressure gradient (Barati, 2011). As a backup constraint, the maximum allowed well injection rate was set to 2.0 Mt per year. All injection wells were started at the same time. This is beneficial for attempting to maximize the quantity injected during 50 years, but is not necessarily representative of an actual field development plan. As a result, injection rate is highest in the first year of injection with lower rates in successive years as average pore pressure increases while the maximum allowed injection pressure remains constant. The injection simulation results are reported for a 50-year injection period, although most cases were executed for 100 years to aid in clarity of the results. Effective dynamic CO_2 storage resource potential and efficiency were determined and, where appropriate, compared to the estimated static values.

Table 2. Properties Used in the Base Case Simulation Model of the Minnelusa Formation

Parameters	Value	Unit
Rock Compressibility	5.58 E-7	L/kPa
Water Compressibility	3.1325 E-7	L/kPa
Brine Salinity	20,000	ppm
Temperature Gradient	0.05	°C/m
Pore Pressure Gradient	9.8	kPa/m
Grid Dimensions	25 × 50	km
Grid Cell Dimensions	250 × 250	m
Grid Cell Average Thickness	1.5	m

An array of simulation cases was selected to expand on the Stage 1 work to reach a better understanding of the variables that limit the ability of potential injection projects to approach volumetric storage efficiency and to define a practical storage efficiency for such projects.

Well Placement and Injection Sensitivity Cases

Table 3 lists the simulation cases for well placement and injection sensitivity investigation. These "drilling" cases are subsequently referred to as Cases D1 through D7. The objective of these cases was to determine the number of wells, and their locations in the simulated area, that could plausibly be used for CO_2 injection and what practical storage efficiency factors could be attained within a reasonable lifetime of an injection project, 50 years.

Table 3. Well Placement and Injection Sensitivity Investigation: Minnelusa Model

Case ID	No. of Wells	No. of Wells, %
D1	684	120
D2 (base case)	576	100
D3	460	80
D4	345	60
D5	230	40
D6	115	20
D7	58	10

A series of preliminary cases were executed with progressively larger numbers of wells, their locations based on favorable permeability–thickness (kh) calculations. As expected, increases in the per well quantity of CO_2 injected eventually decreased as the number of wells continued to increase. This was due not only to progressively poorer locations taken into use, but also to progressively greater degrees of pressure interference and general pressure buildup in the model. This was true even in the cases of simulations with open-boundary conditions. Wells located near the perimeter of the simulation performed better than wells in the central area because perimeter wells had better opportunity to displace formation brine out past the simulation boundary. Both factors are representative of actual conditions that would be encountered in a large-scale onshore storage development that did not benefit from water extraction wells; that is 1) storage developers would prefer to drill the most favorable locations first and 2) large-scale storage development will inevitably be hindered by well interference effects, even in open geologic systems. These cases suggested that for the 1250-km^2 simulated area in the Minnelusa, a total of 576 wells (2.2 km^2 per well) operating for 50 years had reached the point of diminishing returns and that drilling of additional wells was progressively less desirable. This case was deemed to be the base case (D2) and represented full drilling development: 100% of practical drilling locations occupied. All other drilling sensitivity cases presented in Table 3 have a specific percentage of this well count. The well locations selected for all of these cases were based on their kh rank.

Alternative Simulation Scenarios

The well placement sensitivity cases described above include the designation of a base case, D2, which contained 576 wells. Starting from this base case, several alternative cases were also investigated to represent a variety of constraints or geologic settings that might be encountered in a practical development project. Table 4 lists these cases which investigate the effects of reservoir heterogeneity, boundary conditions, formation structural setting, and well distributions on CO_2 storage efficiency.

In terms of reservoir quality, three scenarios were created. The base case (A2) used the same property distributions as the Stage 1 study, whereas the conservative case (A1) assumed 10% less reservoir sand facies, with an associated lesser degree of reservoir continuity, and an optimistic case (A3) which assumed a 10% greater sand distribution.

Table 4. Alternative Modeling Scenarios: Minnelusa Model

Case ID	Reservoir Quality	Boundary Condition	Structural Setting	Plume Design
A1	Conservative	Open	Actual	Dispersed
A2 (D2 base)	Moderate	Open	Actual	Dispersed
A3	Optimistic	Open	Actual	Dispersed
A4	Moderate	Closed	Actual	Dispersed
A6	Moderate	Open, with extractors	Actual	Dispersed
A7	Moderate	Open	Flat	Dispersed
A8	Moderate	Open	Monocline	Dispersed
A9	Moderate	Open	Trap	Dispersed
A10	Moderate	Open	Flat	Concentrated
A11	Moderate	Open	Monocline	Concentrated
A12	Moderate	Open	Trap	Concentrated

Boundary condition variations were considered in Cases A4 and A6 where closed and interior water extraction wells were considered, respectively. Extraction wells were not a focus area of this study, but a single case of this type (Case A6) is helpful in making comparisons with the impact of the boundary condition cases. In Case A6, 525 extraction wells were added and placed between the established injection wells, such that a five-spot pattern was made. Extraction wells were operated with a minimum bottomhole flowing pressure set equal to their initial pore pressure. Thus each extractor produced at a rate proportional to the amount of pressure increase that it experienced. The volume of water produced/volume of CO_2 injected was 37%.

The effect of structural setting was also considered. In Case A7, flat-lying strata were created by removing the structural interpretation from the base case. In Case A8, a simple monocline was created by applying a structural dip of 1 degree west to the flat-lying case. A general structural trap was created in Case A9 by applying a structural dip of 2 degrees south and closing the simulation boundary on the updip sides of the grid such that injected CO_2 could collect at the top of the structure.

Finally, Cases A10, A11, and A12 were created to examine the difference between dispersed drilling activity, based on selecting locations according to kh ranking, and concentrated drilling development, based on larger areas with favorable kh distribution.

Minnelusa Formation Dynamic Simulation Results

Well Placement and Injection Sensitivity Investigation

The results of the simulations after 50 years of injection in the Minnelusa Formation are shown in the Table 5.

Table 5. Minnelusa Simulation Results: Well Placement and Injection Sensitivity Investigations

Case ID	No. of Wells	No. of Wells, %	Mass CO_2 Injected, Mt	Mt per Well	Efficiency, %	Percentage of D2 Efficiency
D1	684	120	253	0.37	4.97	104.55
D2	576	100	242	0.42	4.75	100
D3	460	80	236	0.51	4.64	97.44
D4	345	60	222	0.64	4.37	91.90
D5	230	40	196	0.85	3.84	80.79
D6	115	20	172	1.50	3.39	71.16
D7	58	10	124	2.14	2.43	51.03

The first part of the simulation work focused on the injection sensitivity to well placement and number of wells. As described in the previous section, several test cases were simulated to determine a practical maximum number of wells that could be used in this model to reach a storage capacity and efficiency factor that was comparable to the volumetric assessment. Potential well locations were ranked based on the average kh (permeability × pay thickness) of the area around each well. For the case with the maximum practical number of wells, the top 576 locations were selected from a nominal well spacing of 1250 m × 1250 m. After 50 years of injection, the corresponding CO_2 storage efficiency was 4.75%. Six more cases were performed to examine how the practical storage efficiency changed with different numbers of injection wells. Case D1 had 684 wells, 120% of D2, the base case, but the storage efficiency of D1 was 4.97%, an increase of only 4.55% over that of the base case. The 10% case, D7, with only 58 wells injected 124 Mt CO_2, 51% of the base case. With a longer injection period, 100 years, the top 10% case improves to 63% of the base case. From these cases, it is apparent that the well CO_2 mass injected per well per year decreases for cases with more wells. Results from the optimized well selection process can be seen in Figure 9 where the later years of slow increase in cumulative injection suggest behavior similar to a closed- or restricted-system boundary.

Figure 10 represents the summation of the CO_2 areal plume distributions of the base case. It is apparent that wells on the perimeter of the drilling area maintain higher injectivity than wells in the center of the pattern, regardless of the well kh. This is a condition of the problem description in which maximum practical storage capacity is to be determined for a specific area. In any injection well pattern in which maximum practical capacity is approached, regardless of the size of the area, pressure interference between wells will be experienced; particularly for wells in the interior of the pattern. Images of the summed CO_2 areal distribution for the other cases are presented in Appendix A. Figure 11 shows the plume distribution in cross section, which also demonstrates the lesser quantity of CO_2 injected in the interior parts of the well pattern. Figure 12 is an image of the equivalent pore pressure distribution which shows regional pressure gradients across the domain. The isobars are not horizontal, as would be expected if the regional pore pressure was in equilibrium. It should also be noted there are no significant pressure gradients between wells, suggesting that pressure interference between wells is ubiquitous. Injection rates at Year 50 are low since regional pressure has approached the maximum allowed injection pressure.

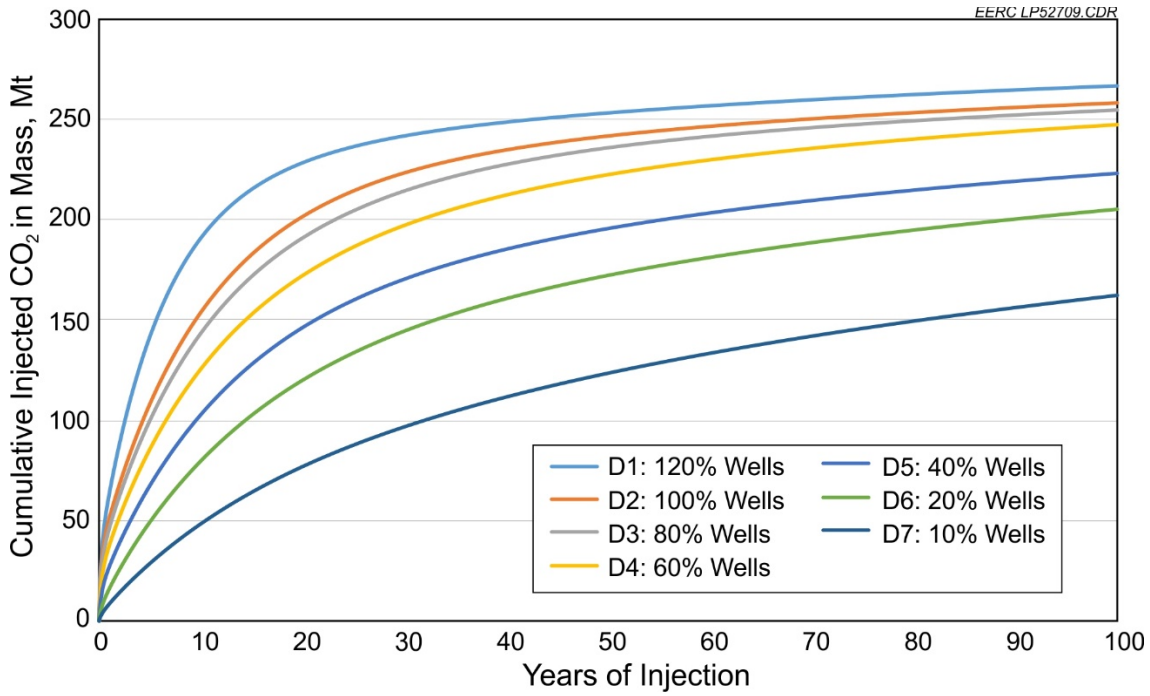

Figure 9. Well placement and injection sensitivity investigation: cumulative CO_2 (mass) with differing well numbers.

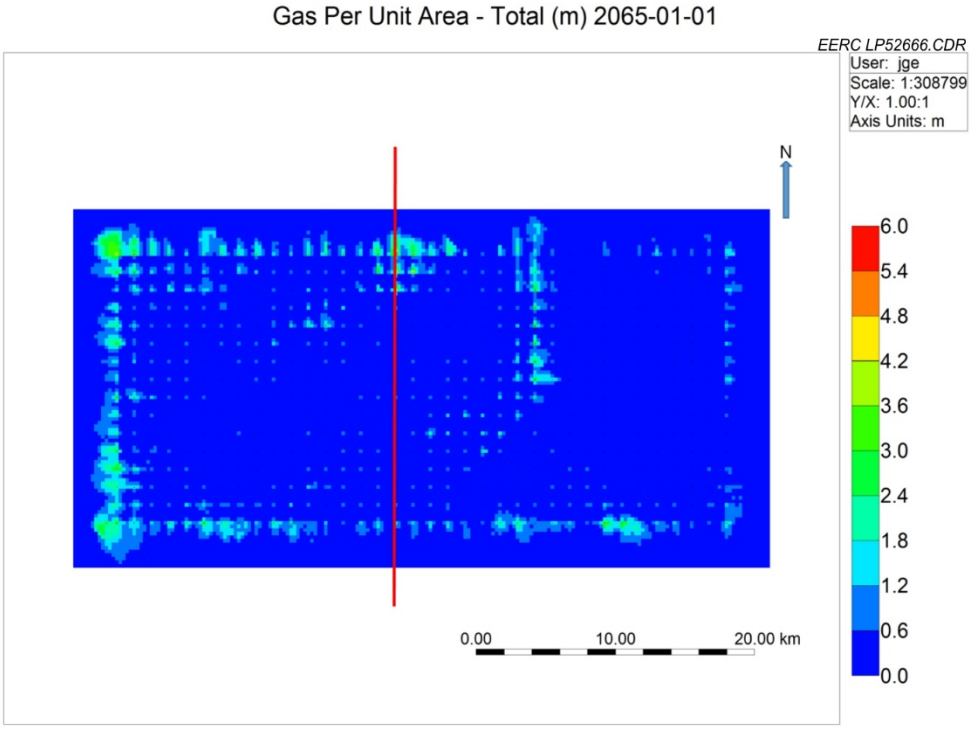

Figure 10. Well placement and injection sensitivity investigation: CO_2 footprint (total gas per unit area in meters) after 50 years of injection in the D2 base case. The red, vertical line indicates the placement of the cross section shown in Figures 11 and 12.

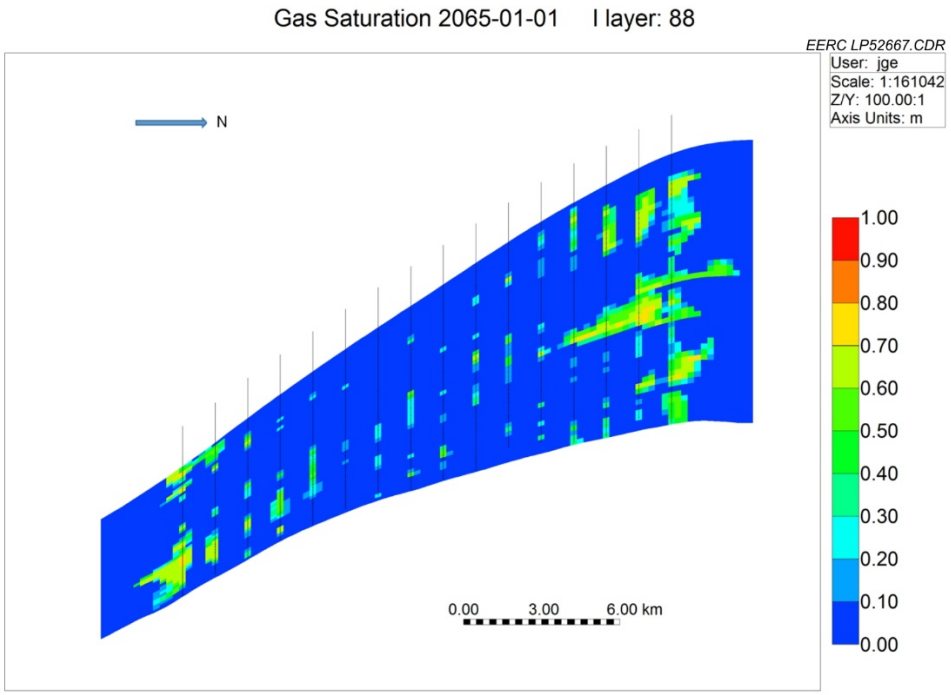

Figure 11. Well placement and injection sensitivity investigation: CO_2 plume in the D2 base case.

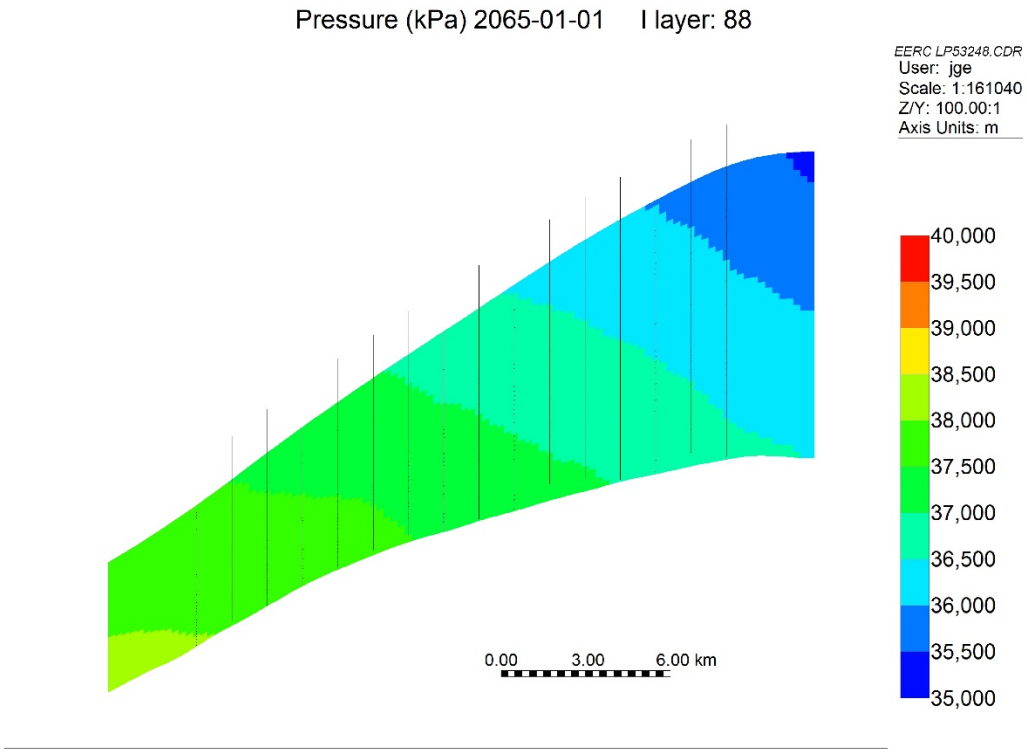

Figure 12. Well placement and injection sensitivity investigation: pore pressure distribution in the D2 base case at the end of injection.

Figure 13 represents the dynamic CO_2 storage efficiency factor vs. the number of wells of the Minnelusa Formation. Compared to the static CO_2 storage efficiency factor which is calculated by the volumetric method, none of the seven cases reached the volumetric storage efficiency within 50 years. This is primarily because of the strong effect from pressure buildup and interference between wells. It also shows that the rate of increase for the dynamic storage efficiency decreases rapidly after the number of wells exceeds 90, which is equivalent to an average well spacing of 13.9 km^2 per well for this model.

Before considering a project-specific economic analysis, optimum can be defined as achieving acceptable storage efficiency with a low number of wells. Based on the analyses on the simulation cases alone, without consideration of economic constraints, the optimum number of wells for this Minnelusa development area appears to be in the range of 58–116 wells, the 10% and 20% cases, respectively, with approximately 90 wells suggested as an ideal number. These two cases represent a practical dynamic storage efficiency range of 2.4% to 3.4%. This fits the initial expectation that a relatively small number of good wells will account for a large fraction of the injection.

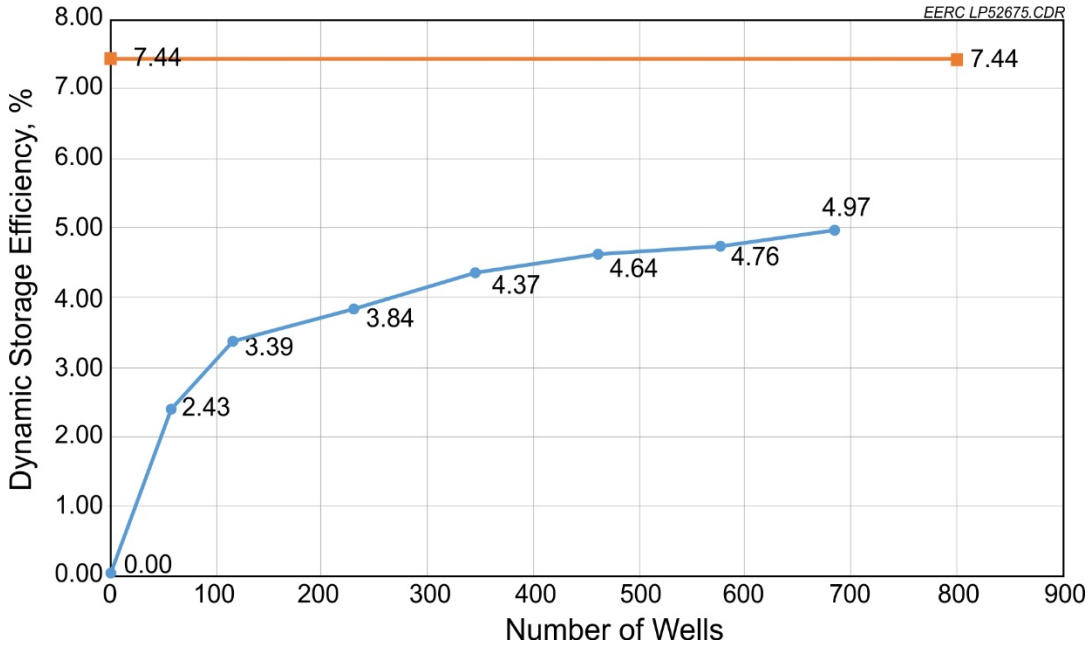

Figure 13. Well placement and injection sensitivity investigation: dynamic CO_2 storage efficiency vs. number of wells for the Minnelusa Formation. Effective efficiency of 7.44% for the base case lithology description is also shown.

Alternative Simulation Scenario Investigation

Minnelusa simulation cases were executed for a 100-year injection period, and all figures that show injection results display a 100-year time period. This is useful to better understand the longer-term trends of these cases and what would be "cut off" as the result of a 50-year injection period.

However, all discussion and tabulated results, unless specifically noted otherwise, are based on injection results at 50 years. Table 6 summarizes the results of the alternative simulation scenarios.

To evaluate the effects of different geologic realizations and reservoir quality on the effective CO_2 storage efficiency, optimistic, base, and conservative lithology distribution cases were generated for the Minnelusa model. These variations were created by increasing and decreasing the reservoir sand fraction in the geologic model, resulting in changes to the percentage of bulk rock volume amenable to storage. These cases resulted in variation of the practical efficiency from 4.04% to 5.36% in the conservative Case A1 and optimistic Case A3 realizations, respectively, as shown in Figure 14. This illustrates that heterogeneity and different model realizations can substantially influence the quantity of injected CO_2. However, these cases also show that exceptional changes did not occur with respect to the ability of the injection program to approach the volumetric storage capacity.

Table 6. Minnelusa Simulation Results: Alternative Modeling Scenarios with 50 years of Injection

Case ID	Case Description	No. of Wells	Mass CO_2 Injected, Mt	Efficiency, %
A1	Conservative lithology	576	206	4.04
A2 (D2)	Base	576	242	4.75
A3	Optimistic lithology	576	272	5.36
A4	Closed boundary	576	64	1.25
A6	With extractors	576 + 525	302	5.94
A7	Flat structure	576	254	5.00
A8	Monocline structure	576	258	5.07
A9	Trap structure	576	232	4.56
A10	Concentrated, flat	58	131	2.57
A11	Concentrated, monocline	58	137	2.69
A12	Concentrated, actual structure	58	168	3.30

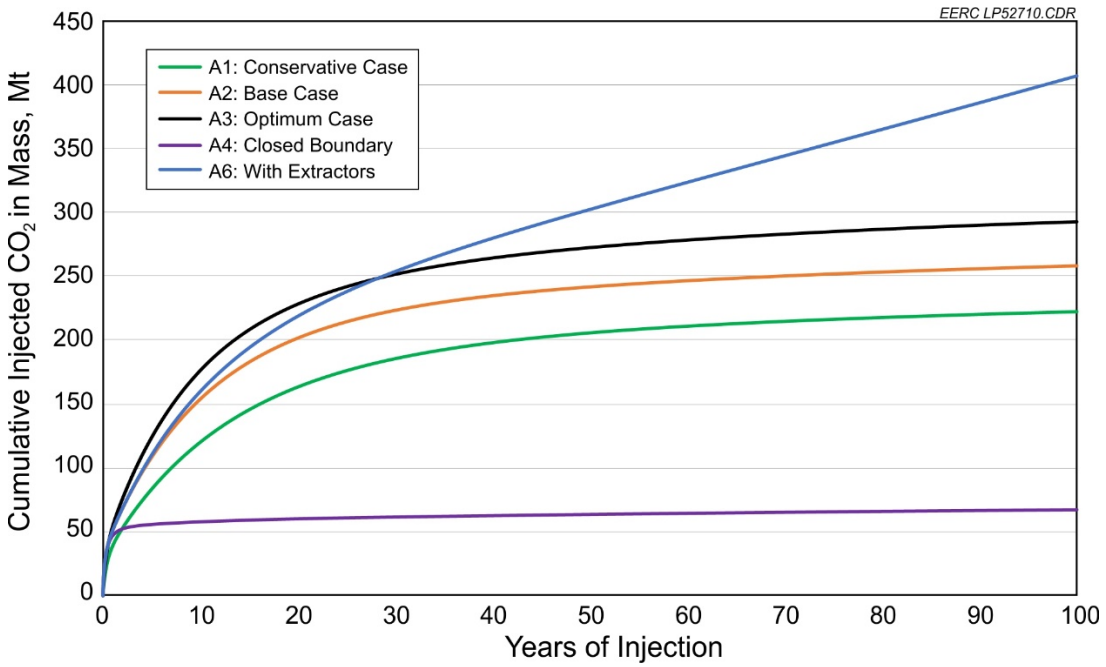

Figure 14. Comparison of the effects of lithology distribution and boundary conditions on CO_2 storage.

Two boundary conditions were considered for this study intended to represent open and closed boundaries at the perimeter of the simulation. The open boundary represents the model boundary connecting to the remainder of the formation outside the simulated area using the same reservoir physical properties as the model boundary cells. The water flux across the boundary is estimated by using the Carter–Tracy approximation, and saline formation water is allowed to flow from the reservoir into the connecting aquifer cells where the pressure of a cell exceeds the adjacent aquifer pressure. CO_2 is not allowed to flow from the reservoir into the connecting aquifer cells. For both the Minnelusa and the Bunter model areas, the actual boundary conditions at the perimeter of the simulations contained no barrier to lateral flow, such as large sealing faults or stratigraphic pinch outs. Therefore, the open-boundary condition cases are considered to be the more representative condition. The closed-boundary case represents a model that is acting as a closed system where no aquifer is connected to the model boundary and no flow out of the system is allowed. Cap rock was not considered in any of the cases. The Stage 1 study did include a low-permeability caprock description. However, that study considered a much longer time frame than this study, and the effect of slow caprock permeation for this study is considered minor. One additional case with 525 water extractors was also examined to check the effects extractors may have on total injection. These extractors were placed between the injectors to form five-spot patterns in the model. As expected, the closed-boundary case, A4, performed poorly and has a much lower efficiency of 1.25% compared to the efficiency of the open-boundary Case A2 (4.75%). However, the case with extractors, Case A6, has the highest efficiency of any case at 5.94%. This is because the pressure interference between injection wells is relieved as formation water is allowed to escape the modeled area by means other than only the boundary conditions, albeit at the cost of nearly doubling the number of wells drilled. The volume of water produced/volume of CO_2 injected for

Case A6 was 37%. The difference in performance of the extractor case continues to grow for continued injection beyond the reported 50-year injection period, as shown in Figure 14.

Three types of structural settings were tested in this study. The actual structural setting represents the actual geologic structure of the sector model area, and this evaluation has focused on this actual structural model, including a regional southwest dip and several structural features that are present in the geologic model. Two hypothetical structural settings, flat (A7) and monocline (A8), were introduced with the same reservoir properties that were used in the actual structural setting model. The reference depth used in these two models was chosen at the average depth of the actual base case scenario. Compared with the flat setting, the monocline setting has a 1 degree dip angle that extends in the simulation's negative x-direction (west). A fourth type of setting, a structural trap, was arranged by using a monocline feature with a 2 degree dip in the negative y-direction (south), with the updip half of the model grid boundary closed and the downdip half of the model boundary open to the aquifer (A9).

Cases A2, A7, A8, and A9 have 576 injection wells, the number determined to be needed to maximize the quantity injected into the 1250-km^2 Minnelusa model domain. These wells were placed in a regular pattern throughout the model. The results presented in Figure 15 show the effects of these varying structural configurations. The cumulative CO_2 injection of the trap structure case, A9, is lower than that of the actual structure case, A2. This case appears to be negatively affected by the partially closed nature of the boundary condition, which was imposed to create an updip closure against which CO_2 could eventually migrate and be trapped. However, the Minnelusa is a heterogeneous and low-permeability formation which inhibits updip migration of the CO_2, preventing it from reaching the updip trap and becoming trapped and concentrated at

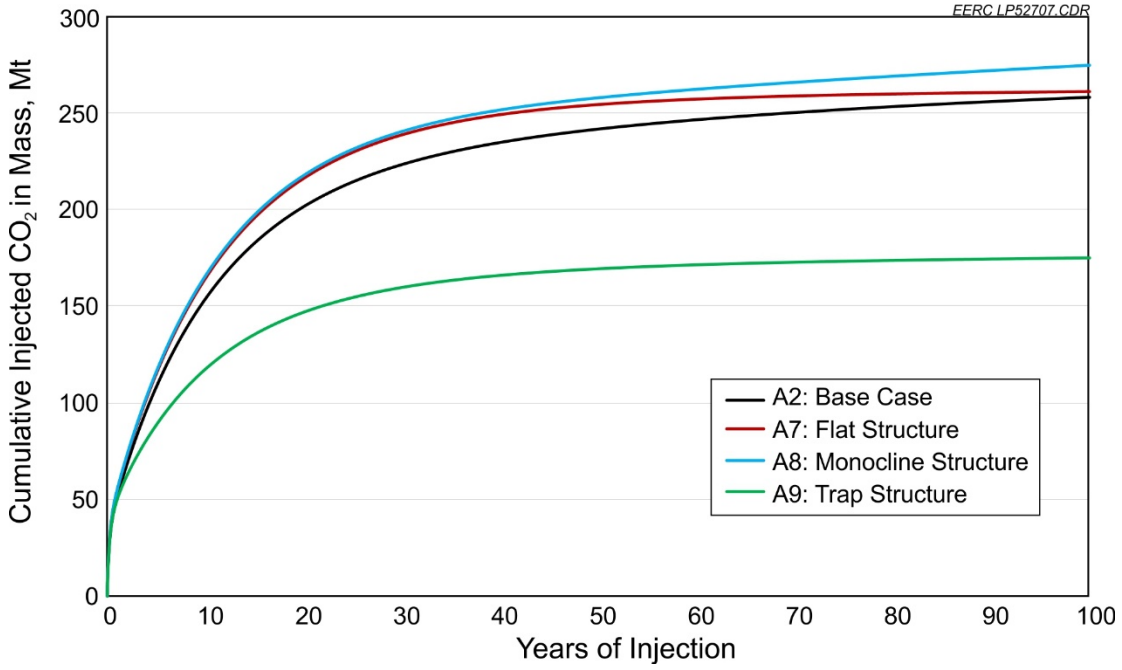

Figure 15. Comparison of the effects of structural setting and well concentration on CO_2 storage.

high saturation. At 50 years, the cases of the flat and monocline structures have slightly higher storage and efficiency than that of the actual structure case, although after a longer period of 100 years of injection, the flat structure case loses its advantage, while the monocline structure maintains its overperformance compared to the actual structural description.

Three additional cases were created from the actual, flat, and monocline structural description cases. Up to this point, well placement in all the cases is based on the kh ranking of the well locations. This provides a somewhat random-looking or "dispersed" drilling pattern.

However, CO_2 storage developers may prefer to concentrate their efforts in localized, favorable areas. The basis for the definition of a favorable area may vary widely among projects, but in this study, larger, continuous areas of relatively higher kh values are used to define such favorable areas. However, the selection of one or a few favorable areas within the simulated area puts a constraint on the number of wells that can be used for these cases. Therefore, as opposed to the 576 wells placed in the other alternative scenarios, these cases have only 58 wells concentrated in three areas with high kh values, as most likely preferred by CO_2 storage operators. The appropriate comparison case for these simulations is not the D2 base case but Case D7, which also contains 58 wells: those with the top 10% of kh locations. Cases A10, A11, and A12 represent flat, monocline, and the actual structure, respectively. Figure 16 shows the results of the effects of these varying structural configurations. All cases performed slightly better than the 58-well dispersed-development case, D7. Under actual conditions, concentrated development might also be reasonably expected to be less costly than dispersed-development scenarios.

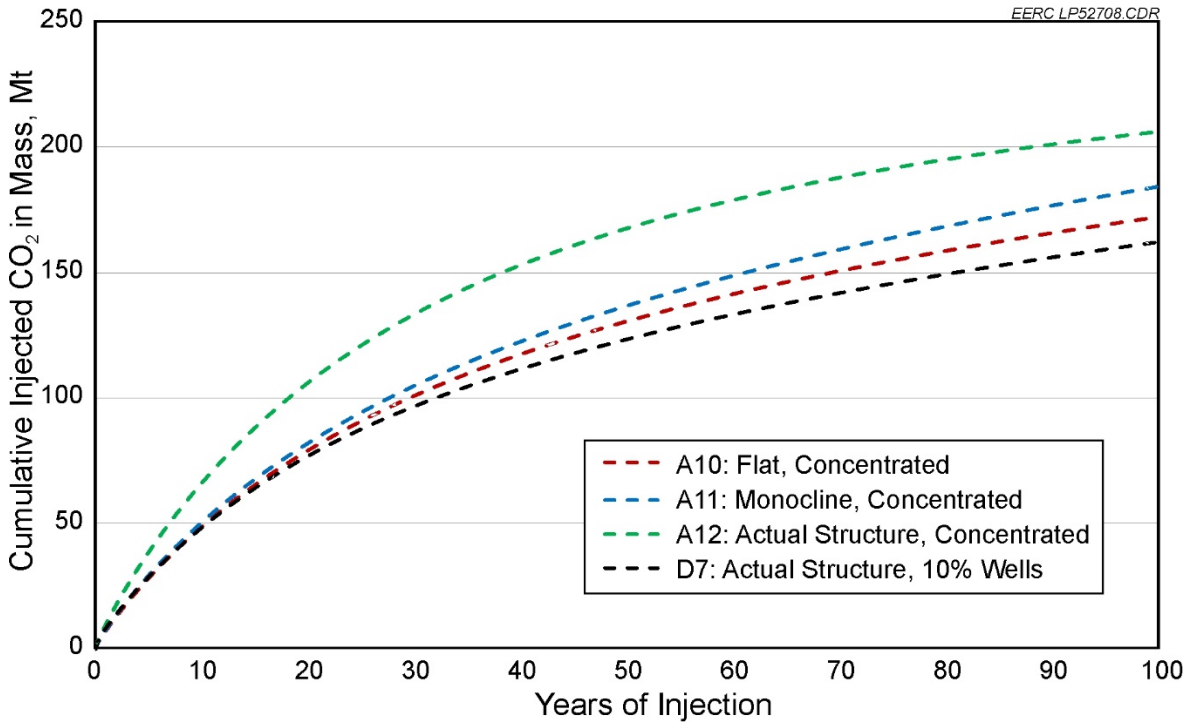

Figure 16. Comparison of the effects of well concentration on CO_2 storage.

Bunter Simulation Work Plan

The Bunter Sandstone DSF of the United Kingdom sector of the southern North Sea is considered likely to have significant CO_2 storage potential (Holloway and others, 2006a,b). The formation has fairly good reservoir properties as required for large-scale CO_2 storage (Chadwick and others, 2008). The Bunter Sandstone contains domed structural traps that could potentially store significant amounts of buoyant CO_2. CO_2 storage potential of the Bunter has been studied by other researchers using a large-scale simulation model (Noy and others, 2012) and one of the Bunter structures (Williams and others, 2013) using publicly available data. In this modeling and simulation study, part of the same area (Bentham, 2006; Smith and others, 2010; Williams and others, 2013) was modeled to provide a consistent basis of comparison.

Dynamic Simulation

Dynamic storage efficiency factors were evaluated through reservoir simulation utilizing GEM, a fully compositional simulator from CMG, for simulating CO_2 storage in saline aquifers. Rock/fluid properties data used in the simulation model were obtained from ETI and other sources (Bentham, 2006; Smith and others, 2010; Bentham and others, 2014), as shown in Table 7. Additional information about the simulation and figures showing results of the cases is presented in Appendix B. Figure 17 shows the top Bunter structure map of the simulated area.

Total dynamic storage efficiency of the Bunter simulated area, E_{Ed}, was calculated as:

$$E_{Ed} = \text{Total Injected } CO_2 \text{ (at reservoir condition)/Total Pore Volume of Model} \quad \text{[Eq. 4]}$$

The total pore volume was calculated at the initial reservoir condition and was found to be $5.19 \times 10^{10} m^3$.

Table 7. Properties Used in the Base Case Simulation Model of the Bunter Formation

Parameters	Value	Unit
Rock Compressibility	5.5675×10^{-7}	L/kPa
Water Compressibility	3.1325×10^{-7}	L/kPa
Brine Salinity	200,000	ppm
Temperature Gradient	0.0365	°C/m
Sea Bed Temperature	4	°C
Pore Pressure Gradient	10.07	kPa/m
Grid Area	24 × 44	km
Grid Cell Area	200 × 200	m
Number of Simulation Layers	33	–
Average Layer Thickness	7.6	m

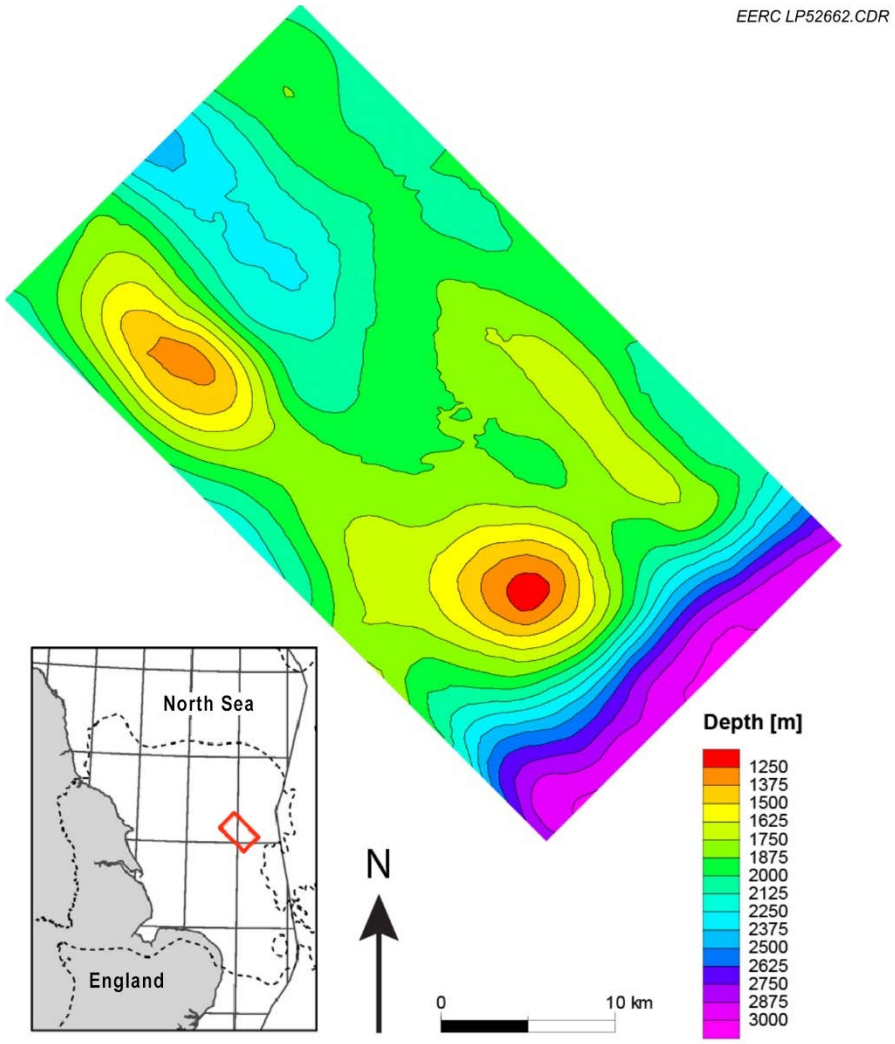

Figure 17. Depth to the top of the Bunter Sandstone, which serves as the upper limit of the geologic model. Inset map (modified from Williams and others, 2013, with permission from Elsevier) depicts the location of the model (red rectangle) within the North Sea and extent of the Bunter Sandstone (dotted line) in relation to the east coast of England.

Well Placement and Injection Sensitivity Cases

As for the Minnelusa Formation simulation, a series of preliminary cases with different well spacings were tested by placing wells over the entire Bunter Sandstone sector model in an attempt to determine a maximum practical efficiency factor for the simulated area. The well spacings that were tested ranged from 2.2 to 5.4 km. That created cases with 32 wells, 91 wells, 112 wells, and 190 wells. Each well was fully perforated through the formation. The well injection rates were limited by injecting at maximum BHP constraint. The BHP limit was calculated based on a pressure gradient of 16.05 kPa/m, approximately 10% lower than the fracture pressure gradient that was assumed in a previous study (Williams and others, 2013). As a backup constraint, the maximum allowed well injection rate was set to 2.9 Mt per year. All injection wells were started

at the same time. This is beneficial for attempting to maximize the quantity injected during 50 years but is not necessarily representative of an actual field development plan. As a result, injection rate is highest in the first year of injection, with lower rates in successive years as average pore pressure increases while the maximum allowed injection pressure remains constant. All cases were executed for a 50-year injection period. These four preliminary cases (32, 91, 112, 190 wells) were used to identify a maximum practical 50-year injection storage efficiency for the Bunter model domain. Results of these cases were plotted, which showed that the 91-well case approaches that maximum with the minimum number of wells (additional discussion is provided in the following Bunter Simulation Results section of the report). Therefore, the 91-well case was selected as the base case (B-D2). Results for these Bunter cases were similar to those performed for the Minnelusa. Both simulation exercises show that additional wells above the base case totals resulted in diminishing returns in terms of cumulative injection and storage efficiency.

With 91 wells as the base case, a series of drilling sensitivities were executed, with the number of wells selected as a specific percentage of the base case. These cases are outlined in Table 8.

As in the case of the Minnelusa simulation exercise, well locations were ranked by kh, and the best locations were selected first and the least prospective locations selected last.

Table 8. Well Placement and Injection Sensitivity Investigation: Bunter Model

Case ID	No. of Wells	No. of Wells, %
B-D1	110	120
B-D2 (base case)	91	100
B-D3	73	80
B-D4	55	60
B-D5	36	40
B-D6	18	20
B-D7	9	10

Alternative Simulation Scenarios

Case B-D2 is used as the base case for a series of alternative investigations to represent a variety of conditions that might be encountered in an actual CO_2 storage development and how they may impact practical storage efficiency. All cases are presented for 50 years of injection. Unless otherwise noted, all cases were executed using the 91-well B-D2 base case as their comparison basis. These cases are listed in Table 9 and represent different boundary conditions, structural settings, and well development patterns.

Table 9. Alternative Modeling Scenarios: Bunter Model

Case ID	Boundary Condition	Structural Setting	Plume Design	Note
B-A2	Open	Actual	Dispersed	B-D2 base case
B-A4	Closed	Actual	Dispersed	
B-A6	Open	Actual	Dispersed	24 extractor wells, fully perfed
B-A6-1	Open	Actual	Dispersed	24 extractor wells, only bottom half perfed
B-A7	Open	Flat	Dispersed	Depth 1800 m
B-A7-1	Open	Flat	Dispersed	Depth 1700 m
B-A8	Open	Monocline	Dispersed	Av depth 1800 m
B-A8-1	Open	Monocline	Dispersed	Av depth 1700 m
B-A8-2	Open	Monocline	Dispersed	A8 with reversed dip
B-A9	Open	Actual traps	Dispersed	15 wells at spill point
B-A10	Open	Flat	Concentrated	15 wells
B-A11	Open	Monocline	Concentrated	15 wells
B-A12	Open	Actual	Concentrated	15 crestal well locations

Bunter Sandstone Dynamic Simulation Results

Preliminary Sensitivity Investigation

The dynamic efficiency factors with 50 years of injection were evaluated for four preliminary cases in order to estimate a reasonable 100% well placement base case for further sensitivity investigations. All of these cases were executed by placing an even pattern of wells across the entire simulation area. The results of these cases, summarized in Table 10, show that increasing the number of wells in the model leads to a higher efficiency factor. However, the incremental efficiency factor is very small when the number of wells exceeds 91, as shown in Figure 18, and it may not be economically practical to drill more wells. Thus the 91-well case serves as the base case for well placement in the injection sensitivity investigation.

Table 10. Summary of Preliminary Case Results for Differing Numbers of Wells and Well Placement: Bunter Model

No. of Wells	Efficiency, %	Well Density, km^2/well	Mass CO_2 Injected, Mt
32	3.39	33.0	1280
91 (base case)	4.66	11.6	1770
112	4.67	9.4	1775
190	4.82	5.6	1838

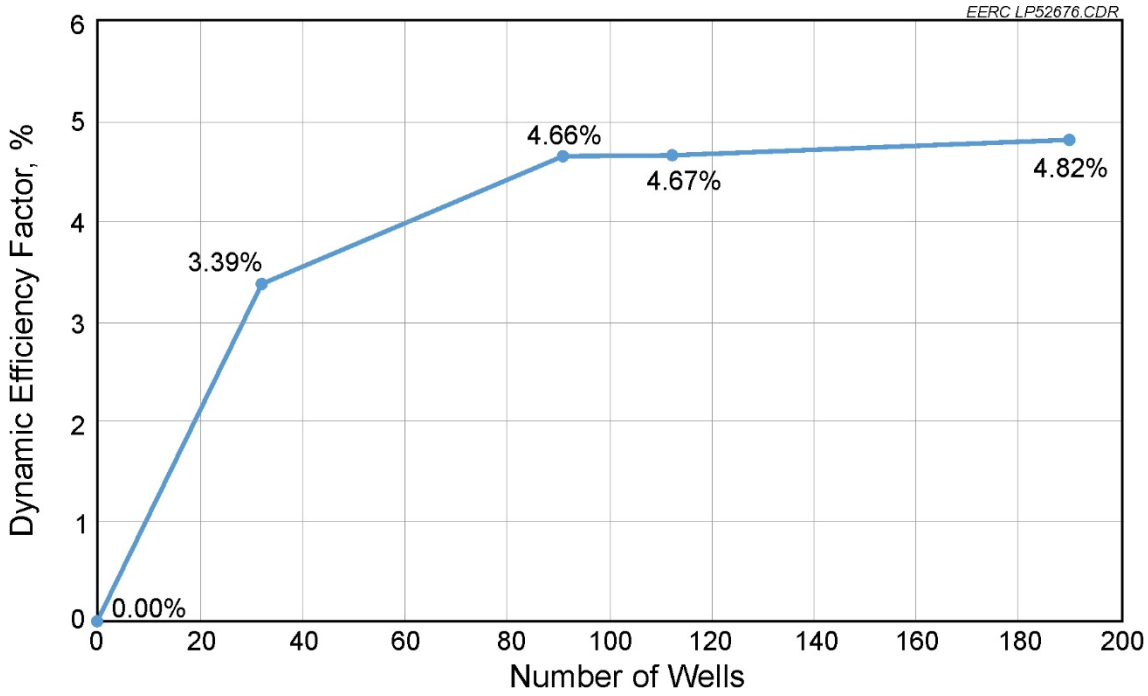

Figure 18. Dynamic efficiency factor vs. number of wells for Bunter Sandstone model area. Volumetric efficiency factor assumed suitable for the Bunter is 14%.

Well Placement and Injection Sensitivity Investigation

The well locations were ranked according to their kh, and a series of sensitivities were executed starting with the best 10% of the wells from the 91-well base case and progressively adding the next-best fraction of wells. These cases were repeated by selecting wells based on their ranking by cumulative injection. Unless otherwise noted, the kh-based ranked cases are used for further discussion, and the cumulative injection-ranked cases are for illustration purposes only. The injection-ranked cases performed better than the kh-ranked cases, but this result is misleading because of simulation edge effects, as discussed below. The results are shown in Table 11 and Figures 19 and 20.

Case D5, with the top 40% of wells for both ranking methods, is shown as Figure 21. Wells placed at the locations that have the best average kh value do not yield the best injection profile because of the heterogeneity of the model. The wells with higher injection are located on the edge of the sector model where there is less pressure buildup effect due to the open-boundary condition or the deeper locations in the formation that allow CO_2 to rise buoyantly so that greater storage would be achieved. However, considering the uncertainty of the boundary condition effects, kh ranking provides a more reasonable possibility for well placement design in field development, if the objective is to obtain a high storage efficiency factor with a minimum number of wells. It is noteworthy that, in both cases, the pattern avoids the structural closures.

Table 11. Bunter Simulation Results: Well Placement and Injection Sensitivity Investigations

Case ID	No. of Wells	No. of Wells, %	Mass CO_2 Injected, Mt (kh ranking)	Efficiency, % (kh ranking)	Mass CO_2 Injected, Mt (cum. inj. ranking)	Efficiency, % (cum. inj. ranking)
B-D1	110	120	1774	4.67	1774	4.67
B-D2	91	100	1770	4.66	1770	4.66
B-D3	73	80	1706	4.49	1762	4.64
B-D4	55	60	1598	4.21	1740	4.58
B-D5	36	40	1390	3.67	1663	4.39
B-D6	18	20	1113	2.94	1327	3.52
B-D7	9	10	830	2.21	795	2.11

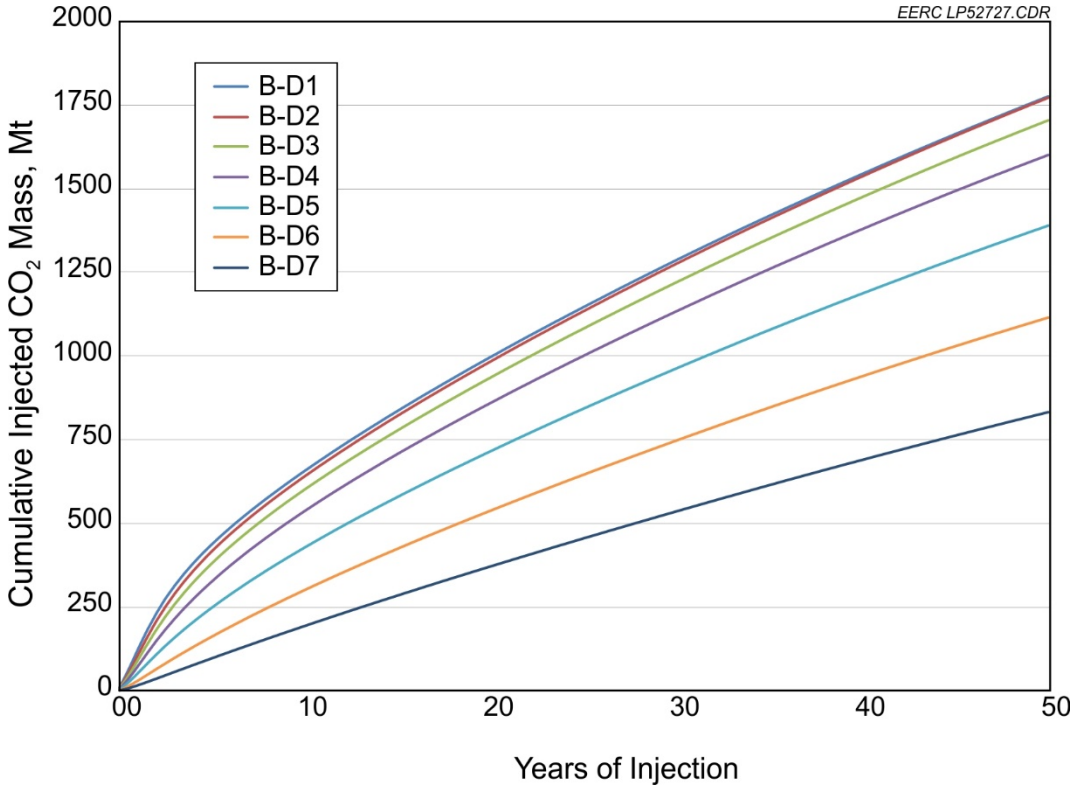

Figure 19. Bunter well placement and injection sensitivity investigation: cumulative CO_2 (mass) with differing numbers of wells.

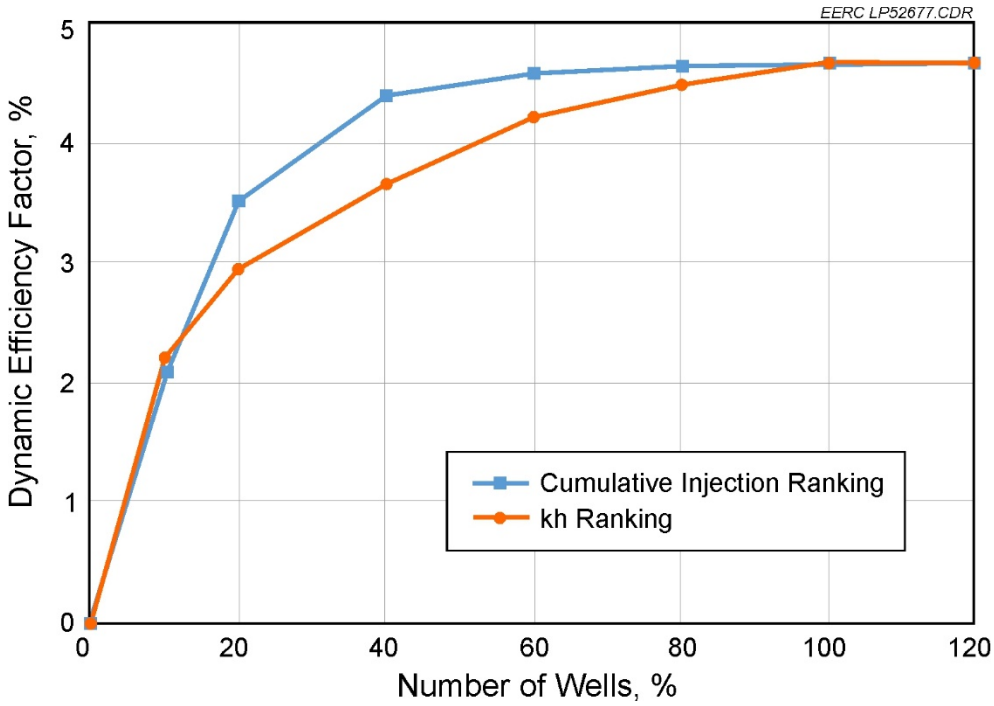

Figure 20. Dynamic efficiency factor vs. number of wells for different performance-ranking methods.

Alternative Simulation Scenarios

Boundary Conditions

DSFs typically have a large areal extent, and it is currently not feasible to model and simulate the entire formation in detail (Williams and others, 2013; IEA Greenhouse Gas R&D Programme, 2014). Modeling efforts normally extend over a limited area and focus on the CO_2 plume evolution and extent. The pressure footprint, however, extends much farther (Smith and others, 2010; Noy and others, 2012), so the proper boundary condition setup is critical to ensure realistic pressure response in the model, which would improve the accuracy of the potential storage capacity calculations.

Two boundary settings were considered in this study: open-boundary conditions and closed-boundary conditions. The formation water flux is estimated using the Carter–Tracy approximation, and water is allowed to flow from the simulated area into the connecting aquifer cells when the pressure of a cell exceeds the adjacent aquifer pressure. Closed-boundary conditions represent the model that is acting as a closed system where no lateral flow is allowed because of a stratigraphic pinchout, sealing faults, equal pressure pulses opposing the pressure within the model, or other flow limitation. An open-boundary system means no lateral boundaries are attached to the sector model so the in situ fluid, specifically brine, can move out of the injection formation. Injected CO_2 does not migrate out of the simulated area. In this study area, there are no identified structural or stratigraphic barriers identified at the model boundaries.

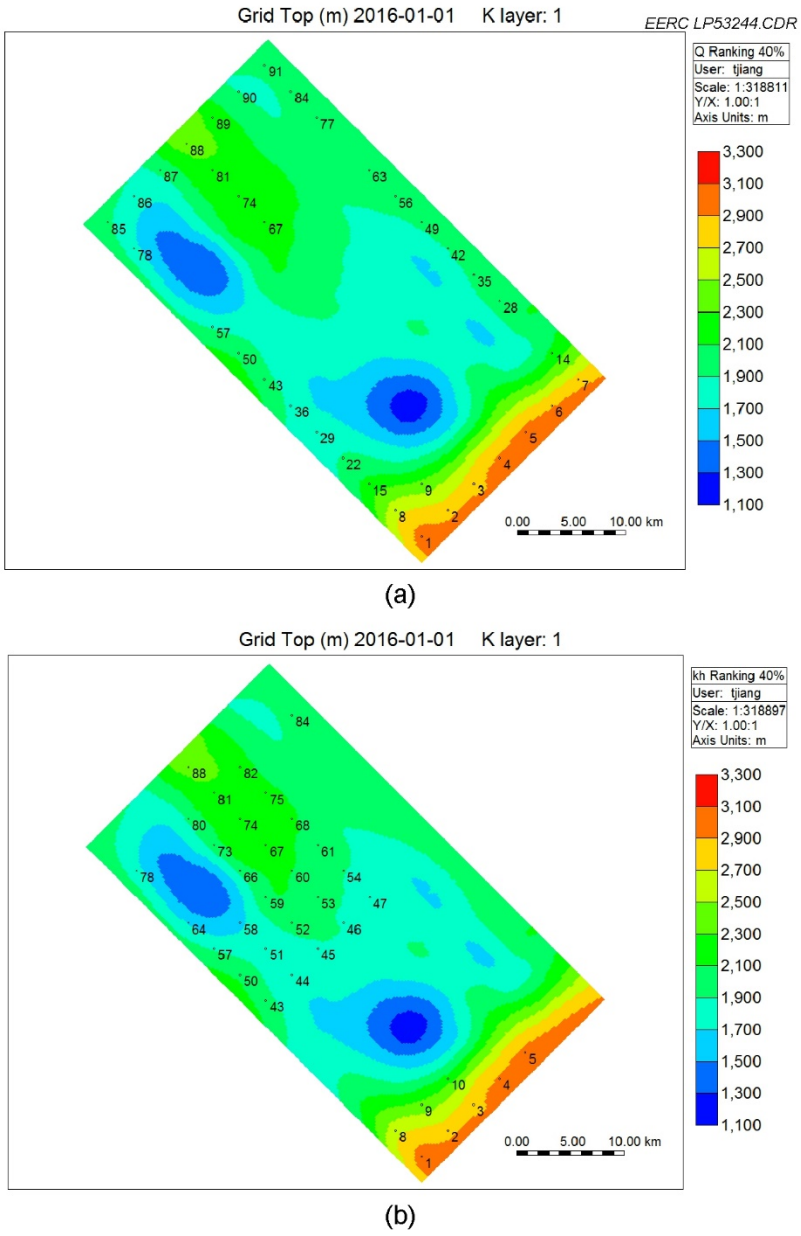

Figure 21. Well placement for different performance-ranking methods (40% of wells): a) cumulative injection ranking and b) average kh ranking.

It should be noted that higher injection rates in the perimeter wells of the well pattern are observed in these simulations and will occur in any open-system model problem. It is not an artifact of the simulation setup; it is in the nature of the problem description. Sectors of the systems in question are here studied at a scale appropriate to large-scale development, and the size of those sectors covers thousands of km^2 and not an entire basin. This problem description is appropriate for CO_2 storage development in new DSF areas where pressure interference from basin boundaries or neighboring competing projects is nil. Thus practical storage capacity and the accompanying efficiency factor determined in this manner (for a 50-year project life in a defined area) are

appropriate until multiple projects in DSF targets begin to severely compete for pore space. Timing for the arrival of such practical development obstacles, and their simulation as closed-boundary problems, likely remains in the intermediate to long-term future.

Structural Setting

Three types of structural settings were also tested in this study. The actual structural setting represents the actual structure of the entire sector model. The efficiency evaluation was focused on the entire sector model, including not only the domal structures present in the model but also the areas between the positive structures. Two other hypothetical structural settings, flat and monocline, were introduced with the same reservoir properties as the actual structural setting model. The reference depth used in these two models was chosen at the depth that was close to the spill point of the structural domes. Compared with the flat setting, the monocline setting has a 1 degree dip angle that extends in the negative x-direction.

The model summary and dynamic efficiency factor results from 50 years of injection are found in Table 12 and Figure 22.

Table 12. Summary of Alternative Simulation Scenarios and Dynamic Efficiency Factor for Each Case: Bunter Model

Case ID	No. of Wells	Boundary	Structure	Mass CO_2 Injected, Mt	Efficiency, %
B-A2 (D2 base)	91	Open	Actual	1770	4.66
B-A4	91	Closed	Actual	426	1.14
B-A7	91	Open	Flat	1613	4.25
B-A8	91	Open	Monocline	1647	4.34

After 50 years of injection, the closed-boundary case (B-A4) has a 1.14% storage efficiency factor, whereas the open-boundary case (B-A2) has a storage efficiency factor of 4.66%. The total CO_2 mass injected for the open-boundary and closed-boundary conditions are 1770 and 426 Mt, respectively.

It should be noted that the efficiency factor achieved in the closed-boundary case, B-4A, is the result of each injection well operating at its maximum allowed bottomhole injection pressure. As previously stated, the BHP limit was calculated based on a pressure gradient of 16.05 kPa/m, approximately 10% lower than the fracture pressure gradient that was assumed in a previous study (Williams and others, 2013). However, this does not consider the long-term pressure distribution throughout the entire reservoir. Buoyancy forces and CO_2 migration to the most shallow point in the reservoir causes the pressure to increase to 1700 kPa above fracture pressure for this simulation case. If this constraint is also considered for the closed-boundary case, then only 366 Mt could be injected, resulting in an efficiency factor of 0.98%. The closed-boundary case is the only simulation case where this level of pressure buildup was observed. All other Bunter cases have open boundaries which allow for more pressure dissipation, mitigating this effect.

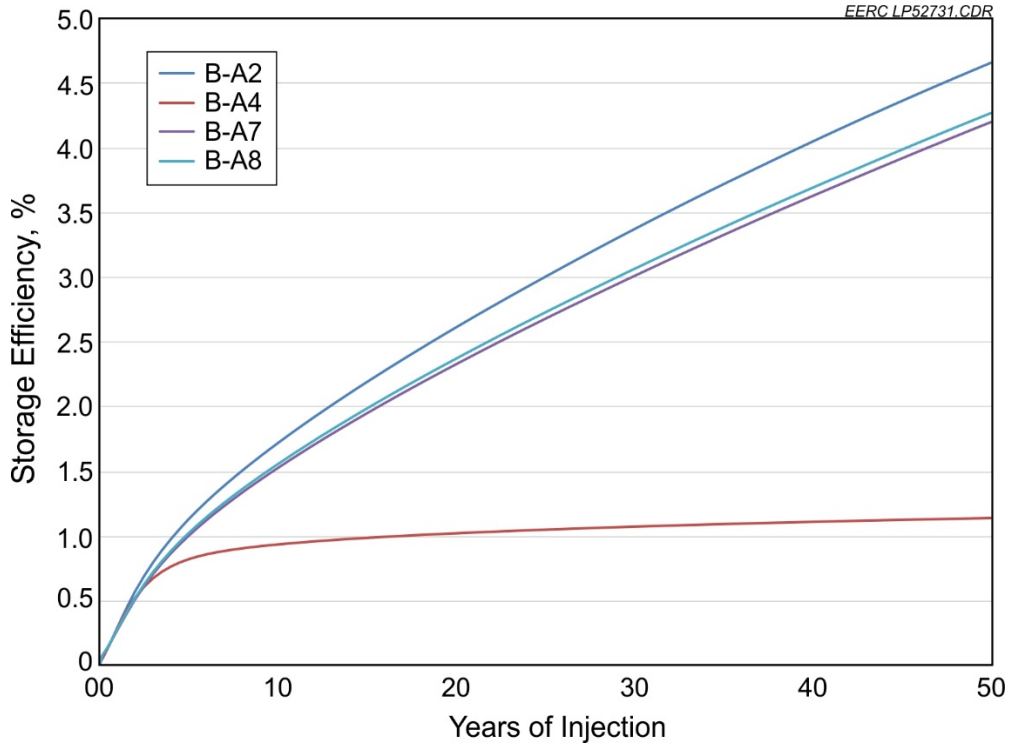

Figure 22. Bunter storage efficiency over time for actual, open, closed, actual with extractor boundary conditions, and flat and monocline structural.

The flat setting, Case B-A7, which is located at depth of 1800 m, has a storage efficiency of 4.25%. The monocline, Case B-A8, has an efficiency factor of 4.34%, slightly higher than the flat-lying case. Both cases have the same average formation depth of 1800 m. The monocline case is better because the tilted formation allows CO_2 flow buoyantly, so a slightly higher efficiency factor could be achieved. Cross sections of CO_2 saturation profiles for these structural settings are shown in Figure 23a, b, and c. In Figure 23c, it should be noted that both water and CO_2 near Well 1 are flowing downdip and away from the interior of the pattern faster than the countering buoyancy force acting on the lower-density CO_2. Thus the CO_2 plume of Well 1 is displaced downdip. Figure 24 is a companion to Figure 23 that shows the pore pressure distribution after 50 years of injection.

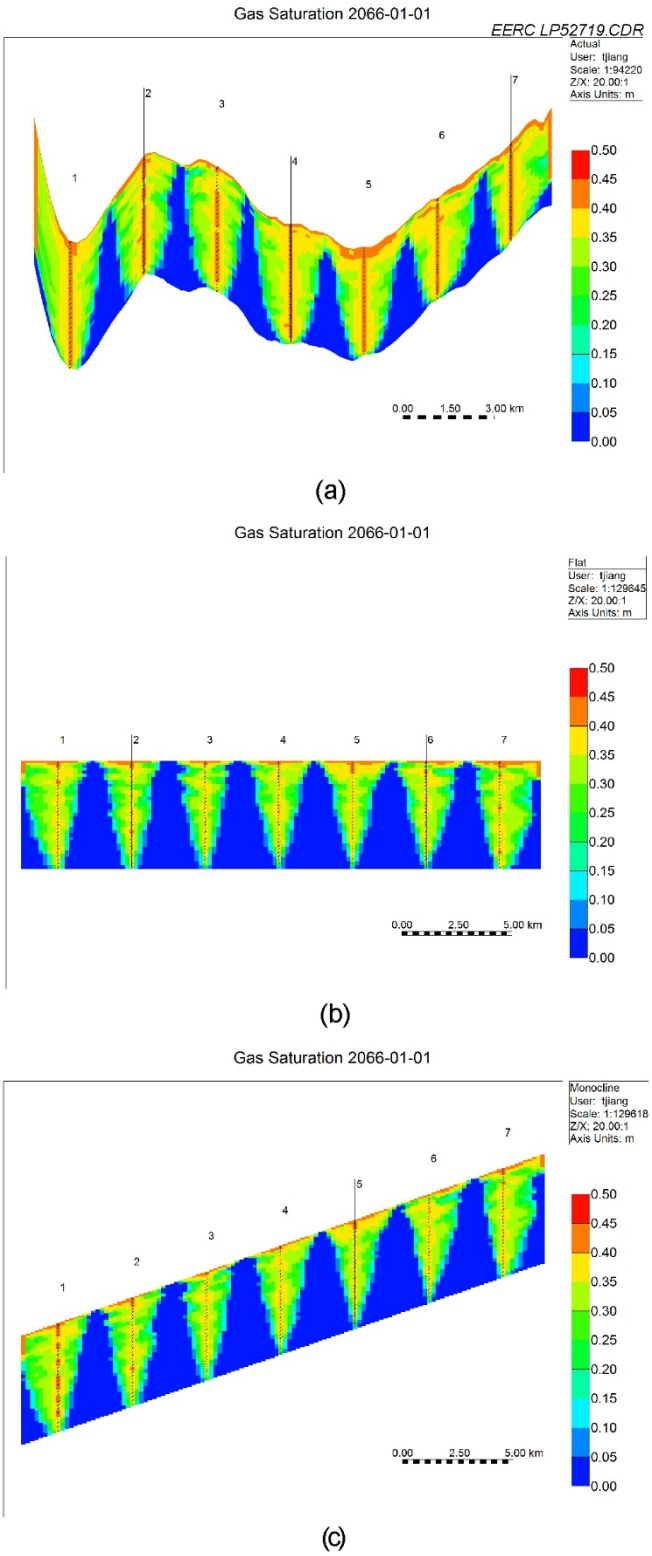

Figure 23. Cross-sectional view of CO_2 saturation profiles at 50 years for a) actual structural, b) flat structural, and c) monocline structural tilt upward.

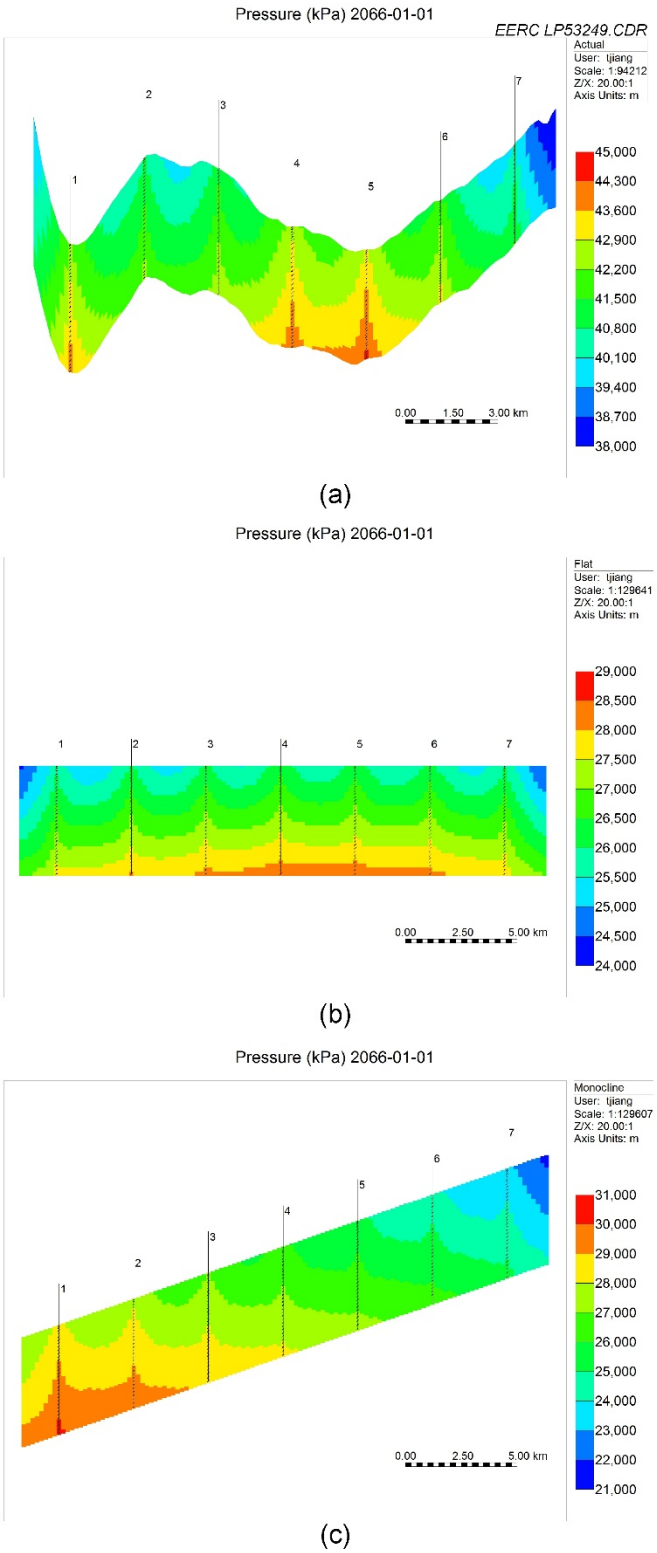

Figure 24. Cross-sectional view of CO_2 pressure profiles at 50 years for a) actual structural, b) flat structural, and c) monocline structural tilt upward.

Three additional cases were built to evaluate the effects of formation depth and dip angle. Cases B-A7-1 and B-A8-1 are constructed with a depth 100 m shallower than that of Cases B-A7 and B-A8. Case B-A8-2 has the same average depth as Case B-A8, but the dip angle is reversed from Case B-A8, as shown in Figure 25. Storage efficiency factors for those cases are shown as Table 13 and Figure 26. Decreasing formation depth by 100 m would reduce storage efficiency for both flat and monocline cases by approximately 0.3%. Reversing the formation dip angle direction changes the storage efficiency by 0.09%. This is mainly an effect of reservoir property heterogeneity.

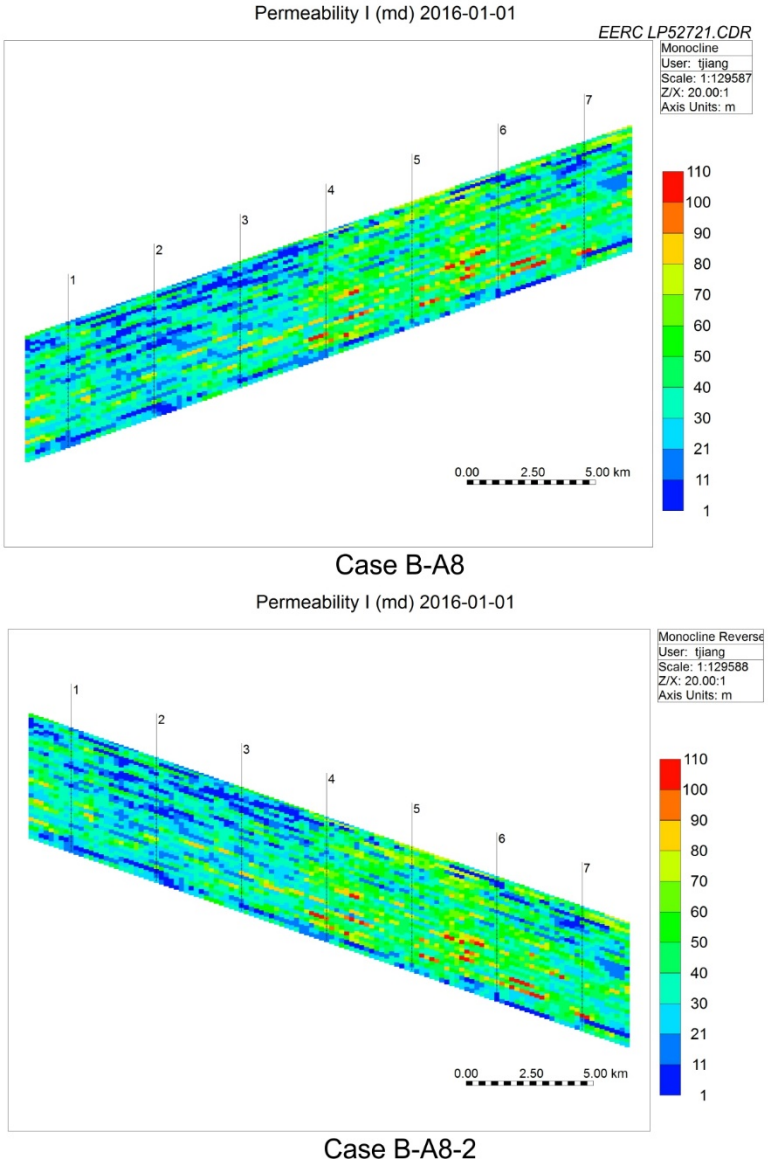

Figure 25. Dip angle difference of Case B-A8 and Case B-A8-2. Case B-A8-2 has reversed dip angle and the same average depth.

Table 13. Summary of Cases for Different Depths and Reversed Dip Angle: Bunter Model

Case ID	Note	Structure	E_{Ed}, %	CO_2 Mass Total, Mt	Mass per Well, Mt
B-A7	Depth at 1800 m	Flat	4.25	1613	18
B-A8	Average depth at 1800 m	Monocline	4.34	1647	18
B-A7-1	100 m shallower	Flat	3.96	1502	17
B-A8-1	100 m shallower in average	Monocline	4.04	1529	17
B-A8-2	Reversed dip angle	Monocline	4.16	1581	17

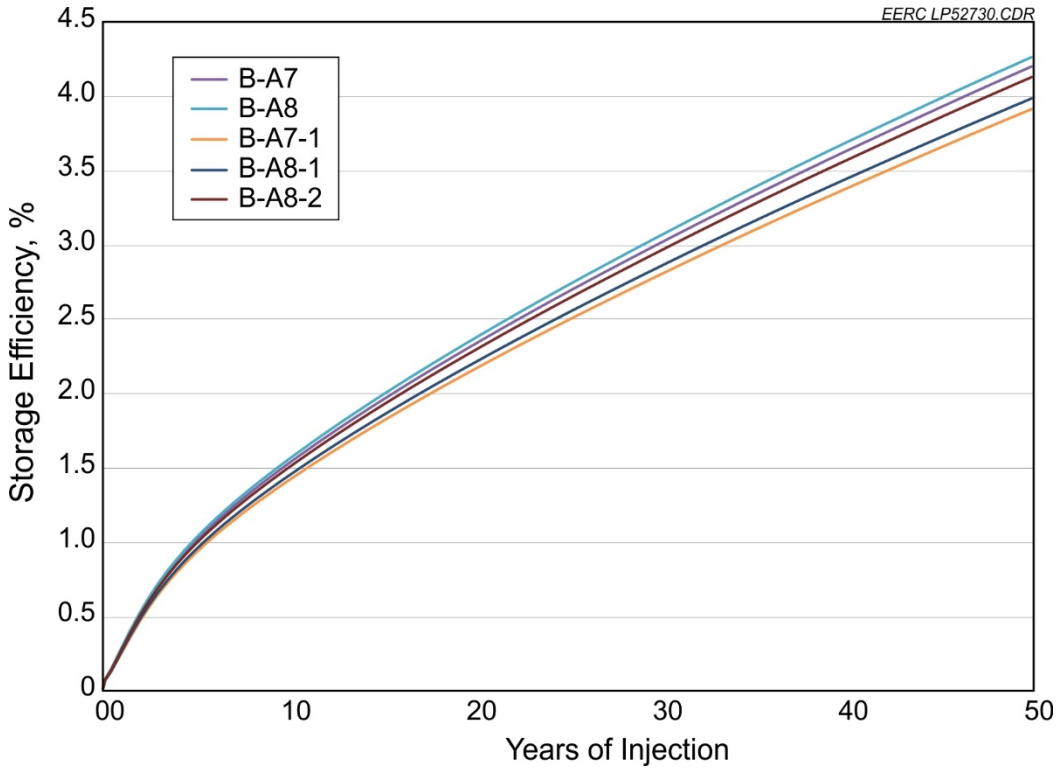

Figure 26. Effects of formation depth and dip angle on flat and monocline structural cases.

Plume Design

Simulation results of cases with different structural settings indicate that structural setting would have significant impact on the storage efficiency because it would affect well injection pressure constraint and fluid flow behavior because of buoyancy effects. Additional cases were proposed to evaluate the concentrated and dispersed well placement for flat, monocline, and trap structural settings. Trap structural setting represents the actual Bunter structure, and rather than evaluate the whole sector model, the wells were located only on the edge of dome structures close to the spill point (dispersed plume) or in the center of dome structures (concentrated plume), shown in Figure 27. The same well placement and configurations were used for the flat and monocline models. Because of the areal size of the dome, the total number of wells used in the model is 15, which is less than 20% of the base case. There are nine wells and six wells for each dome in the model.

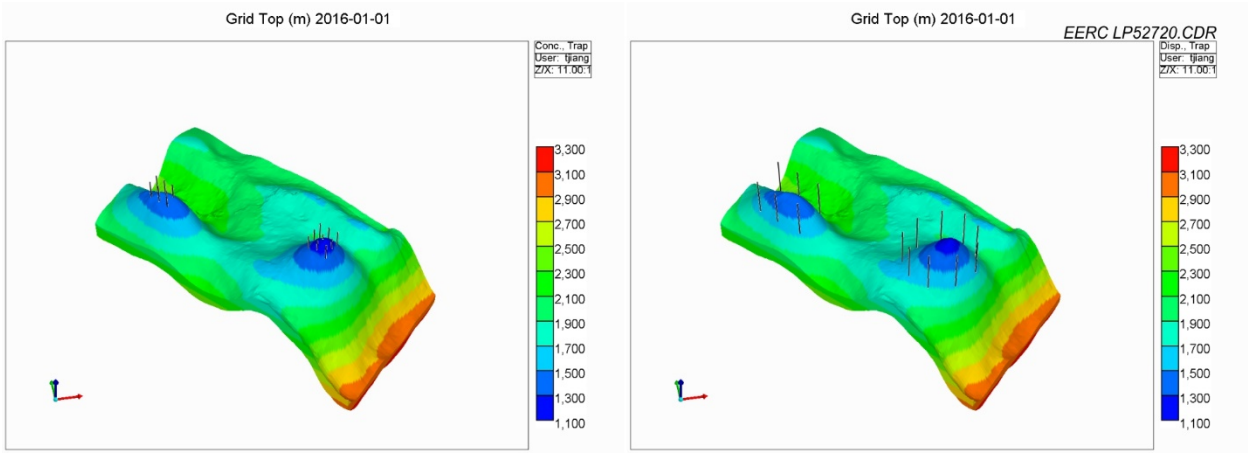

Figure 27. Concentrated well placement (left) and dispersed (right).

The simulation results are shown in Table 14 and Figures 28 and 29. The well placement for the dispersed plume design has overall higher storage efficiency. The more important point is that CO_2 injection per well is the highest of all of the cases discussed. This could be very useful for field development with consideration of cost–benefit.

Table 14. Storage Efficiency, Total CO_2 Mass Injected, and Mass per Well for Plume Design Cases: Bunter Model

Case ID	Structure	Plume Design	Mass CO_2 Injected, Mt	Efficiency, %	Mass per Well, Mt
B-A7D	Flat	Dispersed	818	2.12	55
B-A8D	Monocline	Dispersed	783	2.08	52
B-A9D	Trap	Dispersed	675	1.80	45
B-A10C	Flat	Concentrated	611	1.57	41
B-A11C	Monocline	Concentrated	591	1.56	39
B-A12C	Trap	Concentrated	386	1.02	26

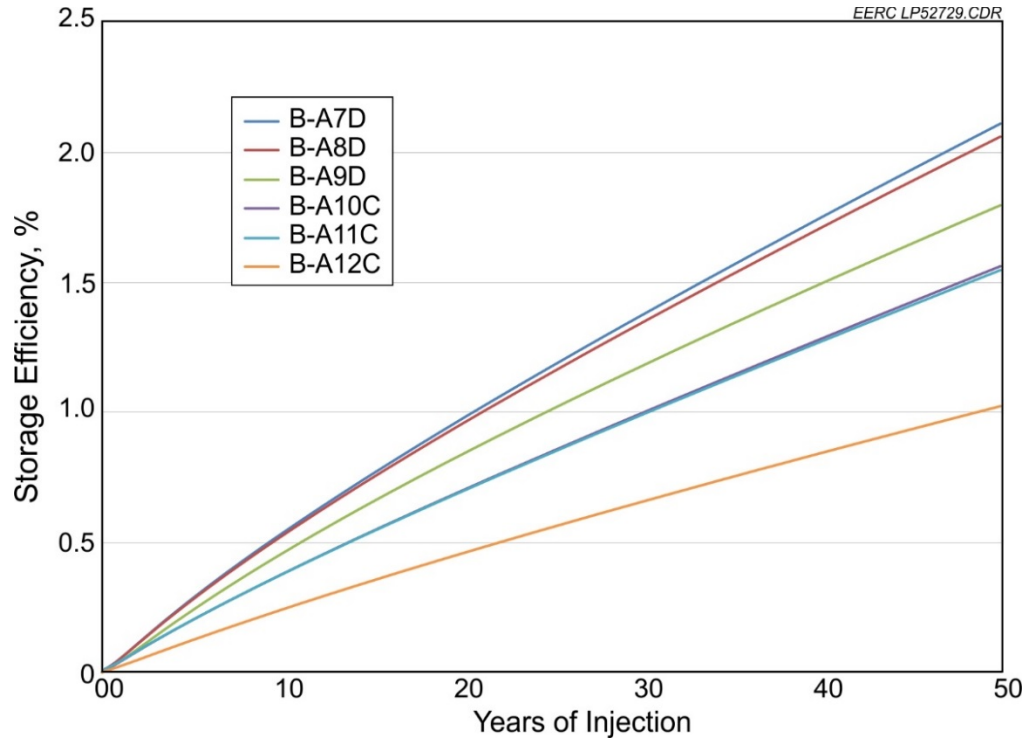

Figure 28. Storage efficiency vs. years of injection.

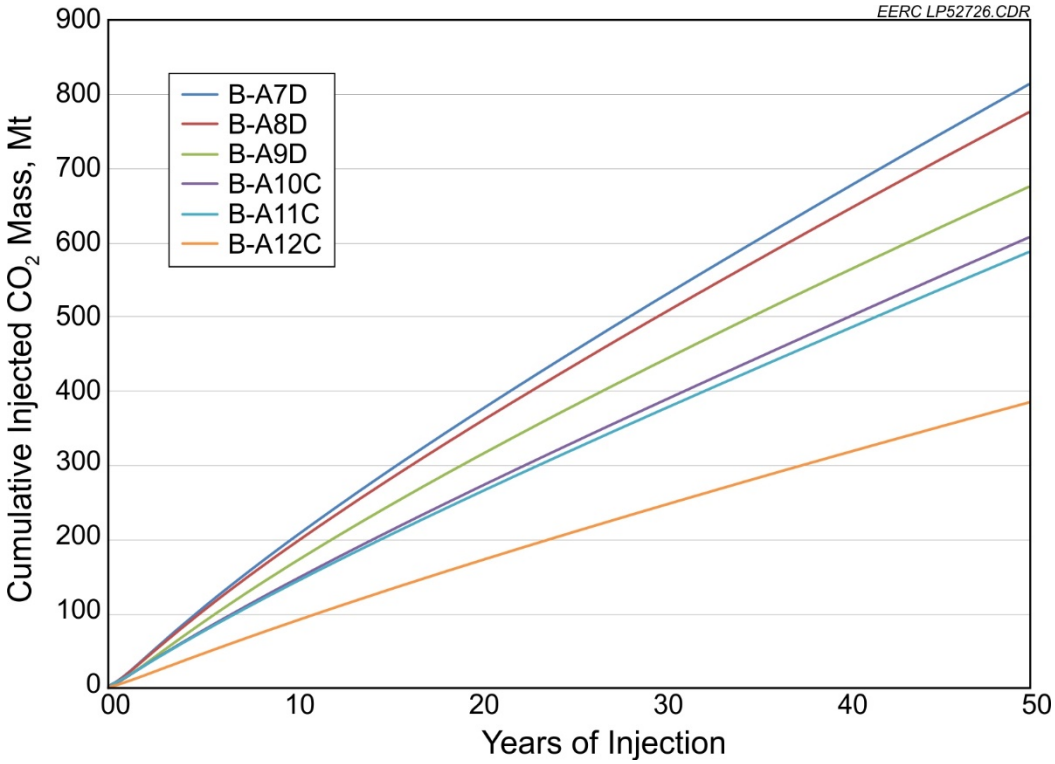

Figure 29. Total CO_2 mass injected vs. years of injection.

Storage Optimization with Water Extraction

As discussed previously, pressure buildup significantly decreases storage efficiency, even in the case of open-boundary conditions. The wells that were located in the middle part of the sector model generally have lower cumulative injection because those wells would reach their injection pressure constraint faster than those located on the outer edge of the model. To verify this effect, two additional cases were built to evaluate potential storage improvement. A total of 24 water extraction wells were introduced to the base case, B-A2, model, as shown in Figure 30a. Extraction well placement for both cases was the same, centrally located between four injection wells to create a five-spot pattern, as shown in Figure 30b. Extraction wells were operated with a minimum bottomhole flowing pressure set equal to their initial pore pressure. Thus each extractor produced at a rate proportional to the amount of pressure increase that it experienced. In the second case, only the bottom half of the formation was perforated in the extraction wells. This reduces the potential for the CO_2 plume to reach extractor well perforations during the course of injection. Removing the top half of the perforation intervals for extractors minimizes early CO_2 breakthrough

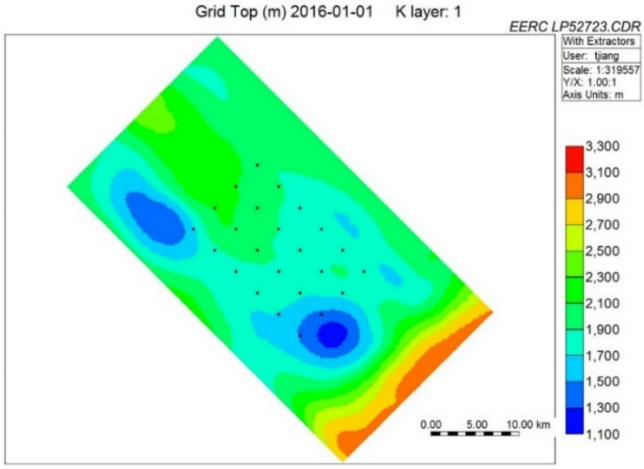

(a) View of Extractors Only

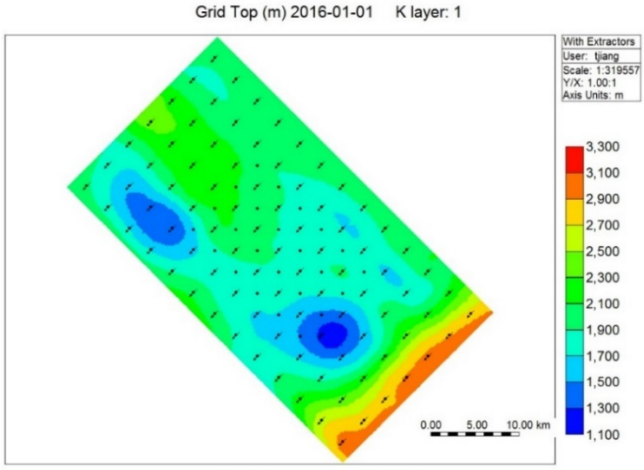

(b) View with All Wells

Figure 30. Schematic view of the model with additional extractors located in the middle of the sector model.

which would result in premature extractor shut-in, thereby allowing more water to be extracted and more CO_2 to be injected.

The results for those two cases are summarized in Table 15. The impact of water extraction was profound, increasing the storage efficiency from 4.66% to 7.39%. Average CO_2 injection per injector would be almost 31 Mt over the course of 50 years of injection. This is more than 10 Mt additional per well than the B-A2 base case. Figure 31 shows the CO_2 plume difference at the locations where the extractors are placed.

Table 15. Comparison of Cases with Different Perforation Intervals for Extraction Wells: Bunter Model

Case ID	No. of Injectors	No. of Extractors	Perforation of Extractors	Mass CO_2 Injected, Mt	Efficiency, %
B-A6	91	24	Full	2710	7.15
B-A6P	91	24	Bottom half	2806	7.39

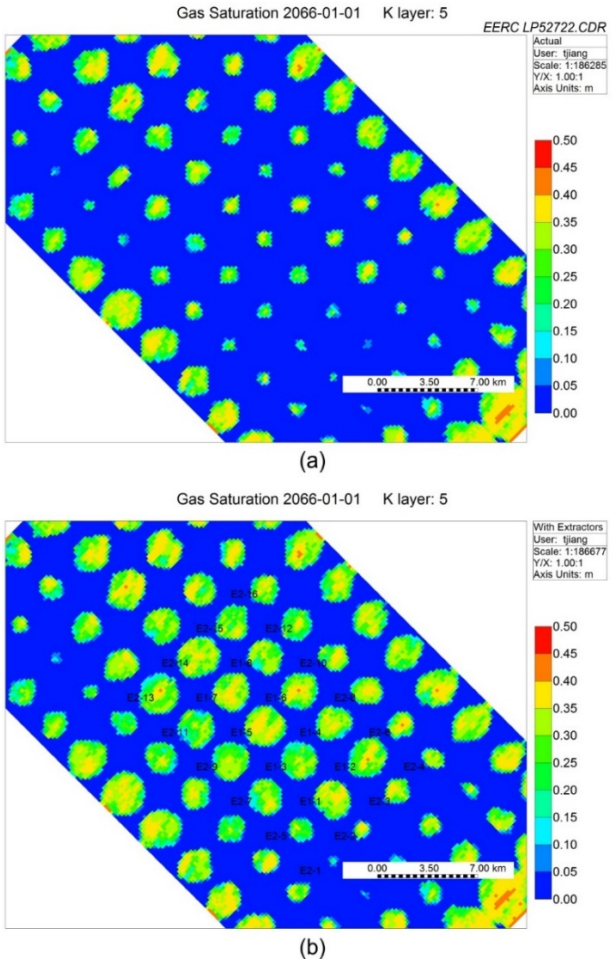

Figure 31. CO_2 plume difference for the cases: a) Case B-A2, no extractor wells and b) Case B-A1 with 24 extractor wells.

SOLUBILITY SENSITIVITY INVESTIGATION

The Stage 1 report noted that results of CO_2 solubility in simulation cases could be affected by simulation grid cell size. To study this, an investigation using the Minnelusa Stage 2 simulation was devised. Ten widely spaced injection well locations were selected to represent a variety of kh values: good, intermediate, and poor. Cases S1 to S4 each use the same well locations but use a different size for the square grid cells, from basin scale (1250 m) to intermediate (417 m), sector (250 m), and fine (139 m) scale. These cell sizes were selected to ensure that well locations maintain the same coordinates for all four cases. All cases retained the 1.5-m average cell thickness. The geologic model was resampled to create these four cases, thus avoiding the complication of upscaling from the static to the dynamic model. The brine condition remains the same as used in the Stage 1 model: 20,000 ppm.

CMG's compositional simulator GEM was used for the investigation. It uses Henry's law to calculate the solubilities of gases in the aqueous phase. A more thorough discussion of all the processes used by CMG to model CO_2 dissolution as a phase equilibrium process is presented in SPE 125848 (Nghiem and others, 2009).

To help create context in describing the magnitude of the grid sensitivity effect, additional cases using the more widely recognized solubility variables of brine salinity and reservoir temperature were also executed to provide points of comparison. Using a slightly modified version of Case S3 (S3-A) as a base for these additional cases, Cases S5 and S6 have higher salinity: 200,000 and 100,000 ppm, respectively. Cases S7 and S8 represent higher reservoir temperature ($\Delta T + 20°C$) and lower reservoir temperature ($\Delta T - 20°C$), respectively.

As suggested by Table 16, injection rate and cumulative injection can vary considerably with grid cell size, even when using the same static model and well locations. Larger grid cells result in lower injection rates when the maximum injection pressure is regulated by the specified pore pressure gradient of 13.6 kPa/m. This is due at least in part to relative permeability effects and a slower buildup of average CO_2 saturation in the larger grid blocks. Therefore, comparison of the quantities of dissolved CO_2 at the same point in time is not representative and not listed in the table. To resolve this, the wells in Cases S1, S2, and S3 were set up with cumulative injection limits determined by the quantities injected in Case S4 for each well at 50 years of injection. Cases S1, S2, and S3 all required more than 50 years to reach their cumulative well injection limits established by Case S4, 50.5, 68, and 83 years, respectively.

Table 16. Minnelusa Simulation Results: Solubility Sensitivity Grid Cell Investigation

Case ID	Cell Width, m	Salinity, ppm	Temperature, °C, av	Injected CO_2, Mt at 50 years	Efficiency, %
S1	1250	20,000	75.7	82.7	1.53
S2	417	20,000	75.7	97.4	1.80
S3	250	20,000	75.7	101.9	1.88
S4	139	20,000	75.7	102.1	1.89

Figure 32 shows the cumulative CO_2 mass dissolved into the reservoir for each gridding (cell size) system during injection. The rate and amount of dissolution varies widely. Case S4 injected 102.1 Mt CO_2 at 50 years, the point in time indicated by the vertical red line crossing the curve for Case S4. The other cases also have red lines marking the point in time when 102.1 Mt is injected. Differences in the quantity of dissolved CO_2 for each case are apparent in Figure 30. In Appendix A, Figures A-10 through A-13 show the free-phase CO_2 plume size for each case at the same cumulative injection. The coarse grid case, S1, shows the plume in less detail than the fine grid case, S4. The S1 plume is actually slightly smaller than for S4 since a greater fraction of the injected CO_2 is dissolved, leaving less observable free-phase CO_2.

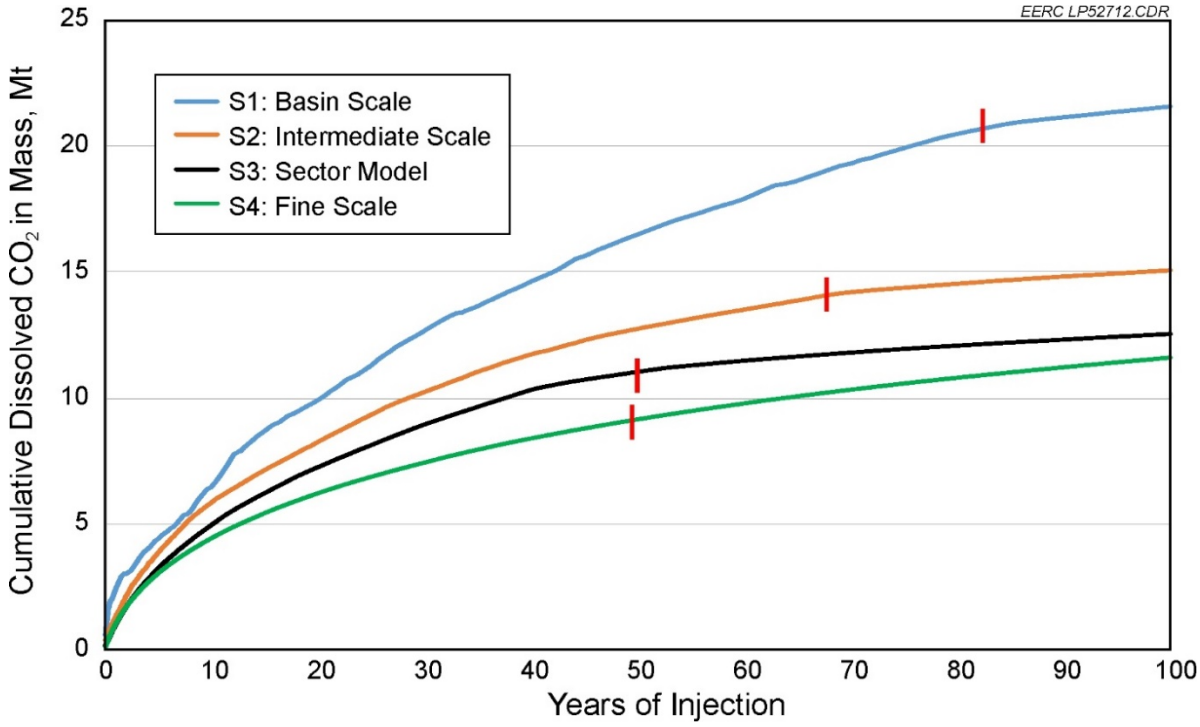

Figure 32. Cumulative dissolved CO_2 mass with time for different gridding systems. Red lines indicate the point in time when 102.1 Mt injection is reached.

Figure 33 describes the change of dissolved CO_2 with the cumulative injected CO_2 of each grid cell size case. From this plot, we can see that the dissolved CO_2 increases with increasing cell size for the same amount of CO_2 injected. At 50 Mt injected, Case S1 has 10.4 Mt dissolved, Case S2 has 6.0 Mt dissolved, Case S3 has 5.1 Mt dissolved, and Case S4 has 4.4 Mt dissolved. This effect is more clearly defined in Figure 34, which shows the dissolved CO_2 change with cell size for the same value of cumulative injection, 50 Mt. The trend line extrapolates to an intercept of 3.74 Mt of dissolved CO_2 at a grid cell dimension of zero. This value may more accurately indicate the quantity of CO_2 that should actually dissolve in the reservoir brine for these model conditions, absent gridding effects. Dissolution of 3.74 Mt for the 50-Mt injection yields 7.48% dissolved CO_2 for these conditions. Note that for the 1250-m grid cell case, 10.4 Mt of dissolved CO_2 is

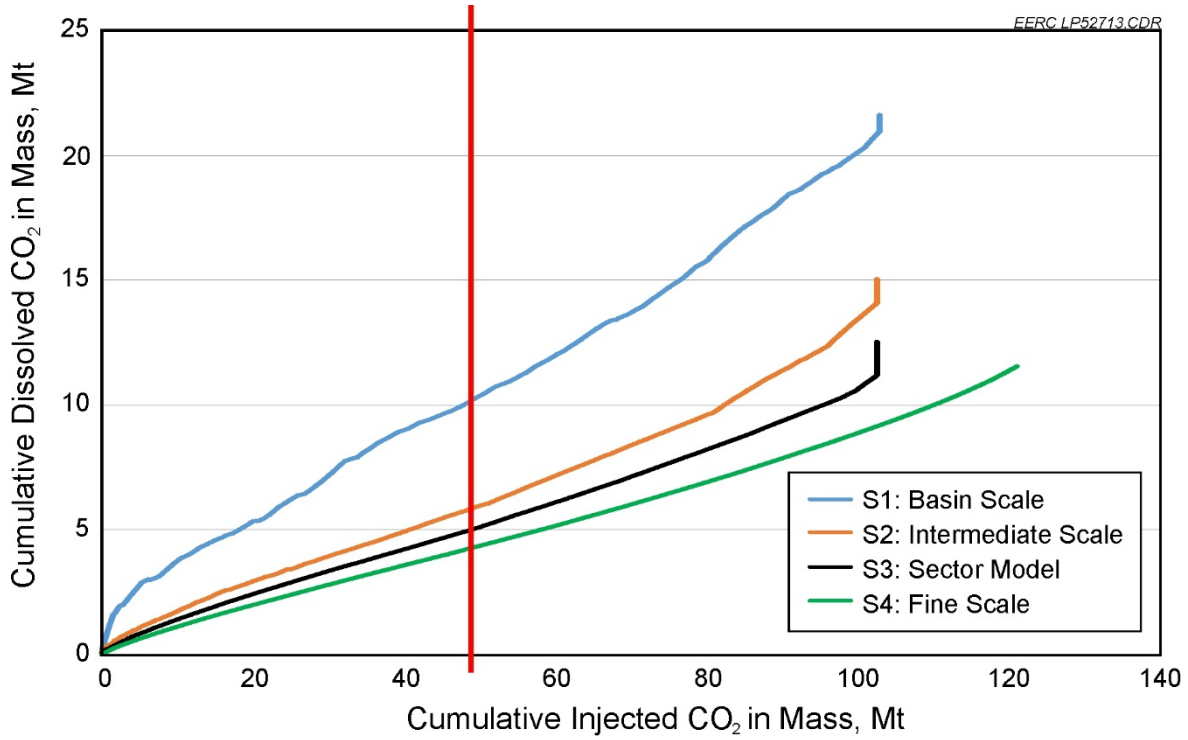

Figure 33. Cumulative dissolved CO_2 vs. cumulative injected CO_2 mass. Vertical line denotes 50 Mt injected.

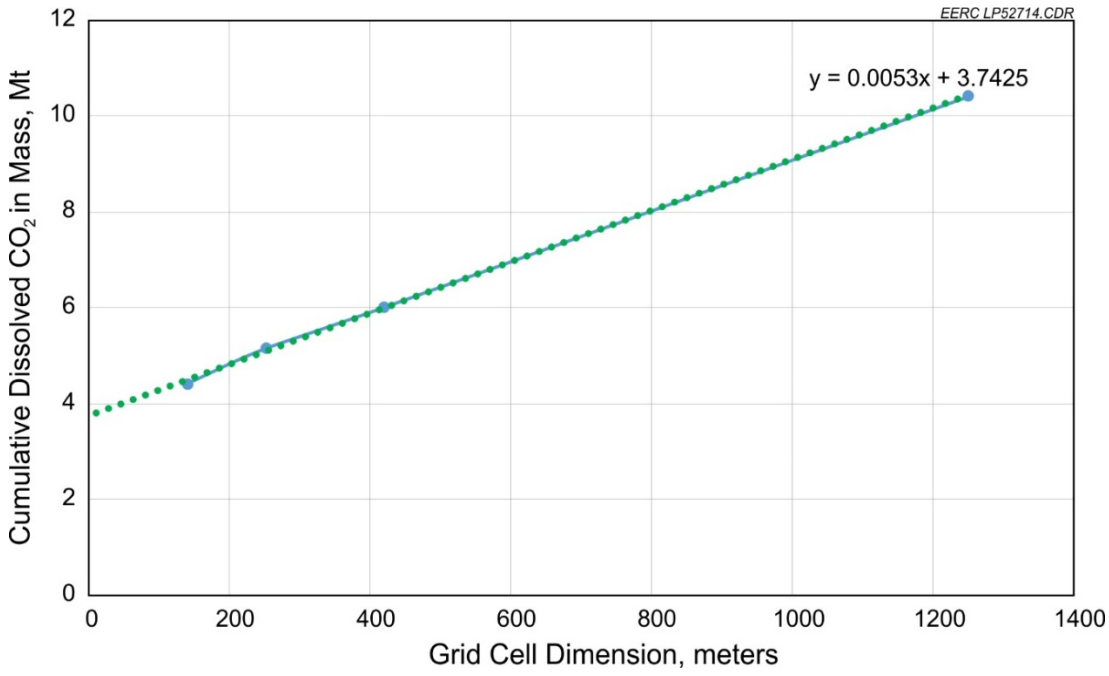

Figure 34. Effect of grid cell size on the simulated dissolved CO_2 in the Minnelusa Formation for 50 Mt injected.

calculated, or 20.74% of the total injected, nearly 3 times the amount suggested as a more accurate estimate. As is true for any extrapolation, it is uncertain if a straight line extrapolation is accurate. However, four data points on a single straight line with a very high regression coefficient is good evidence, particularly when the range of values spans 6.0 Mt (10.4–4.4 Mt) and the extrapolation is only 0.7 Mt (an extrapolation of the data by ~12%). The issue is not about the physical properties of the brine, but more about the quantity of brine contacted by CO_2 in the simulation and numerical dispersion. With coarse grid cells, a much larger quantity of brine is contacted at the perimeter of the plume compared to smaller cells, allowing more CO_2 to become dissolved.

Sensitivity cases to show the effects of changing salinity and temperature on CO_2 dissolution are summarized in Table 17 and shown in Figure 35. These results are independent of gridding effects, but they present an instructive point of comparison to the gridding exercise results. From Figure 35, it is clear that the higher the formation salinity, the lower the quantity of dissolved CO_2 in the formation, and the higher the reservoir temperature, then the higher the quantity of dissolved CO_2 in the formation. However, even with the large range in the salinity cases from 20,000 to 200,000 ppm, the largest variation in the amount of dissolved CO_2 is approximately a factor of 2×. Even in the unlikely case of a very poor estimate of formation salinity, the impact to the calculated dissolved CO_2 quantity is considerably less than grid cell size sensitivity. Variation as a result of formation temperature change is smaller than either grid cell sensitivity or salinity.

The conclusion to be drawn from this solubility sensitivity investigation is that grid cell size is an important parameter when considering CO_2 dissolution and may be more important than more widely recognized variables such as brine salinity or reservoir temperature.

Table 17. Minnelusa Simulation Results: Solubility Sensitivity Comparison Cases

Case ID	Cell Width, m	Salinity, ppm	Temperature, °C, av	Injected CO_2, Mt at 50 years	Efficiency, %
S3-A	250	20,000	75.7	119.0	2.20
S5	250	200,000	75.7	97.8	1.81
S6	250	100,000	75.7	109.0	2.01
S7	250	20,000	95.7	117.7	2.18
S8	250	20,000	55.7	117.9	2.18

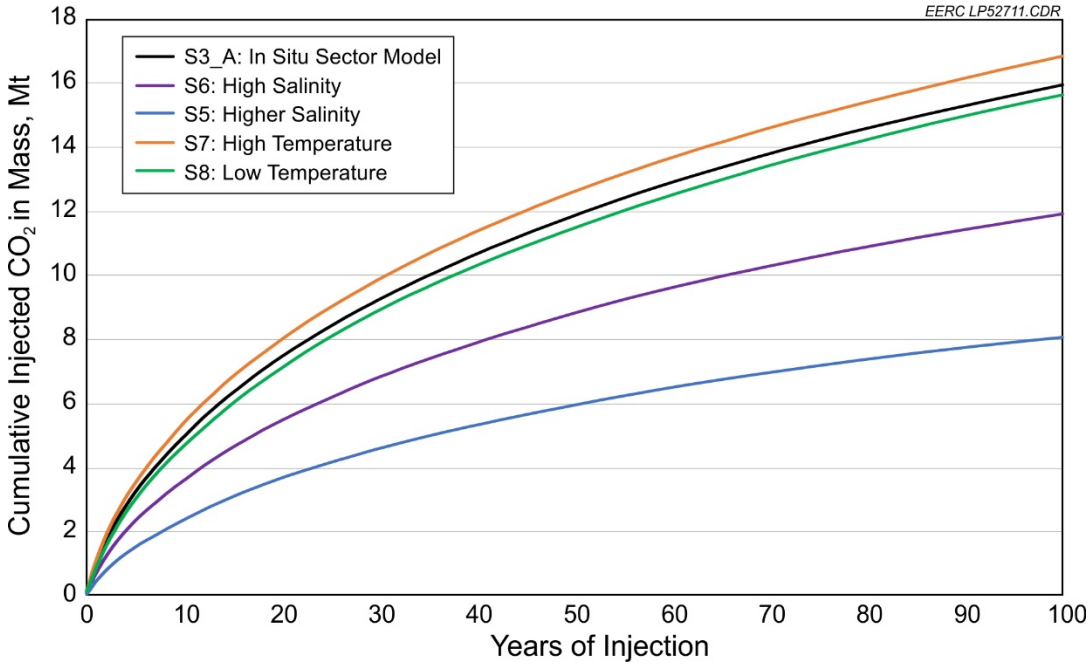

Figure 35. Effect of salinity and temperature on the simulated dissolved CO_2 (it should be noted that S3-A is the same as the S3 case, but without the well injection limits).

COST–BENEFIT ANALYSIS

Objectives

Previous studies performed by the EERC for IEAGHG focused on the maximum storage efficiency achievable in modeled saline formations without optimizing storage on a time frame reasonable for an actual CO_2 storage project or considering the cost of storage (IEA Greenhouse Gas R&D Programme, 2014). This task was focused on addressing the latter, with the goal of gaining an understanding of the relationship between total CO_2 stored in each of the simulated formations and relative cost.

Cost–benefit analysis, in a generic sense, is an evaluation of the financial cost of a project/ activity compared to its overall value (benefit) to the one conducting it. A primary reason for performing this type of analysis is to determine whether the project/activity is worth undertaking or continuing, thereby supporting go/no-go decisions. This analysis can be of particular interest for CO_2 storage projects, which can be long-term (50 or more years of injection plus a postinjection monitoring period), have multiple drivers and stakeholders (e.g., tax incentives, regulatory agencies), and have high capital and operating expenditures (e.g., wells, pipelines).

Because of the time line and budget for this project, a detailed breakdown and estimation of costs for storing CO_2 in each of these real-world formations, the level of which could be used to guide final investment decisions (FIDs), was beyond the scope of this evaluation. Rather, the goal was to establish a relationship between CO_2 stored in the simulation scenarios and high-level cost

estimates. If established, this relationship could provide insight into the configuration that may offer the best CO_2 storage value.

Approach

With the overall goal of this task in mind, the discrete objectives were to 1) determine an approximate generic cost of storing CO_2 in an onshore and offshore DSF for each of the phases of a CO_2 storage project, 2) use those representative costs to develop a cost per tonne estimate for each of the simulated scenarios, and 3) analyze the relationship of storage to cost by plotting cost per tonne vs. total tonnes stored. The following further delineates these objectives:

1. It is generally accepted that a CO_2 storage project in a DSF will undergo several distinct phases throughout its life cycle, e.g., site screening, feasibility, design, construction/ operation, and closure/postclosure. Throughout these phases, costs can be classified into a few primary groups, e.g., preproject costs (exploration, appraisal, and FEED [front-end engineering and design]), surface facilities (including pipelines and offshore platforms), well-drilling costs, and operating costs (including maintenance, monitoring, compliance, and closure). The first objective of this task was to determine approximate costs for as many of the phases and cost categories as possible, relying heavily on publicly available literature and EERC experience with CCS (carbon capture and storage).

2. Using the costs cataloged from literature, the second objective was to develop a total estimated cost of storage in the simulation scenarios for each formation. Combining this number with the total mass of CO_2 stored results in a unit cost per tonne estimate for the simulated scenarios. Because the goal of this study was not to determine the precise cost of storage in the formations modeled, the estimated cost per tonne value for each scenario was normalized to create a unitless cost factor.

3. The third objective was to plot the cost factor with the total tonnes stored to identify a relationship between total storage in each injection scenario to cost. Analysis of these functions would provide insight into the relative CO_2 storage value for money spent and potentially indicate the optimum injection scenario for each of the models.

Challenges

Although straightforward in nature, completing this task was met with several challenges, primarily related to the first objective listed above (i.e., finding publicly available costs for each phase). First, although public documents containing cost information are available, there is a lack of consistency with how costs are categorized. For example, a DOE National Energy Technology Laboratory (NETL) study (U.S. Department of Energy National Energy Technology Laboratory, 2014a) included the drilling and completion of wells within a category labeled “Permitting.” In contrast, Zero Emissions Platform (2011) does not list a permitting category but instead includes costs for permitting and injection well drilling in two separate categories. This example helps illustrate that while often the same costs are considered across studies, it can require significant effort to examine the details of the work, if such details are available, and may inhibit immediate, direct comparison of the results without manipulation (increasing odds for introducing error).

Second, given that CO_2 storage in DSFs as an industry is in the early stages of development, much of the existing literature relates to costs associated with research projects or hypothetical scenarios. Many of the research projects that have injected CO_2 into DSFs have focused on testing new techniques and technologies to determine their applicability/efficacy related to characterization and monitoring of CO_2 storage. While these types of projects are necessary and the costs associated with them can be useful, they may not be indicative of actual costs associated with a commercial CO_2 storage project. For example, monitoring technologies installed at a commercial project will likely be focused on meeting regulatory requirements rather than validating cutting-edge technology. As a result, current research programs may overestimate the cost of storage.

Finally, while the technique of injecting CO_2 in the subsurface has existed for decades, doing so purely for the purpose of storage is a relatively new concept, especially in DSFs. As such, no commercial CO_2 storage projects in a DSF have progressed through all phases (i.e., site screening, feasibility, design, construction/operation, and closure/postclosure). This results in a paucity of cost data based on real-world experience, especially for the latter development phases.

Method

In spite of the above challenges, much work has been published on cost analyses for the transport and geologic storage of CO_2 (e.g., Rubin and others, 2015; U.S. Department of Energy National Energy Technology Laboratory, 2014b; Energy Technologies Institute, 2016b; Eccles and others, 2012; Anderson, 2016; Zero Emissions Platform, 2011), with the results of two recent efforts forming the primary basis for conducting the remainder of this task. The first is a cost model developed by DOE NETL (U.S. Department of Energy National Energy Technology Laboratory, 2014c). This spreadsheet-based model was created to help estimate the cost of storing CO_2 in onshore DSFs within the United States and is capable of incorporating costs from the major phases of a storage project (defined in the cost model as regional evaluation, characterization, permitting, operations, postinjection site care, and site closure) (U.S. Department of Energy National Energy Technology Laboratory, 2014a). The second effort is a study commissioned by ETI to investigate the development of CO_2 storage potential in the United Kingdom (Energy Technologies Institute, 2016b). Part of ETI's work, presented across multiple detailed reports, was the development of cost estimates for transporting and storing CO_2 at five potential offshore storage sites. The ETI case studies include three DSFs, including a portion of the Bunter Sandstone Formation, and two depleted gas fields. The ETI study displays costs in terms of traditional business expense categories (e.g., capital expenditures [CAPEX], operating expenditures [OPEX]) for the life cycle of a hypothetical CO_2 storage scenario in each of the three DSFs.

The NETL cost model was used to complete the Minnelusa portion of this task, while the detailed cost estimates reported by ETI were used for the Bunter, with some important notes:

- The NETL cost model calculates well costs based on U.S. Environmental Protection Agency (EPA) Class VI specifications, which at this time are only relevant in the United States and do not account for certain costs important to offshore storage (e.g., platform construction and operation). For these reasons, this model was not deemed appropriate for use with the Bunter Sandstone Formation scenarios in this project.

- While different assumptions are used in the NETL cost model and ETI study and the cost categories are not identically presented in each, there are many overlaps, particularly between the primary CAPEX and OPEX for a CO_2 storage project.

- A thorough vetting of the validity of the NETL cost model and economic analysis presented by ETI is beyond the scope of this work. The analysis, results, and conclusions presented in this section are not intended to prove or disprove these previous studies. While some inaccuracies may exist in costs associated with specific items, in light of the overall goal of this project (identifying a relationship between CO_2 storage in the simulations and relative cost), they are believed to be sufficient.

- The NETL cost model gives results in terms of 2008 U.S. dollars, while the ETI study is presented in 2015 pounds sterling. To allow easier comparison of results, all costs were converted to 2015 U.S. dollars.

Analysis

Minnelusa Formation

The NETL CO_2 storage cost model has default settings for each of its many adjustable variables. Since the ultimate objective of this task was to determine a relationship between CO_2 stored and cost from a broad standpoint, rather than a rigorous calculation of the exact cost of storage in these formations, many of the default settings were deemed sufficient for this purpose. The variables that were adjusted to make the cost model scenario most similar to the project's Minnelusa simulations included the following:

- Selection of the Minnelusa Formation
- Number and depth of wells
- 3-D seismic area and collection interval

Selection of Formation

The NETL cost model comes preloaded with detailed geologic and petrophysical data for over 220 formations existing in the United States, one of which is the Minnelusa. As the Minnelusa Formation is regionally expansive and covers the entire Powder River Basin, multiple entries for this formation exist in the cost model. The Wyoming portion of the Minnelusa Formation (designated Minnelusa1 in the cost model) was selected and the properties compared to the geologic model used in the simulations. Comparing basic parameters of the Minnelusa1 in the cost model to the geologic model used in the simulations indicated a close match, supporting the use of the default geologic settings in the cost model.

Number and Depth of Wells

As discussed in the simulation section of this report, seven cases with varying well numbers were developed for the Minnelusa Formation to investigate the effect of well number on CO_2 storage. These simulation cases were used as the basis for the cost–benefit assessment of the Minnelusa Formation simulations. The base case (or 100% case) for these simulations used

576 wells, with the other six cases having a percentage of this number (Table 18). The wells were ranked based upon their permeability thickness (kh), and the best wells were sequentially selected to use for injection in each scenario. The well depth in the cost model was set to 8700 feet (2652 m) to match the average depth in the Minnelusa simulation efforts.

Table 18. Minnelusa Formation Simulation Cases Used for the Cost–Benefit Assessment

Case ID	No. of Wells	% of 576 Wells	Total CO_2 Stored, Mt	Mt per Well
D7	58	10	123.5	2.13
D6	115	20	172.2	1.50
D5	230	40	195.5	.85
D4	345	60	222.4	.64
D3	460	80	235.8	.51
D2	576	100	242	.42
D1	684	120	253	.37

3-D Seismic Area and Collection Interval

The default schedule of collecting 3-D seismic surveys in the cost model is one survey every 5 years during CO_2 injection and a defined postinjection monitoring period. The total cost of each survey increases based on the estimated rate of expansion of the CO_2 plume (performed in the model using an analytical method). The CO_2 plume area is dependent on the total mass of CO_2 injected over the course of operations and constrained by a maximum project area set by the user. To make the cost estimate better align with the Minnelusa Formation simulation scenarios in this project, the project area was changed to 1500 km^2 (579 mi^2) to approximate the area of the simulation model. The collection interval of 3-D seismic was changed from every 5 years during operations and site closure to a more conservative schedule indicative of a commercial operation scenario: one baseline survey during site characterization, two during the 50 years of injection operations, and two during postinjection monitoring.

Other Assumptions

Although not included in the NETL cost model, a 100-mile (~161-km) pipeline was assumed for each simulation scenario. The pipeline cost was based on a NETL study presenting a unit cost of $93,250 per inch-mile (Agalliu and others, 2016). Although each simulation case had a different annual injection rate, the same length and diameter of pipe were estimated to be sufficient for all the scenarios based on data from Carbon Management GIS (2008). An injection period of 50 years, followed by 50 years of postinjection monitoring, was assumed. All dollar amounts in the NETL cost model are in 2008 U.S. dollars. All costs (pipeline and NETL cost model) were converted to 2015 U.S. dollars to allow comparison between the case studies. Cost conversions were performed with the following cumulative inflation rates (US Inflation, 2017):

- Pipeline: −1.2% deflation (2016 U.S. dollars to 2015)
- Cost model totals: 10.1% inflation (2008 U.S. dollars to 2015)

Bunter Sandstone Formation

The economic assessment conducted by ETI for the appraisal of CO_2 storage in the Bunter Closure 36 (Energy Technologies Institute, 2016a,b) served as the basis for the cost estimates of the Bunter Sandstone simulations in this project. In addition to the reports available on ETI's Web site, a spreadsheet was graciously provided by ETI that contained additional granularity in the costs used in its assessment. The ETI analysis separated costs into four main categories (pre-FID, post-FID [CAPEX], OPEX, and abandonment expenditures [ABEX]) with four subcategories in each (i.e., Transportation, Facilities, Wells, and Other). Some of the key assumptions used by ETI in its analysis included the following:

- 40 years of CO_2 injection
- 160-km pipeline
- Ten injection wells drilled
- 280 Mt of total injection

In an effort to remain consistent with ETI's work and minimize potential error, these categories and subcategories were left unchanged; however, total costs were recalculated based on variables used in the simulation scenarios (e.g., number of wells) to make total costs applicable to this project. Table 19 shows the subcategory unit costs used for all categories to perform the calculations. The assumptions used to develop costs for the current study are discussed below.

Table 19. Unit Costs Developed Based on the ETI Work

Subcategory	Unit Cost
Transportation	£/km
Wells	£/well
Facilities	£/platform
Other	CAPEX Other was converted to £/well; all remaining Other costs were fixed.

Number of Wells

Similar to the Minnelusa Formation model, the wells in the simulations were ranked based on their kh, and the top wells were sequentially chosen for each case (Table 20). The ETI study assumed a steel jacket platform capable of handling 12 wells. The same assumption was used in this study, and the number of platforms required for each scenario was calculated accordingly.

The original simulation scenarios created for the Bunter Formation well sensitivity analysis were designed based on a percentage of the number of wells in the base case scenario, rather than making efficient use of platforms. For example, assuming 12 wells per platform, the 80% (73 wells) case results in a need for seven platforms. With six platforms accommodating 72 wells, the seventh platform in this scenario had only one well, but the cost to build and operate the platform was included in the cost analysis. The authors felt that this was not representative of how an operator would design an offshore storage project in reality. As a result, an alternate set of

Table 20. Bunter Formation Simulation Cases Used for the Cost–Benefit Assessment

Case ID	No. of Wells	% of 91 Wells	Total CO_2 Stored, Mt	Mt per Well
B-D7	9	10	830	92.22
B-D6	18	20	1113	61.83
B-D5	36	40	1390	38.61
B-D4	55	60	1598	29.05
B-D3	73	80	1706	23.37
B-D2	91	100	1770	19.45

simulation cases was developed to maximize the use of the number of platforms by increasing the number of wells in increments of 12 (Table 21). The results of both the original and alternate simulation scenarios are discussed below. Because of time constraints, the alternate simulation scenarios were not performed numerically using the simulation software. Instead, the total CO_2 stored for each case was calculated analytically based on storage efficiencies observed in the original simulation scenarios.

Table 21. Bunter Formation Alternate Scenarios Optimized for 12 Wells per Platform

No. of Wells	% of 91 Wells	Total CO_2 Stored, Mt	Mt per Well
12	13	965	80.40
24	26	1220	50.83
36	40	1390	38.61
48	53	1530	31.88
60	63	1635	27.25
72	79	1700	23.61
84	92	1750	20.83
96	105	1774	18.48

Other Assumptions

To be consistent with the simulation scenarios conducted for this project, an injection period of 50 years was assumed. A postinjection monitoring period of 20 years was assumed by ETI in its estimation of costs. This assumption was left unchanged.

A 160-km pipeline was assumed. In order to account for additional pipeline needed between platforms for simulation cases over 12 wells, an additional 5 km of pipeline was added per platform.

Costs used from the ETI study were in 2015 pounds sterling and were converted to 2015 U.S. dollars to allow comparison between the case studies. A conversion factor of 1.57 $/£ was used (Xe, 2017).

Results

Using the data from the NETL cost model (Minnelusa) and the ETI study (Bunter), a total estimated transport and storage cost was calculated for each of the well sensitivity simulation cases and converted to 2015 U.S. dollars. Each total cost was divided by the total tonnes of CO_2 stored in that case to create a unit cost (i.e., $/tonne). These data points were normalized to create a unitless cost factor and plotted vs. total tonnes stored and the number of wells for each simulation case. The resulting plots (subsequently presented) show a trend relating the cost of transport and storage in these simulation cases to total quantity of CO_2 stored. Because of the site-specific nature of geologic CO_2 storage and the volatility of service and materials pricing, this work is not intended to represent the actual cost of storing CO_2 in these formations or to replace rigorous site-specific appraisals to support go/no-go or investment decisions. Rather, this work is meant to provide a high-level relationship between cost of transport and storage and total CO_2 storage to approximate relative CO_2 storage value.

Minnelusa Formation

The results of the cost analysis for the Minnelusa Formation simulations are shown in Figure 36.

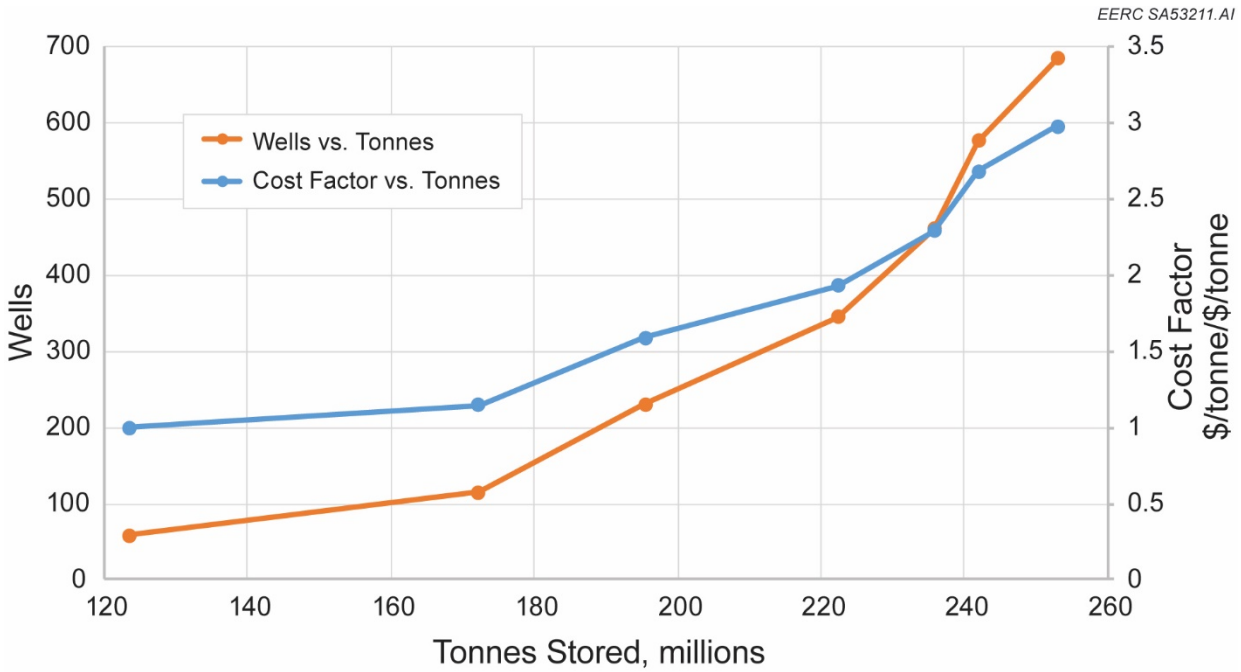

Figure 36. Relationship between number of wells, total tonnes stored, and cost factor for the Minnelusa simulation scenarios.

Several key observations can be made by looking at Figure 36. First, a large increase in total storage occurs between the 10% (58 wells) and 20% (115 wells) cases, followed by smaller gains in storage until the 60% (345 wells) case. Increasing the number of wells beyond the 60% (345 wells) case results in only incremental gains, even after adding nearly six times the number of wells from the 20% (115 wells) case to the 120% (684 wells) case. This result is not surprising and has been observed elsewhere (IEA Greenhouse Gas R&D Programme, 2014; Gorecki and others, 2015) and indicates that a relatively small number of wells inject the majority of the total CO_2 stored. As mentioned in the discussion of simulation results, this is due not only to variations in geology (kh) in the Minnelusa Formation model, but also to increasing pressure interference effects between wells as the attempt is made to increase the practical storage efficiency factor within the defined area. With a lower number of injection wells, the best geologic locations are selected, and interference effects are reduced. Adding wells beyond the 20% case results in an increasing number of wells injecting into a poorer-quality reservoir, in turn lowering injectivity, resulting in less additional storage per additional well. Second, the increase in cost factor observed between the 10% (58 wells) and 20% (115 wells) cases is quite small compared to the increase in total CO_2 stored (14% increase in cost factor, compared to 39% increase in CO_2 stored). This small increase is due to the large gain in total CO_2 stored for the 20% (115 wells) case, which offsets the increased total cost for this case because of drilling, completing, and operating the additional wells. Third, between the 20% (115 wells) and 60% (345 wells) cases, the cost factor increases moderately but increases dramatically for cases over 60% (345 wells).

The primary drivers in cost factor for the Minnelusa Formation simulations include number of wells and frequency and extent of 3-D seismic surveys. The relationship between number of wells and cost factor is straightforward: the higher the number of wells, the higher the overall cost. Well number initially affects CAPEX but also influences OPEX (higher maintenance and well-based monitoring total costs).

The NETL cost model estimates the cost of a 3-D seismic survey using a unit cost of dollars per square mile, with the area based on an analytical calculation of the extent of the CO_2 plume (dependent on total mass of CO_2 injected) at the time of the survey, limited by a user-defined maximum project area (U.S. Department of Energy National Energy Technology Laboratory, 2014a). The implication of this is that the simulation cases with more wells have a larger injected mass of CO_2, resulting in a bigger CO_2 plume (and related seismic survey area), in turn leading to a higher cost for seismic surveys.

Bunter Formation

The results of the cost analysis for the Bunter Formation simulations are shown in Figure 37.

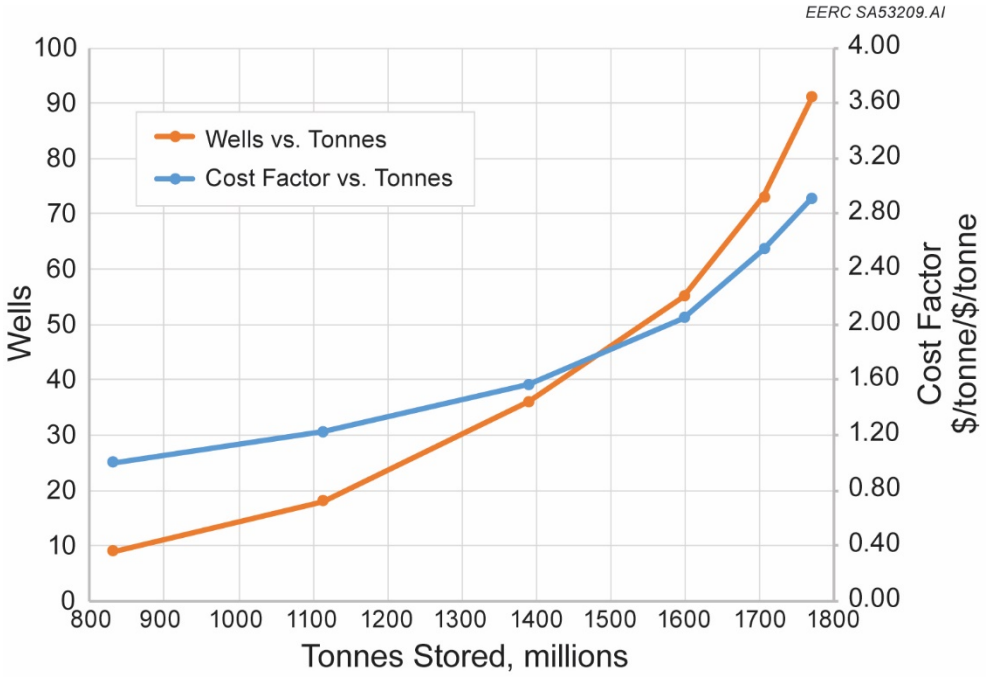

Figure 37. Relationship between number of wells, total tonnes stored, and cost factor for the Bunter Formation simulation scenarios.

Original Scenarios

Similar to the results of the Minnelusa Formation analysis, a large increase in total CO_2 stored is observed between the 10% (nine wells) and 20% (18 wells) cases. However, while the Minnelusa Formation simulations saw smaller gains in total CO_2 stored beyond the 20% case, the Bunter Sandstone simulations showed nearly the same increase in total CO_2 stored between the 20% (18 wells) and 40% (36 wells) cases. This is likely due to the more consistently distributed "good" geologic properties of the Bunter model compared to the Minnelusa Formation model (which contains more geologic variability). For cases above 40% (36 wells), there is a steady decline in the gains of total CO_2 stored in spite of increasing the number of wells. These reduced gains in total CO_2 stored are likely due to pressure interference between wells in the Bunter simulations. The cost factor shown in Figure 37 increases consistently with the increase in total CO_2 stored between the 10% (nine wells), 20% (18 wells), and 40% (36 wells) cases but increases more dramatically for cases after 40% (36 wells), with less benefit of CO_2 stored.

Alternate Scenarios

Like the results of the original Bunter simulation scenarios, the largest increase in total CO_2 stored compared to the increase in cost factor occurs between the first two scenarios, here the 13% (12 wells) and 26% (24 wells) cases (Figure 38). The next three cases (40% [36 wells], 53% [48 wells], and 60% [60 wells]) see moderate increases in storage compared to the increase in cost factor. Beyond the 63% (60 wells) case, the gains in total CO_2 stored are much smaller compared

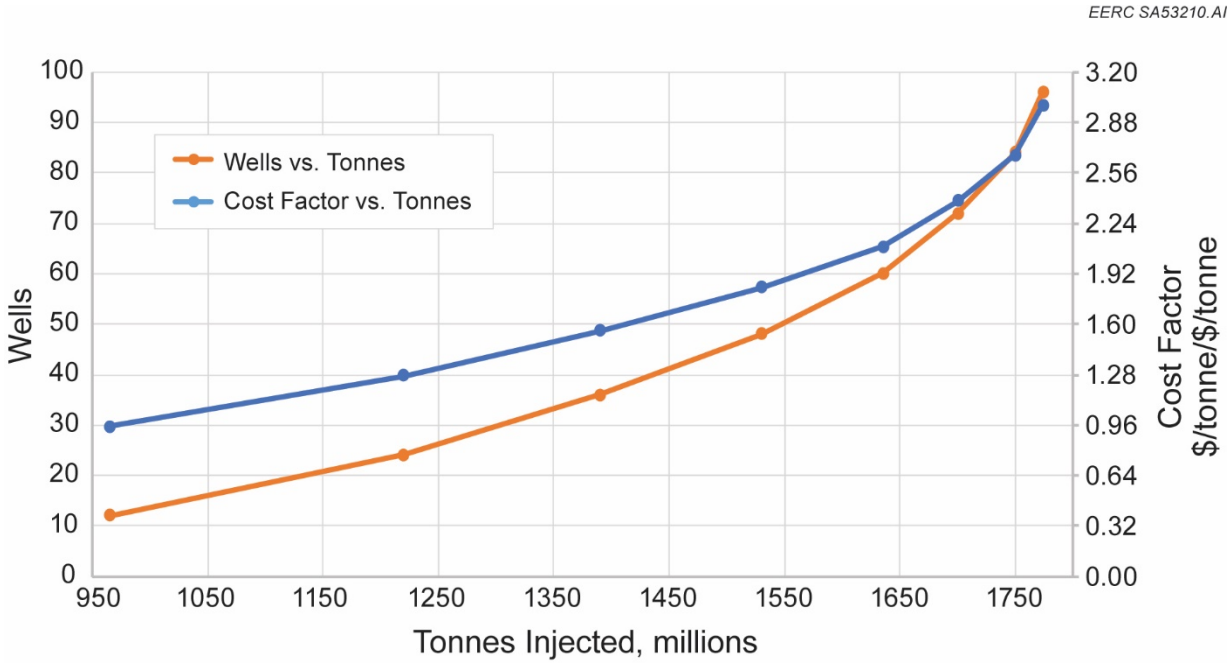

Figure 38. Relationship between number of wells, total tonnes stored, and cost factor for the alternate Bunter Formation scenarios. Data points are created in increments of 12 wells to better optimize platform-based well groupings.

to the increasing cost factor. One thing to note about the results shown in Figure 38 is that there are consistent moderate gains in CO_2 stored through the 63% (60 wells) case, compared to moderate gains through the 40% (36 wells) case in the original scenarios. This is likely due to the cost savings realized from increased efficiency in using platforms in the alternate scenarios.

The primary influences in the cost factors for the Bunter simulations include well number, number of platforms, and operational costs (primarily wells and facilities). Similar to the Minnelusa, as the total number of wells increases, both CAPEX and OPEX increase. Being offshore, the wells for the Bunter Sandstone require platform facilities for their operation. The platforms contribute significantly to the CAPEX and OPEX, with the number of platforms required for each simulation scenario directly related to the total number of wells.

Comparison of Minnelusa and Bunter

In order to make a direct comparison between the two modeled case studies, two additional figures are shown: 1) the cost factors for both the Minnelusa and Bunter scenarios plotted vs. total tonnes of stored CO_2 (Figure 39) and 2) the total number of wells plotted vs. total tonnes of stored CO_2 (Figure 40). In contrast to the separate analyses in Figures 36–38 where each scenario's $/tonne value was normalized to the lowest $/tonne value for that model, the data points presented in Figure 39 were all normalized to the same value (i.e., the lowest well number scenario for the Bunter). This was done to allow a direct comparison for all data points, and accounts for the difference in cost factors for the Minnelusa between Figures 36 and 37. The alternate Bunter scenarios shown in Table 21 were not included in the case study comparison below.

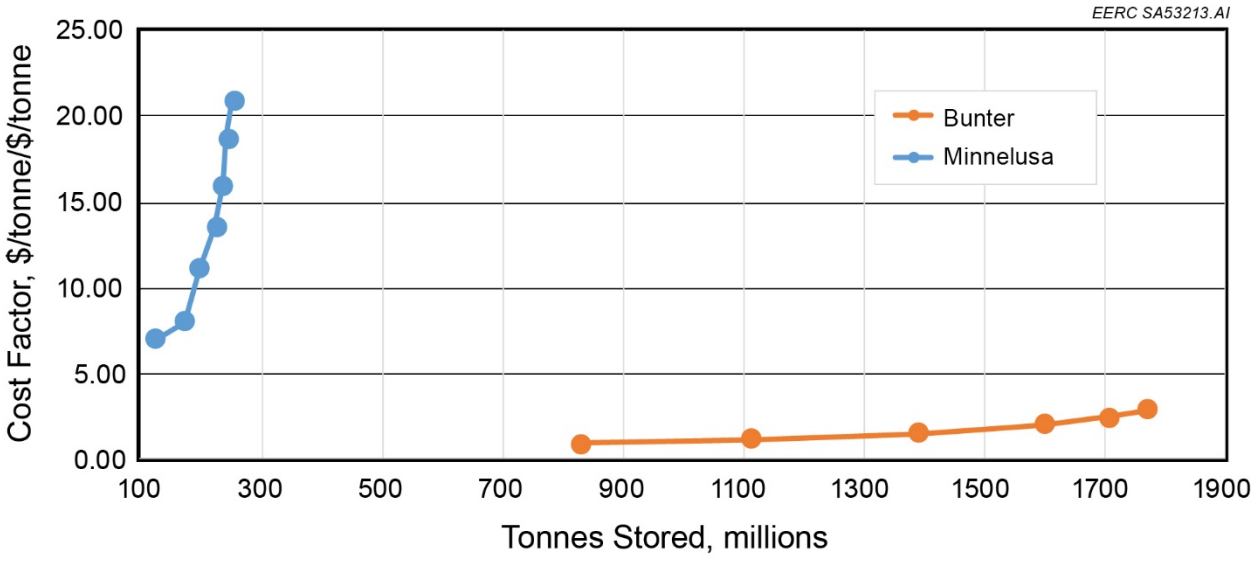

Figure 39. Comparison of the relationship between cost factor and total tonnes stored in both Minnelusa and original Bunter Formation scenarios.

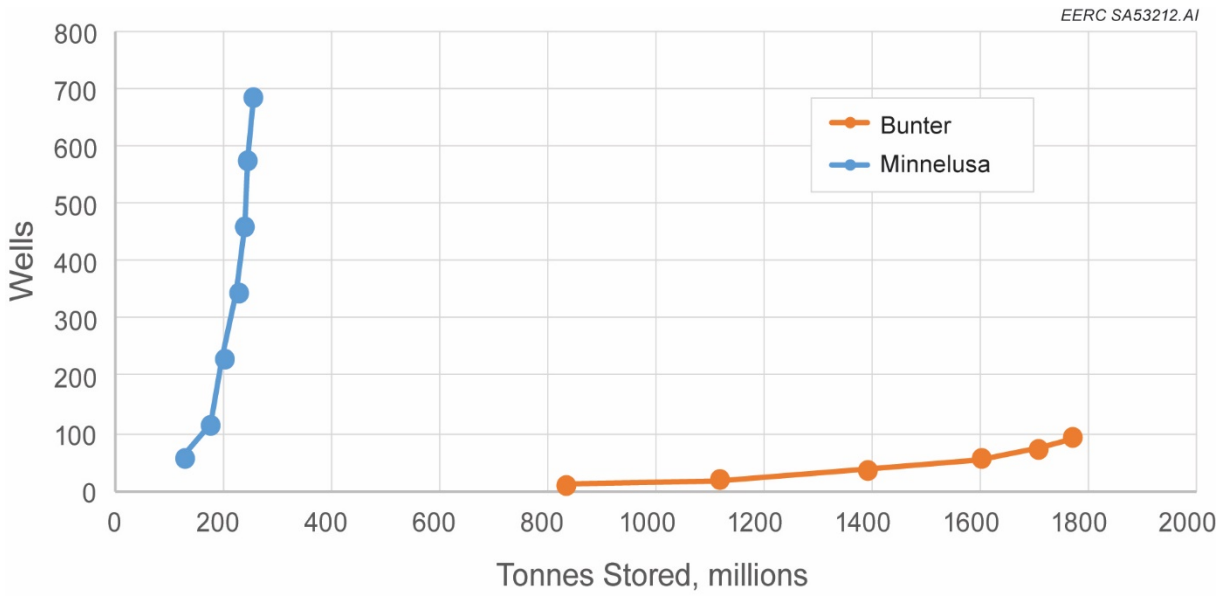

Figure 40. Comparison of the relationship between total number of wells plotted and total tonnes stored in both Minnelusa and original Bunter Formation scenarios.

It is clear from examining Figures 36, 38, and 39 that the Bunter was able to store significantly more CO_2 over 50 years for a similar overall cost factor, thus representing a better relative value for CO_2 stored in this particular study. There are two driving factors behind this result. The first is made apparent by examining Figure 40—the Minnelusa model required a substantially higher number of wells to inject the CO_2. In fact, the highest number of wells (684) in the Minnelusa simulation cases used in the cost–benefit analysis was seven times the highest number of wells (91) in the Bunter. It is worth noting that even with significantly more wells in the Minnelusa scenarios, the cost factor is quite similar to the Bunter (Figures 36 and 37), pointing to the high unit cost of the wells and offshore platforms needed in the Bunter. The second factor is related to the geologic properties in the models. As previously mentioned, the Bunter model had more consistently "good" rock properties, while the Minnelusa contained higher variability, resulting in a lower per well injectivity (Tables 18 and 20). It should be noted that these results are true for this specific study and may not be indicative of actual/future storage projects in these formations.

Conclusions

The analyses of both the Minnelusa and Bunter Sandstone (original scenario) simulations conducted for this project indicate that the 20% well case is the configuration offering the best CO_2 storage value and most favorable cost–benefit ratio. For the Minnelusa Formation simulations, the 20% case (115 wells) was able to inject and store 68% of the maximum stored amount of CO_2. This case also offered the smallest increase in cost compared to the gain in additional total CO_2 storage of all of the examined Minnelusa Formation simulations. Similarly, for the Bunter Sandstone simulations, the 20% case (18 wells) was able to inject 63% of the maximum stored amount of CO_2 and had the smallest increase in cost factor (between 10% to 20%) compared to the increase between all the other cases, showing the best value in increased storage between the Bunter cases. For the alternate Bunter simulations, the 26% (24 wells) case saw the most gain in total CO_2 stored compared to the increase in cost factor, indicating this case also offered the best CO_2 storage value. Comparing the Minnelusa and original Bunter scenarios indicates that the Bunter Formation represents the best relative value for CO_2 stored in this study. In both of the modeled formations, the number of wells was the primary variable in determining cost factor, a conclusion supported by other work (Eccles and others, 2012). It should be noted that in a real-world application, a project developer would likely experience a cost savings related to drilling and completing a large number of wells as well as building multiple platforms at one time. This cost savings would likely be realized in a few ways. First, if a project operator were able to buy a large number of supplies such as casing, tubulars, wellheads, and other tangible cost items all at once, a price break may be realized by "buying in bulk." Second, in a similar way, signing a multiwell contract with the same drilling company may result in a discount over the life of the drilling program. Finally, the "learning curve" of drilling successive wells in the same location can lead to an increase in efficiency over time as the drilling company becomes quicker, thereby reducing cost (Hellstrom, 2010; Ikoku, 1978). A similar learning curve would likely be realized in building multiple platforms offshore. Unfortunately, the authors were not able to account for these economies of scale; however, design work for specific projects should attempt to consider these aspects.

RESULTS AND DISCUSSION

Comparison to the Stage 1 Report

The Stage 1 report used dynamic modeling techniques to determine if injection scenarios can be created to achieve storage efficiency factors that approach volumetric estimates for basin-scale applications. The open-boundary Minnelusa Formation and the closed-boundary Qingshankou–Yaojia System were the object areas for this work.

The Stage 2 report used dynamic modeling techniques to determine storage efficiency factors that can be achieved with injection scenarios representing realistic potential commercial-scale applications. The open-boundary Minnelusa Formation and the open-boundary Bunter Formation were the object areas for this work.

The differences in efficiency factors achieved in these works are considerable, but understandable, in the context of the most important premises applied to each:

1) The area of investigation is much smaller in the Stage 2 work.
2) The well density is much higher in the Stage 2 work.
3) The length of simulated time is much shorter in the Stage 2 work.

The variation of these premises and their impact on simulated results are summarized in Table 22. This brings into better focus the differences between calculations of basin-scale storage resource efficiency estimates and calculations that attempt to account for some of the limitations imposed by commercial execution that lead toward estimations of practical storage efficiency. It

Table 22. Comparison of Stage 1 and Stage 2 Simulation Premises and Results

Model, Report Stage	Boundary Condition	Model Area, km^2	No. of Injection wells	Well Density, km^2/well	E, % at 50 years	E, % at 2000 years
Minnelusa, 1	Open	58,632	238–820	246.3–71.5	0.6–1.7	3.4–17.7
Q–Y, 1	Closed	45,995	216–827	212.9–55.6	0.3–0.4	0.5–0.7
Minnelusa, 2	Open	1250	115–576	10.9–2.2	3.4–4.8	N/A[1]
Bunter, 2	Open	1056	18–91	58.7–11.6	2.9–4.7	N/A

[1] Not applicable.

is clear from these studies that commercial execution in a localized area will not achieve volumetric efficiency estimates for that area. It is also clear that after 50 years of injection, local storage efficiency from commercial project execution can be much higher than that surmised from basin-scale evaluations. The efficiency achieved by the Stage 2 cost–benefit optimal solutions for the Minnelusa and Bunter, 3.4 % and 2.9%, respectively, are much higher than any 50-year result from the Stage 1 study.

Well density and pressure interference among wells play a very important role in the variation of these efficiency estimates. Commercial execution of large-scale injection projects in the foreseeable future will demand a higher well density than wide-spaced pattern drilling of an entire

basin, as was simulated in the Stage 1 work. In either scenario, wells will normally be operated at or near their maximum injection pressure capability. Thus the higher well density scenario, as simulated in the Stage 2 work, will create greater pressure interference among injectors. This condition is a well-known phenomenon, but it has significant negative impact on injection capacity and storage efficiency, even in open-boundary reservoir systems such as the Minnelusa and Bunter. It plays a large role, perhaps a dominant role, in limiting storage efficiency in the Stage 2 study areas.

The degree to which pressure interference, and the corresponding difficulty of displacing formation water away from the injectors, suppresses storage efficiency is subject to many variables; however, in high-density pattern well development scenarios, such as those simulated in this study, the project scale and number of wells are critical. The greater the number of wells in the drilling pattern, the greater the fraction of wells that are located in the interior of the pattern where interference is greatest. This effectively creates a closed-boundary condition for a large percentage of the wells, in turn limiting their performance. Thus the larger the pattern, the more the efficiency factor will trend toward a closed-boundary system. For this reason, smaller projects and early projects in a given area will enjoy higher storage efficiency than larger projects or those starting later in a developed area. For commercial development, considerable engineering optimization efforts should be expected, which may yield significantly higher storage efficiencies than those presented in this report.

Other Results and Discussion Items

1) This work has benefited from adopting previous work to build upon. In particular, it was efficient to use geologic models that were previously developed and willingly shared with the project. This was also true of existing economic analysis models. Where reasonably practical, this practice should be repeated for future work.

2) Practical storage capacity estimates have been developed for both the Minnelusa and Bunter Sandstone study areas. These estimates are a function of the assumed project constraints, and results could be different if different assumptions are used. For example, the simulation results suggest that a 50-year injection period for the Minnelusa was adequate to approach the practical storage efficiency factor, while the Bunter would likely benefit from a longer injection period; therefore, the Bunter capacity and efficiency factor results may be slightly conservative. However, for both study areas, the so-called 20% cases, D6 and B-D6 for Minnelusa and Bunter, respectively, are considered to have achieved the best value in terms of cost per tonne stored. These cases achieved similar 3.39% and 2.94% practical storage efficiencies, respectively. The maximum drilling, or the so-called 100% cases, D2 and B-D2, also achieved similar efficiency factors after 50 years of injection. These results and the relative cost factors for these cases are given in Table 23.

Table 23. Minnelusa and Bunter Selected Simulation and Economic Results

Case ID	Well No.	Percentage of Wells	Mass CO_2 Injected, Mt	Efficiency, %	Relative Cost Factor
Minn. D2	576	100	242	4.75	18.7
Minn. D6	115	20	172	3.39	8.0
Bunt. B-D2	91	100	1770	4.66	2.9
Bunt. B-D6	18	20	1113	2.94	1.2

3) The use of extractor wells was not considered an integral part of this study, but extraction cases were run for both study areas, and they achieved superior storage capacity and efficiency, even for open-boundary conditions.

4) Low levels of structural dip, 1 or 2 degrees, had marginally better storage efficiency than flat-lying geology. Fifty years may not have been a long enough simulation time to fully account for updip fluid migration. Updip migration may affect storage efficiency for the following reasons:
   a) Reservoir heterogeneity may contribute because of the CO_2 encountering formation rock with differing properties.
   b) Compared to flat-lying strata, the plume will migrate to areas farther away from the high pressure at the injection wells and toward areas of lower pore pressure.
   c) Migration encourages CO_2 to come into greater contact with formation brine, increasing dissolution. Brine density increases but brine volume change is relatively small, thus reducing pore pressure and allowing additional injection volume.

5) Bunter sensitivity cases executed to examine the effect of reservoir depth showed significant improvement in injectivity at greater depth, assuming no change in reservoir porosity and permeability. Maximum allowed injection pressure is typically defined as a function of formation-fracturing pressure. Since fracture gradient is generally higher than pore pressure gradient, the pressure difference between the two increases with depth. This means that higher injection pressure can be applied to deeper wells, thereby increasing injection rate. This effect can be significant and may more than justify the added cost of drilling to deeper areas of a target reservoir. In the case of the Bunter, significant advantage may be realized by drilling in structurally low areas, below 1800 m depth, compared to drilling on structural highs at 1300 m depth. This improved performance may be partially offset by CO_2 migration into updip areas, creating excessive pressure in these areas. Caution should be used to ensure that formation fracture pressure is not exceeded. Additional comment is included in the next discussion point.

6) Concentrated vs. dispersed plume development scenarios gave differing results between the Minnelusa and Bunter. Minnelusa sensitivities used selected areas of relatively high kh as the basis for concentrating 58 well locations, and cumulative injection was better than for the dispersed development scenario using the 58 highest individually kh-ranked wells. For the Bunter, structural closure was the basis for concentrating well locations, and that case was significantly poorer than the more dispersed well pattern that placed wells deeper, near the

structure spill points. The concentrated wells at the top of the structures have comparatively lower injection pressure limits and were also obliged to displace formation water downdip into higher-pressure areas. The dispersed, downdip pattern allowed higher injection pressure and did not have an equivalent limitation on displacement, allowing higher injection.

7) The sensitivity investigation of CO_2 solubility as a function of grid cell dimensions yielded a wide variation in the amount of dissolved CO_2. Figure 34 shows a very good relationship between cell dimension and the amount of dissolved CO_2, with the large cell simulation calculating much higher values. For the given Minnelusa conditions, extrapolation of the data trend to an infinitely small cell size resulted in 3.74 Mt dissolved for 50 Mt injected, 7.48%, whereas a simulation using 1250-m × 1250-m grid cells calculated 10.37 Mt dissolved for 50 Mt injected, 20.74%. All cases used ten injection wells positioned at the same locations.

8) Cost data for carbon storage projects are limited because of the low number of actual projects for which data have been reported. Also, most reported projects are small-scale and have a considerable research component attached to the work; therefore, unit costs are higher and appear not representative of commercial applications. Reported cost data are not always easily comparable because costs may be classified or grouped differently or described using different terminology.

9) Cost evaluation methods are available and useful. However, they are inevitably of limited flexibility, and no common method was found suitable to both onshore and offshore conditions.

10) The analyses of both the Minnelusa and Bunter Sandstone (original scenario) simulations conducted for this project indicate that the 20% well case is the configuration offering the best CO_2 storage value and most favorable cost–benefit ratio.

11) For Minnelusa Formation simulations, the 20% case (115 wells) was able to inject and store 68% of the maximum stored amount of CO_2. This case also offered the smallest increase in cost compared to the gain in additional total CO_2 storage of all of the examined Minnelusa Formation simulations.

12) Similarly, for the Bunter Sandstone simulations, the 20% case (18 wells) was able to inject 63% of the maximum stored amount of CO_2 and had the smallest increase in cost factor (between 10% to 20%) compared to the increase between all the other cases, showing the best value in increased storage between the Bunter cases. For the alternate Bunter simulations, the 26% (24 wells) case saw the most gain in total CO_2 stored compared to the increase in cost factor, indicating this case also offered the best CO_2 storage value.

13) In both of the modeled formations in this study, the number of wells was the primary variable in determining cost factor, a conclusion supported by other work (Eccles and others, 2012). It should be noted that in a real-world application, a project developer would likely experience a cost savings related to drilling and completing a large number of wells (from purchasing supplies, such as casing, tubing, etc., in bulk), as well as building multiple platforms, at one time. The authors were not able to account for this economy of scale in these results.

FUTURE WORK

The results of the study demonstrate that practical storage efficiency factors can be determined for a given set of premises. However, efficiency results can be as variable as the premises used to define the case of interest. Several areas of investigation may be appropriate to lead toward a standardized understanding of practical storage efficiency:

1) Storage efficiency evaluations have largely been a function of geoscience and numerical simulation. Practical efficiency is much more affected by what an evaluation team deems to be reasonable operating and cost assumptions for the project at hand, including the following:

   - Length of injection period
   - Area available for evaluation
   - Injection rate
   - Injection pattern
   - Use of extraction wells
   - Total cost
   - Cost per tonne stored

   Obviously, a wide range of potential values is possible for all of these premises. Without a common understanding of what reasonable premises are to project evaluators, it will be a challenge to establish a common understanding of practical storage efficiency. Therefore, an area of useful future work may be to establish a framework of expectations for effective storage premises. The list above represents only a starting point for consideration.

2) During the Bunter investigation of this study, it was apparent that the most successful injector locations, in terms of cumulative injection, were located in the structurally deeper portions of the study area. Excluding wells located near the perimeter of the simulated area, none of the top 25% of injector locations was on either of the two prominent structural closures. This performance justifies closer investigation into the pros and cons of placing injectors in off-structure locations, particularly in an offshore setting where wide-scale pattern drilling may not be feasible. If upon closer scrutiny this observation is sustained, better development planning and improved practical storage efficiency may be achievable.

3) It is apparent in both study areas that large-scale development using pattern drilling techniques, even if favorable areas are targeted, is self-restricting because of pressure interference effects among injection wells. The impact of this is apparent from the much-improved storage efficiency achieved when water extraction wells were added to the development plan. Additional simulation and cost estimation efforts may be justified to investigate project development scenarios intended to mitigate interference effects in these study areas and/or other CO_2 storage target formations.

4) The most complex and elusive of the premises listed above is cost. Without the limitation of cost placed on this process, the limits of practicality cannot be judged. Not only is indicative project cost needed, but incremental costs are also needed to determine how unit storage costs increase. It is this incremental unit cost that ultimately determines if further increase in practical storage efficiency is justified. This project, within its scope of work, found it challenging to collect, prepare, and manipulate publicly available cost data for carbon storage. Data that were available were not presented in a consistent manner, making cost comparisons difficult. Therefore, an avenue for future work may be an attempt to collate existing cost data, classify major elements in a consistent manner, and present general cost indices that can be used as a first approximation to help determine what is practically achievable and what is cost-prohibitive.

CONCLUSION

The work performed has shown a significant difference between volumetric static storage efficiency and practical storage efficiency. Simulation cases can be designed to address almost any list of design premises, but the selection of satisfactory premises to define practical storage efficiency is a challenge that deserves careful consideration.

The primary premises used in this evaluation were an assumed injection lifetime of 50 years and an area of investigation of approximately 1000 km^2. Both appear reasonable for the determination of practical storage efficiency for large-scale CO_2 storage development. However, while for the lower permeability and heterogeneous Minnelusa a 50-year injection period appears sufficient to approach a practical storage efficiency, the Bunter would have continued to accept significant quantities of CO_2 for 100 years or longer. Practical efficiency for the Bunter would be higher relative to the Minnelusa if the term “practical” were defined to assume 100 years of injection or greater. The size of the study area, nominally 1000 km^2 for each model, was practical for the purpose of this study, yet in many cases, injection was clearly limited in both areas by interwell pressure interference, even for open-boundary conditions. Practical efficiency would have been higher if the study areas were smaller or even if they were constructed with a different areal geometry. Practical efficiency might also be affected by other factors not considered here, such as surface conditions. Onshore, significant areas of prospective storage locations may be excluded from development because of cultural features. Offshore, pattern drilling of large areas is not practical. While this study provides a useful step toward defining and demonstrating practical storage efficiency, it also points toward concepts that require more work to establish commonly recognized ranges of conditions to be used in the definition of practical.

Cost is also a critical factor in the definition of practical since unit storage costs rise considerably as well density increases. However, available cost information is limited, much more so than simulation study examples. Cost information is also not easily comparable. Costs can vary significantly for different parts of the world, onshore vs. offshore, and are also affected by differing expectations for operational and monitoring security.

The above uncertainties notwithstanding, the simulations of two study areas produced very similar results. In terms of maximum drilling intensity, 4.7% efficiency was achieved for both study areas.

The unit storage cost-optimized drilling intensity was deemed to be 20% of maximum for both study areas, and practical efficiency for the cost-optimized development was 3.4% for the Minnelusa and 2.9% for the Bunter. Both values are considerably less than volumetric estimates of storage efficiency for these areas but greater than estimates that would assume closed-boundary systems.

REFERENCES

Agalliu, I., Smith, C., Tavallali, M., Rao, M., Adams, S., Montero, A., Levesque, L., Coughlin, C., Yang, D., and Gallagher, S., 2016, CO_2 EOR potential in North Dakota—challenges, policy solutions, and contribution to economy and environment: Consulting report, IHS Energy, June.

Anderson, S.T., 2016, Cost implications of uncertainty in CO_2 storage resource estimates—a review: Natural Resource Research, p. 1–23, DOI: 10.1007/s11053-016-9310-7.

Anna, L.O., 2009, Geologic assessment of undiscovered oil and gas in the Powder River Basin Province: U.S. Geological Survey Digital Data Series DDS–69–U, 93 p.

Bachu, S., 2015, Review of CO_2 storage efficiency in deep saline aquifers: International Journal of Greenhouse Gas Control, v. 40, p. 188–202.

Bachu, S., Bonijoly, D., Bradshaw, J., Burruss, R., Holloway, S., Christensen, N.P., and Mathiassen, O.M., 2007, CO_2 storage capacity estimation—methodology and gaps: International Journal of Greenhouse Gas Control, v. 1, no. 4, p. 430–443, ISSN 1750–5836

Barati, R., 2011, EORI collaboration in solving the challenges of Minnelusa: Presented at the EOR Commission and Technical Advisory Board Meeting, Laramie, Wyoming, www.uwyo.edu/eori/_files/eroctab_july_2011/reza%20-minelusapres%2007-19-2011%20tab_reza.pdf (accessed November 2016).

Bentham, M., 2006, An assessment of carbon sequestration potential in the UK – southern North Sea case study: Tyndall Centre for Climate Change Research, Working Paper 85.

Bentham, M., Mallows, T., Lowndes, J., and Green, A., 2014, CO_2 STORage evaluation database (CO_2 stored)—the UK's online storage atlas: 12th International Conference on Greenhouse Gas Control Technologies (GHGT-12), v. 63, p. 5103–5113.

Birkholzer, J.T., and Zhou, Q., 2009, Basin-scale hydrogeologic impacts of CO_2 storage—capacity and regulatory implications: International Journal of Greenhouse Gas Control, v. 3, no. 6, p. 745–756.

Blondes, M.S., Brennan, S.T., Merrill, M.D., Buursink, M.L., Warwick, P.D., Cahan, S.M., Cook, T.A., Corum, M.D., Craddock, W.H., DeVera, C.A, Drake, R.M., II, Drew, L.J., Freeman, P.A., Lohr, C.D., Olea, R.A., Roberts-Ashby, T.L., Slucher, E.R., and Varela, B.A., 2013, National assessment of geologic carbon dioxide storage resources—methodology implementation: U.S. Geological Survey Open-File Report 2013–1055, 26 p., http://pubs.usgs.gov/of/2013/1055/.

Bradshaw, J., Bachu, S., Bonijoly, D., Burruss, R., Holloway, S., Christensen, N.P., and Mathiassen, O.M., 2007, CO_2 storage capacity estimation—issues and development of standards: International Journal of Greenhouse Gas Control, v. 1, no. 1, p. 62–68.

Brennan, S.T., Burruss, R.C., Merrill, M.D., Freeman, P.A., and Ruppert, L.F., 2010, A probabilistic assessment methodology for the evaluation of geologic carbon dioxide storage: U.S. Geological Survey Open-File Report 2010–1127, 31 p., http://pubs.usgs.gov/of/2010/1127 (accessed February 2013).

Brook, M., Shaw, K., Vincent, C., and Holloway, S., 2003, GESTCO Case Study 2a-1—storage potential of the Bunter Sandstone in the UK sector of the southern North Sea and the adjacent onshore area of eastern England: Nottingham, UK, British Geological Survey, 44 p. (CR/03/154N).

Carbon Management GIS, 2008, CO_2 pipeline transport cost estimation, carbon capture and sequestration technologies program: Massachusetts Institute of Technology.

Carbon Sequestration Leadership Forum, 2005, A task force for review and development of standards with regards to storage capacity measurement—Phase I: CSLF-T-2005-9 15, August 8, 2005, 16 p., www.cslforum.org/publications/documents/PhaseIReportStorage CapacityMeasurementTaskForce.pdf (accessed February 2013).

Carbon Sequestration Leadership Forum, 2007, Estimation of CO_2 storage capacity in geological media—Phase II report: June 15, 2007, www.cslforum.org/publications/documents/ PhaseIIReportStorageCapacityMeasurementTaskForce.pdf (accessed February 2013).

Carbon Sequestration Leadership Forum, 2008, Comparison between methodologies recommended for estimation of CO_2 storage capacity in geologic media—Phase III report: April 21, 2008, www.cslforum.org/publications/documents/PhaseIIIReportStorageCapacity EstimationTaskForce0408.pdf (accessed February 2013).

Carman, P.C., 1956, Flow of gases through porous media: New York City, Academic Press Inc.

Chadwick, R.A., Arts, R., Bernstone, C., May, F., Thibeau, S., and Zweigel, P., 2008, Best practise for the storage of CO_2 in saline aquifers: British Geological Survey, Keyworth (Occasional Publications 14).

Craig, J., Gorecki, D.C., Ayash, S.C., Liu, G., and Braunberger, J.R., 2014, A comparison of volumetric and dynamic storage efficiency in deep saline reservoirs—an overview of IEAGHG study IEA/CON/13/208: 12th International Conference on Greenhouse Gas Control Technologies.

Eccles, J.K., Pratson, L., Newell, R.G., and Jackson, R.B., 2012, The impact of geologic variability on capacity and cost estimates for storing CO_2 in deep-saline aquifers: Energy Economics, v. 34, p. 1569–1579.

Energy Technologies Institute, 2016a, D10: WP5A—Bunter storage development plan: Report of DECC Strategic UK CCS Storage Appraisal Project, commissioned by the Energy Technologies Institute and funded by the Department of Energy and Climate Change, prepared

by Pale Blue Dot Energy and Axis Well Technology, United Kingdom, 10113ETIS-Rep-13-03, March.

Energy Technologies Institute, 2016b, Progressing development of the UK's strategic carbon dioxide storage resource—a summary of results from the Strategic UK CO_2 Storage Appraisal Project: Report of study commissioned by the Energy Technologies Institute and funded by the Department of Energy and Climate Change, prepared by Pale Blue Dot Energy, Axis Well Technology, and Costain, United Kingdom, April, 48 p.

Gorecki, C.D., Ayash, S.C., Liu, G., Braunberger, J.R., and Dotzenrod, N.W., 2015, A comparison of volumetric and dynamic CO_2 storage resource and efficiency in deep saline formations: International Journal of Greenhouse Gas Control, v. 42, p. 213–225.

Hellström, A.H.K., 2010, Statoil drilling and well learning curves, experience and theory—is there a learning curve from drilling the first well with a new rig and onwards?: Master thesis, Department for Industrial Asset Management, University of Stavanger, Stavanger, Norway, June 15.

Holloway, S., Vincent, C.J., Bentham, M.S., and Kirk, K.L., 2006a, Top-down and bottom-up estimates of CO_2 storage capacity in the United Kingdom sector of the southern North Sea Basin: Environmental Geosciences, v. 13, no. 2, p. 71–84.

Holloway, S., Vincent, C.J., and Kirk, K.L., 2006b, Industrial carbon dioxide emissions and carbon dioxide storage potential in the UK, *in* DTI Report COAL R308: DTI/Pub URN 06/2027, DECC, London.

IEA Greenhouse Gas R&D Programme, 2009, Development of storage coefficients for CO_2 storage in deep saline formations: 2009/12, October.

IEA Greenhouse Gas R&D Programme, 2010, Pressurisation and brine displacement issues for deep saline formation CO_2 storage: 2010/15, November.

IEA Greenhouse Gas R&D Programme, 2014, CO_2 storage efficiency in deep saline formations—a comparison of volumetric and dynamic storage resource estimation methods: 2014/09, October.

Ikoku, C.U., 1978, Application of learning curve models to oil and gas well drilling: Presented at the Society of Petroleum Engineers (SPE) of AIME (American Institute of Mining, Metallurgical and Petroleum Engineers) California Regional Meeting, San Francisco, California, April 12–14, 1978, SPE 7119.

Litynski, J., Deel, D., Rodosta, T., Guthrie, G., Goodman, A., Hakala, A., Bromhal, G., and Frailey, S., 2010, Summary of the methodology for development of geologic storage estimates for carbon dioxide: Prepared for U.S. Department of Energy National Energy Technology Laboratory Carbon Storage Program, www.netl.doe.gov/File%20Library/Research/Coal/carbon-storage/natcarb/geologic-storage-estimates-for-carbon-dioxide.pdf (accessed January 2014).

Nghiem, L., Shrivastava, V., Tran, D., Kohse, B., Hassam, M., and Yang, C., 2009, Simulation of CO_2 storage in saline aquifers: Presented at the Society of Petroleum Engineers (SPE) of AIME (American Institute of Mining, Metallurgical and Petroleum Engineers) Reservoir Characterization and Simulation Conference, Abu Dhabi, United Arab Emirates, October 19–21, 2009, SPE 125848.

Nicot, J.P., 2008, Evaluation of large-scale CO_2 storage on fresh-water sections of aquifers—an example from the Texas Gulf Coast Basin: International Journal of Greenhouse Gas Control, v. 2, p. 582–593.

Noy, D.J., Holloway, S., Chadwick, R.A., Williams, J.D.O., Hannis, S.A., and Lahann, R.W., 2012, Modelling large-scale carbon dioxide injection into the Bunter Sandstone in the UK Southern North Sea: International Journal of Greenhouse Gas Control, v. 9, p. 220–233.

Peck, W.A., Glazewski, K.A., Klenner, R.C.L., Gorecki, C.D., Steadman, E.N., and Harju, J.A., 2014, A workflow to determine CO_2 storage potential in deep saline formations: Energy Procedia, v. 63, p. 5231–5238.

Rubin, E.S., Davison, J.E., and Herzog, H.J., 2015, The cost of CO_2 capture and storage: International Journal of Greenhouse Gas Control, v. 40, p. 378–400.

Szulczewski, M.L., MacMinn, C.W., Herzog, H.J., and Juanes, R., 2012, Lifetime of carbon capture and storage as a climate-change mitigation technology: PNAS, v. 109, no. 14.

Smith, D.J., Noy, D.J., Holloway, S., Chadwick, R.A., 2010, The impact of boundary conditions on CO_2 storage capacity estimation in aquifers: Energy Procedia, v. 4, p. 4828–4834.

U.S. Department of Energy, 2007, National Energy Technology Laboratory carbon sequestration atlas of the United States and Canada.

U.S. Department of Energy, 2008, National Energy Technology Laboratory carbon sequestration atlas of the United States and Canada, 2nd ed.

U.S. Department of Energy National Energy Technology Laboratory, 2010, Carbon sequestration atlas of the United States and Canada, 3rd ed.

U.S. Department of Energy National Energy Technology Laboratory, 2012, Carbon sequestration atlas of the United States and Canada, 4th ed.

U.S. Department of Energy National Energy Technology Laboratory, 2014a, FE/NETL CO_2 saline storage cost model—user's manual: Report by Energy Sector Planning and Analysis (ESPA) for U.S. Department of Energy National Energy Technology Laboratory Contract No. DE-FE0004001, DOE/NETL-2012/1582.

U.S. Department of Energy National Energy Technology Laboratory, 2014b, Quality guidelines for energy system studies—carbon dioxide transport and storage costs in NETL studies: Report for U.S. Department of Energy National Energy Technology Laboratory Contract No. DE-FE0004001, DOE/NETL-2014/1653.

U.S. Department of Energy National Energy Technology Laboratory 2014c, FE/NETL CO_2 saline storage cost model—Cost model spreadsheet, U.S. Department of Energy National Energy Technology Laboratory, DOE/NETL-2014/1669, www.netl.doe.gov/research/energy-analysis/analytical-tools-and-data/co2-saline-storage (accessed October 2016).

U.S. Inflation, 2017, www.usinflation.org (accessed March 2017).

Vangkilde-Pedersen, T., Vosgerau, H., Willscher, B., Neele, F., van der Meer, B., Bossie-Codreanu, D., Wojcicki, A., Le Nindre, Y-M., Kirk, K., von Dalwigk, I., and Anthonsen, K.L., 2009, EU geocapacity—assessing European capacity for geological storage of carbon dioxide: Geological Survey of Denmark and Greenland, Project No. SES6-518318, 45 p.

Williams, J.D.O., Jin, M., Bentham, M., Pickup, G.E., Hannis, S.D., and Mackay, E.J., 2013, Modelling carbon dioxide storage within closed structures in the UK Bunter Sandstone Formation: International Journal of Greenhouse Gas Control, v. 18, p. 38–50, Copyright 2013, modifications with permission from Elsevier.

Xe, 2017, www.xe.com (accessed March 2017).

Zero Emissions Platform, 2011, The costs of CO_2 storage—post-demonstration CCS in the EU: Report for the Advisory Council of the European Platform for Zero Emission Fossil Fuel Power Plants, July 2011, available at www.zeroemissionsplatform.eu/ (accessed August 2016).

Zhou, Q., and Birkholzer, J.T., 2011, On scale and magnitude of pressure buildup induced by large-scale geologic storage of CO_2 greenhouse gases: Science and Technology, v. 1, no. 1, p. 11–20.

Zhou, Q., Birkholzer, J. T., Tsang, C.-F., and Rutqvist, J., 2008, A method for quick assessment of CO_2 storage capacity in closed and semiclosed saline formations: International Journal of Greenhouse Gas Control, v. 2, no. 4, p. 626–639.

APPENDIX A

ADDITIONAL FIGURES FOR THE MINNELUSA SIMULATIONS

ADDITIONAL FIGURES FOR THE MINNELUSA SIMULATIONS

The rock–fluid settings of the Minnelusa Formation were based on the lithologies found in the static geologic model. Pitts and Surkalo (1995) and Barati (2011 and 2012) reported relative permeability curves and capillary pressure based on the sedimentary lithologies, including the sandstone and dolomite, in the Minnelusa Formation. The relative permeability and capillary pressure curves used for the system are shown in Figures A-1 and A-2.

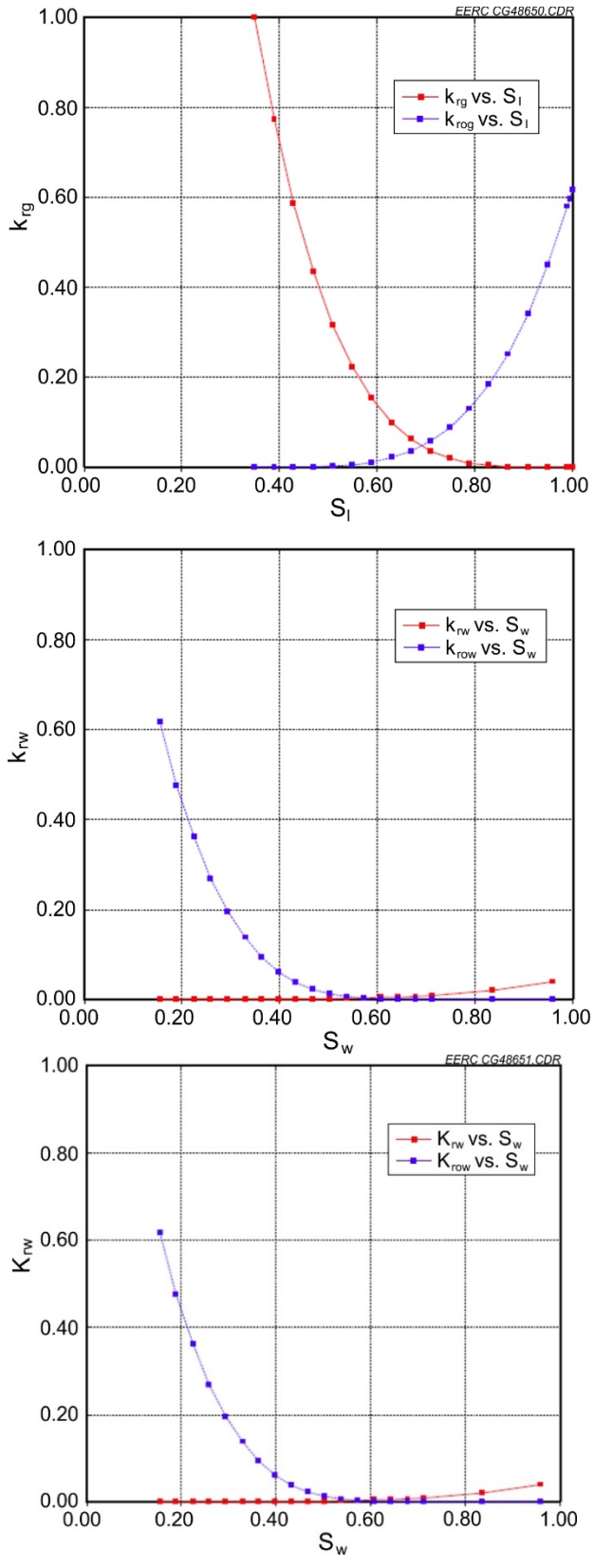

Figure A-1. Relative permeability curves of the Minnelusa system (Garcia, 2005).

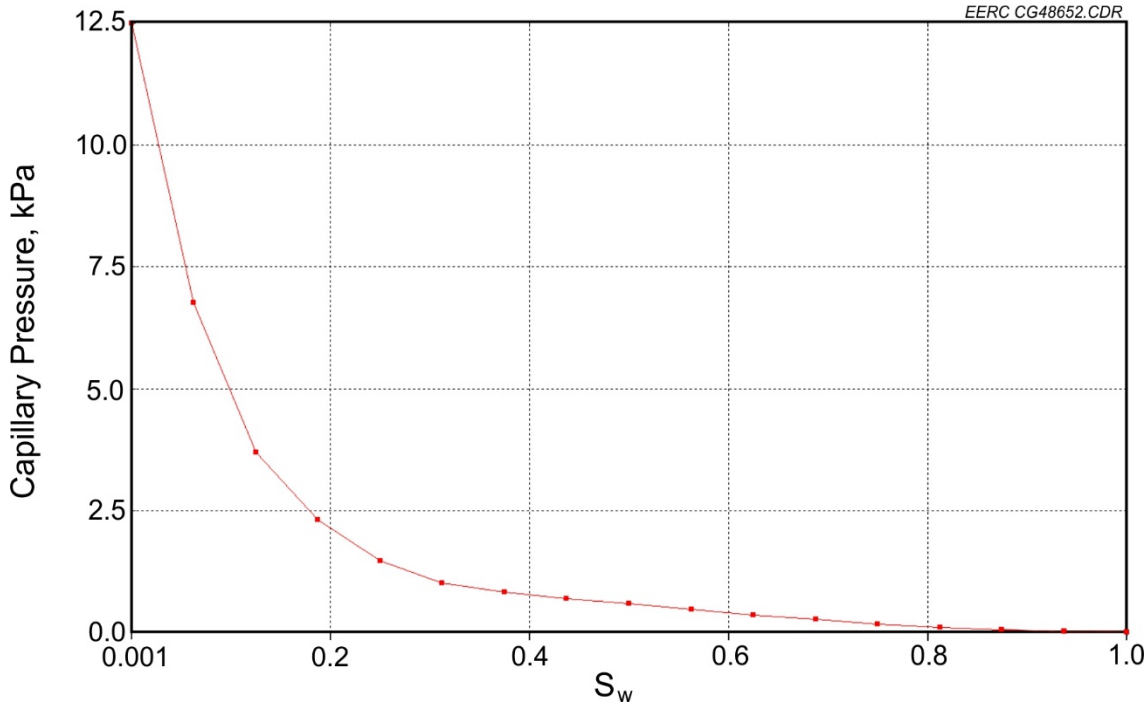

Figure A-2. Capillary pressure curve of the Minnelusa system (Barati, 2011).

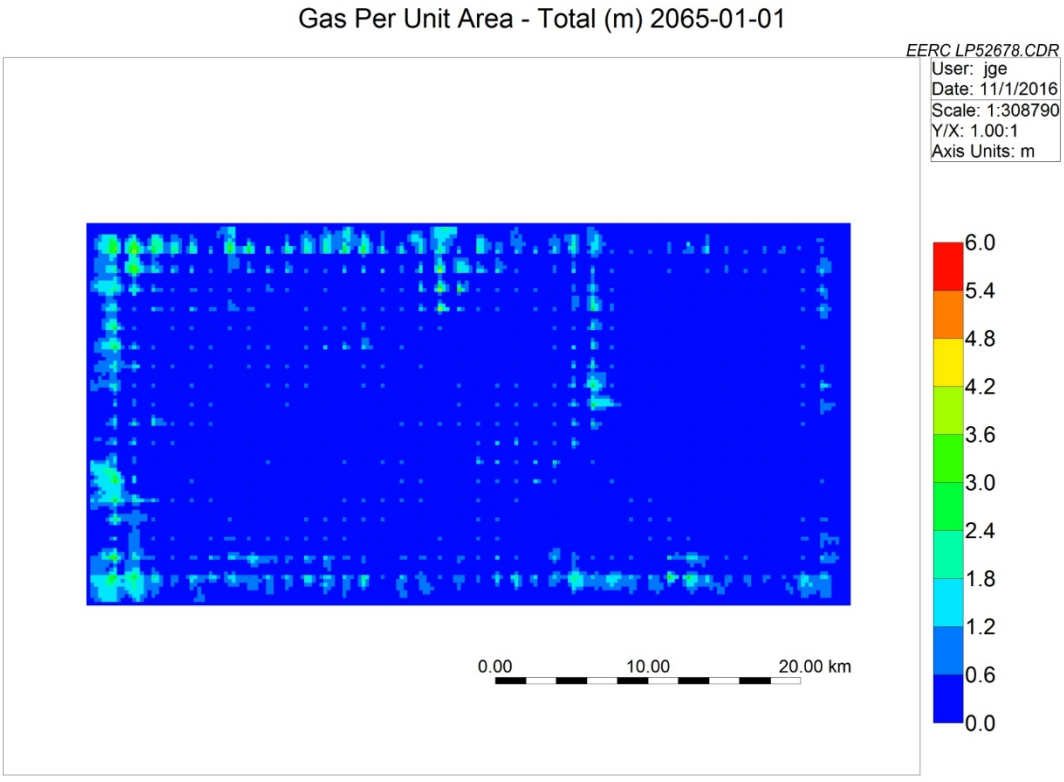

Figure A-3. Case D1: CO_2 footprint (total gas per unit area in meters) after 50 years of injection.

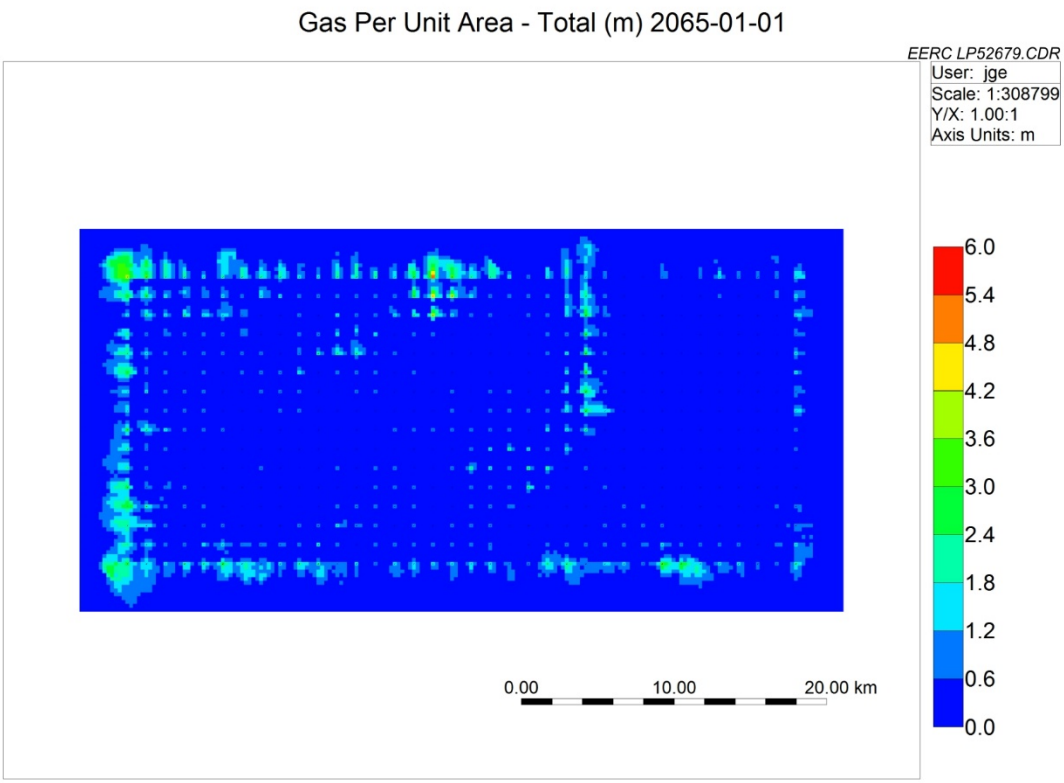

Figure A-4. Case D2: CO_2 footprint (total gas per unit area in meters) after 50 years of injection.

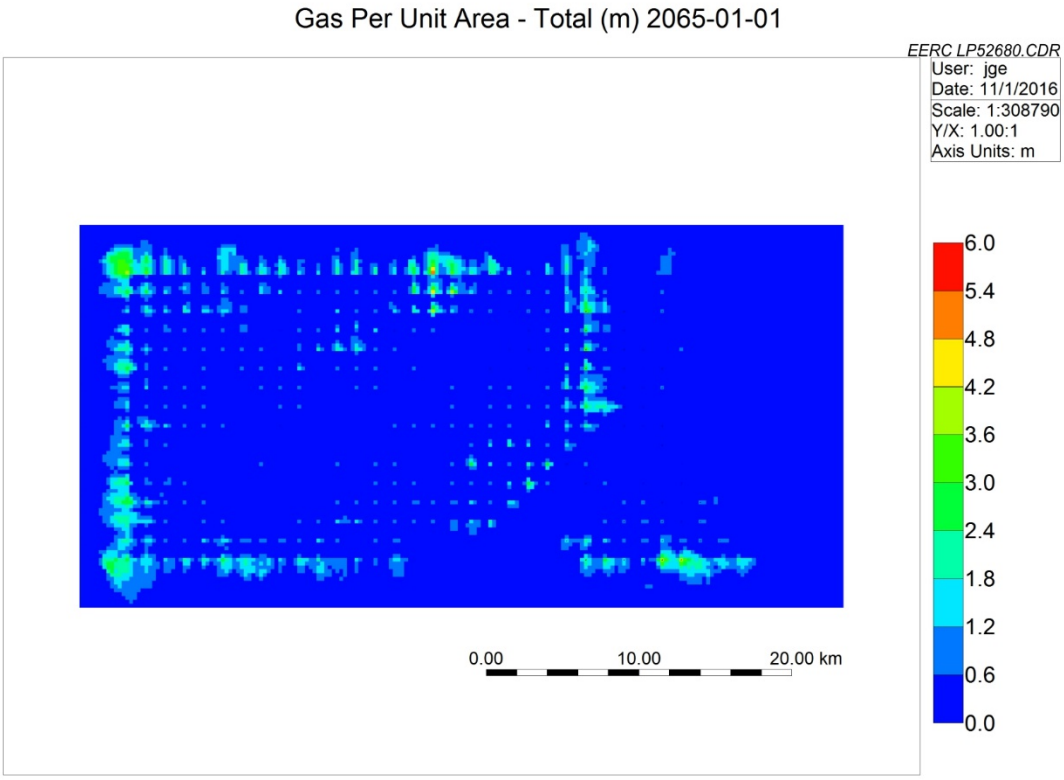

Figure A-5. Case D3: CO_2 footprint (total gas per unit area in meters) after 50 years of injection.

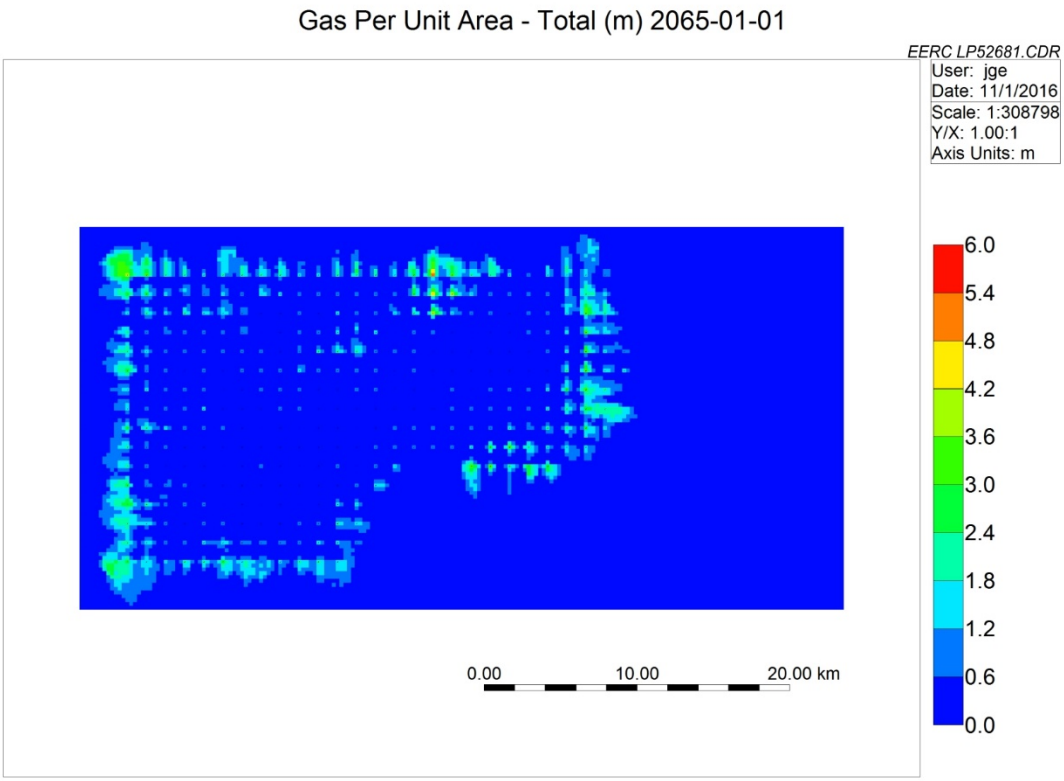

Figure A-6. Case D4: CO_2 footprint (total gas per unit area in meters) after 50 years of injection.

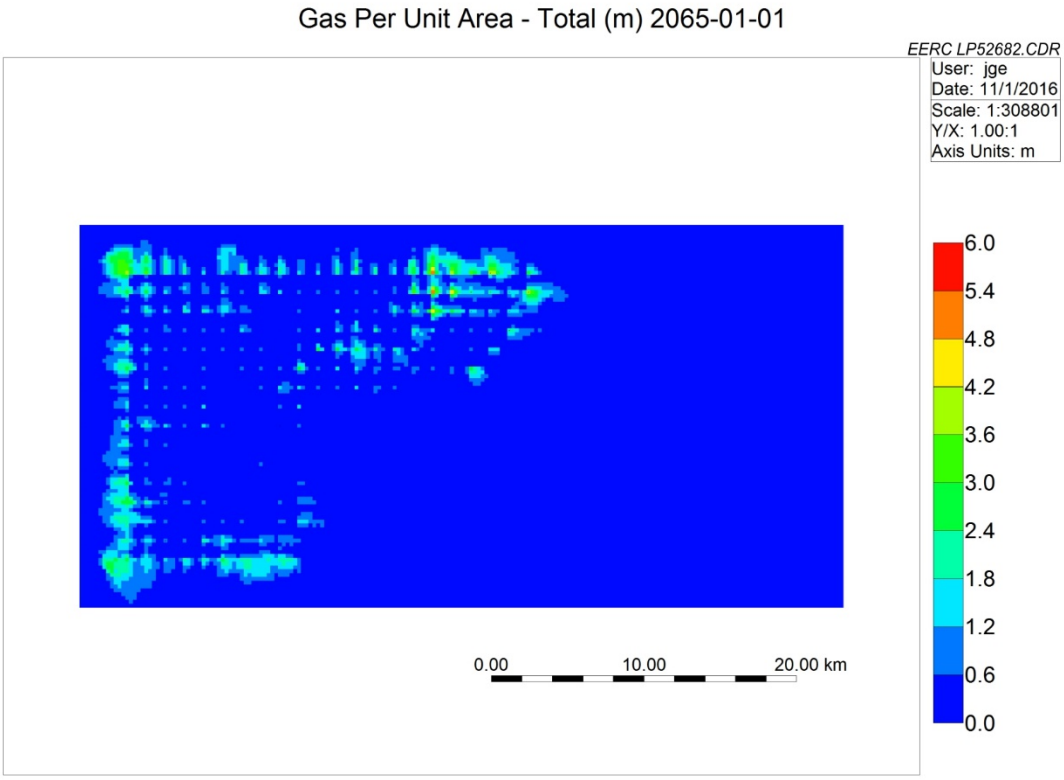

Figure A-7. Case D5: CO_2 footprint (total gas per unit area in meters) after 50 years of injection.

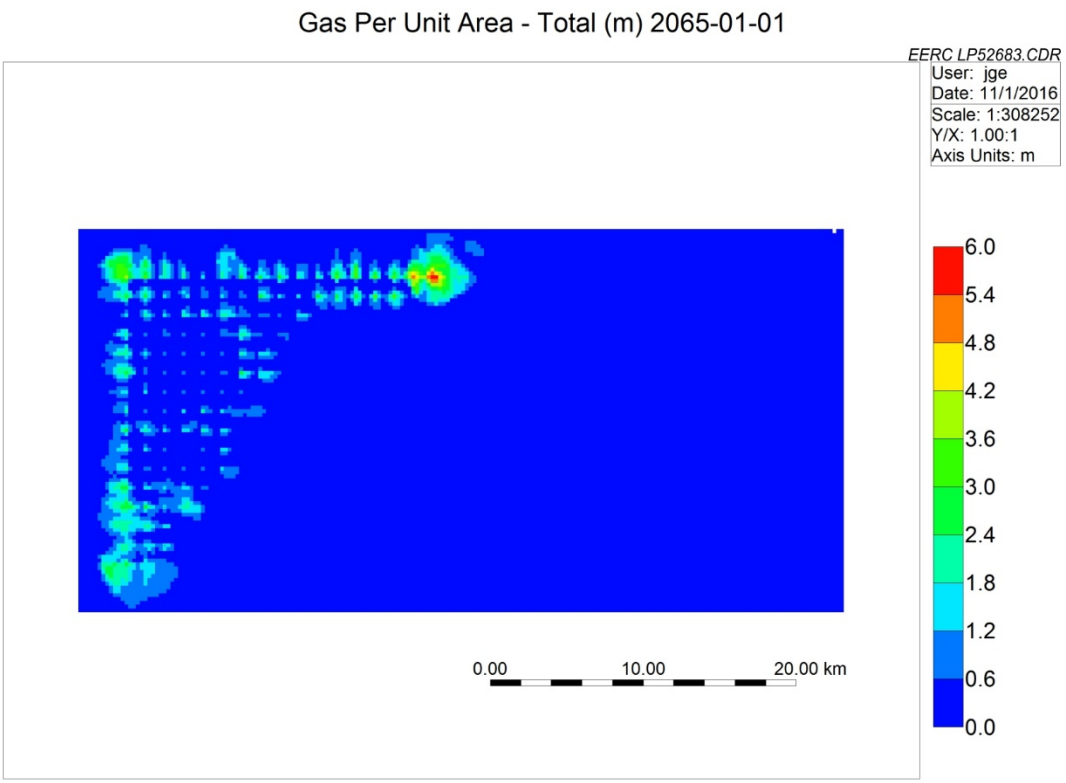

Figure A-8. Case D6: CO_2 footprint (total gas per unit area in meters) after 50 years of injection.

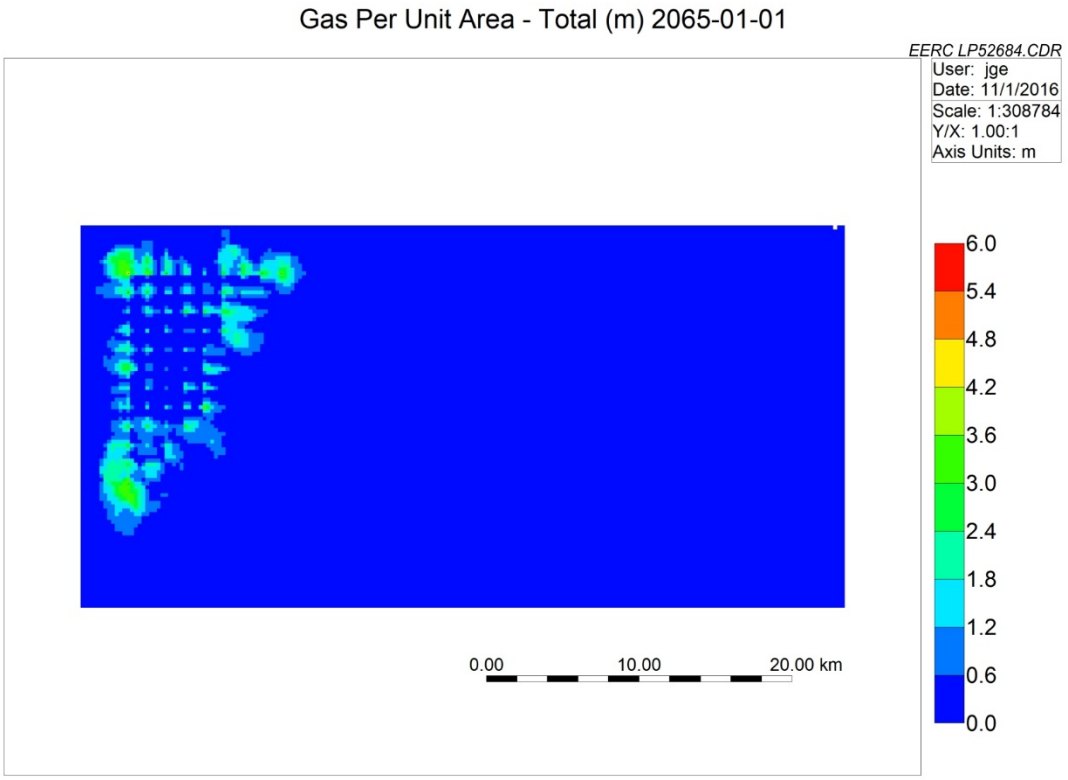

Figure A-9. Case D7: CO_2 footprint (total gas per unit area in meters) after 50 years of injection.

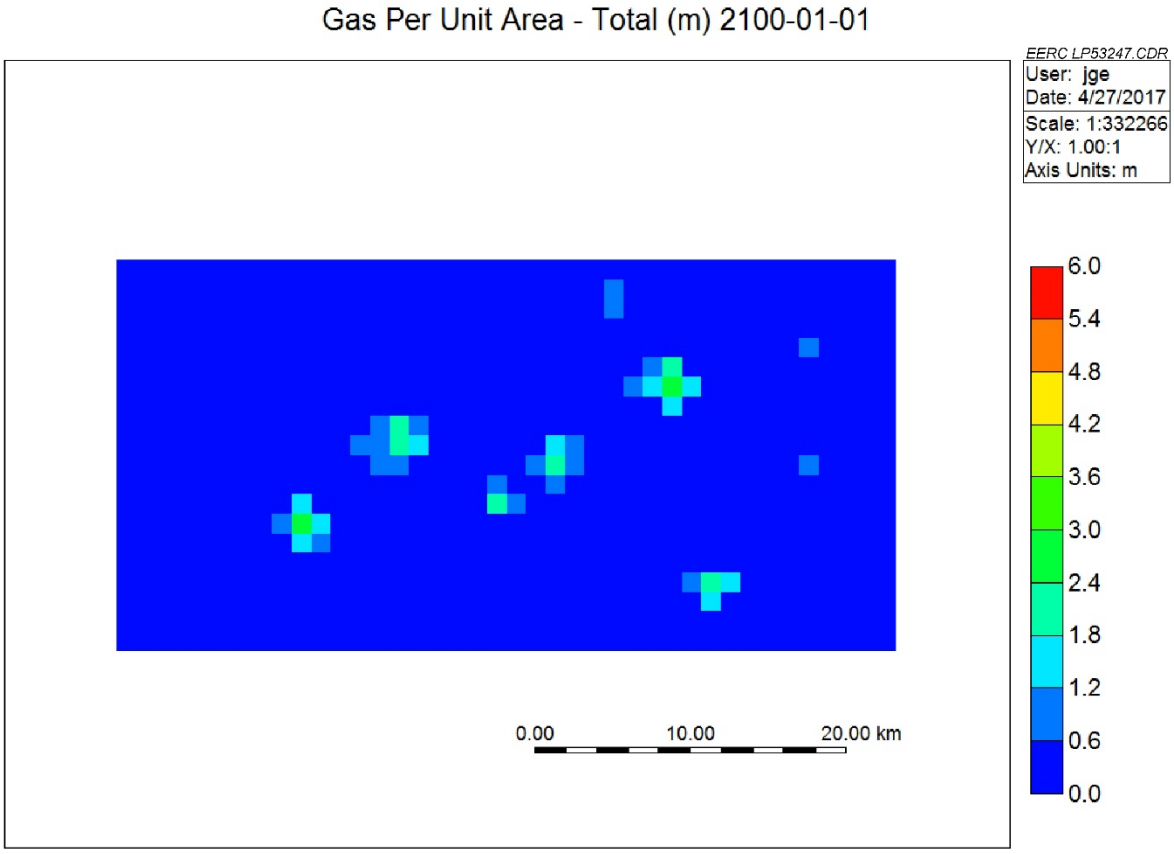

Figure A-10. Case S1: CO_2 footprint (total gas per unit area in meters) after 50 years of injection.

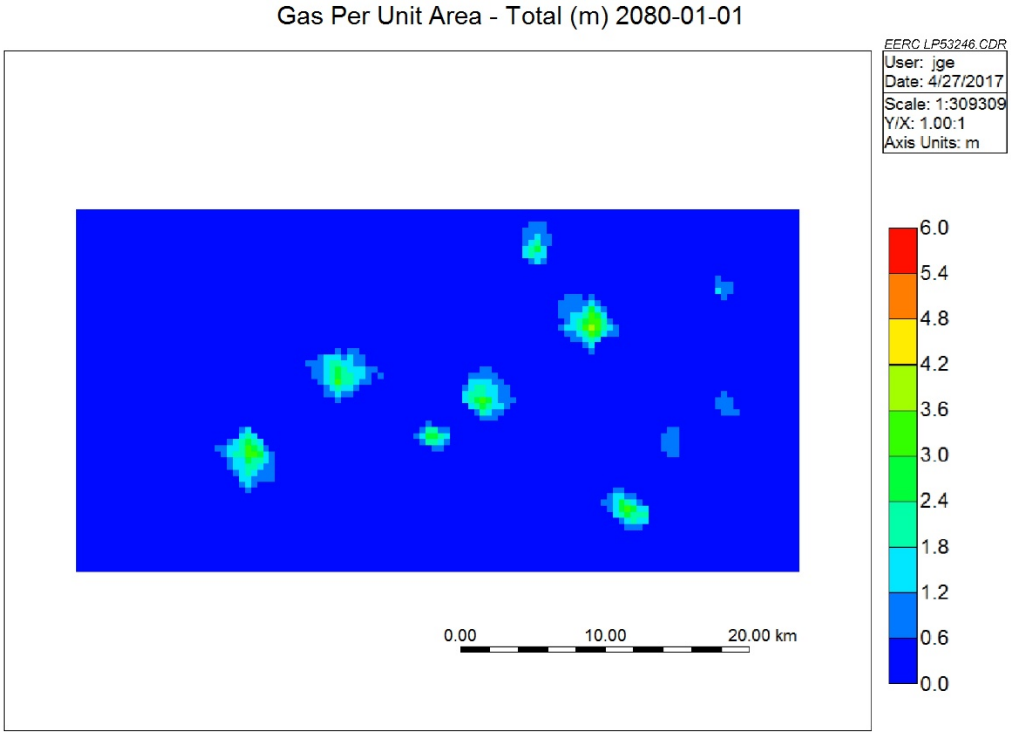

Figure A-11. Case S2: CO_2 footprint (total gas per unit area in meters) after 50 years of injection.

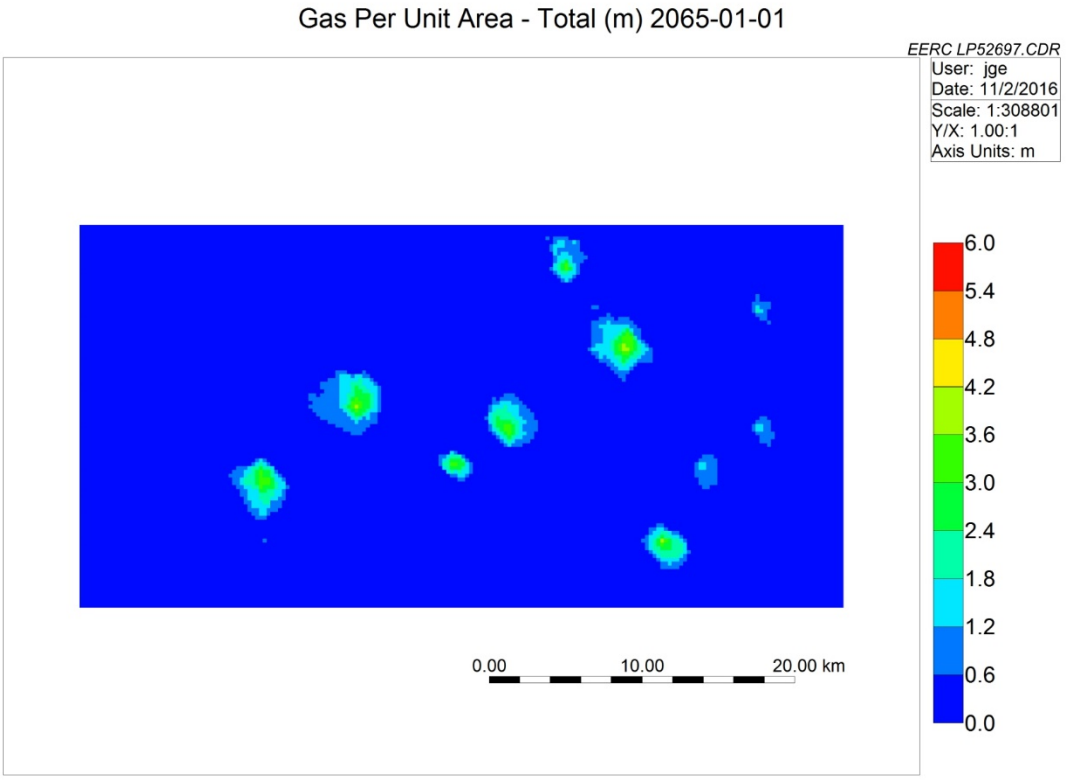

Figure A-12. Case S3: CO_2 footprint (total gas per unit area in meters) after 50 years of injection.

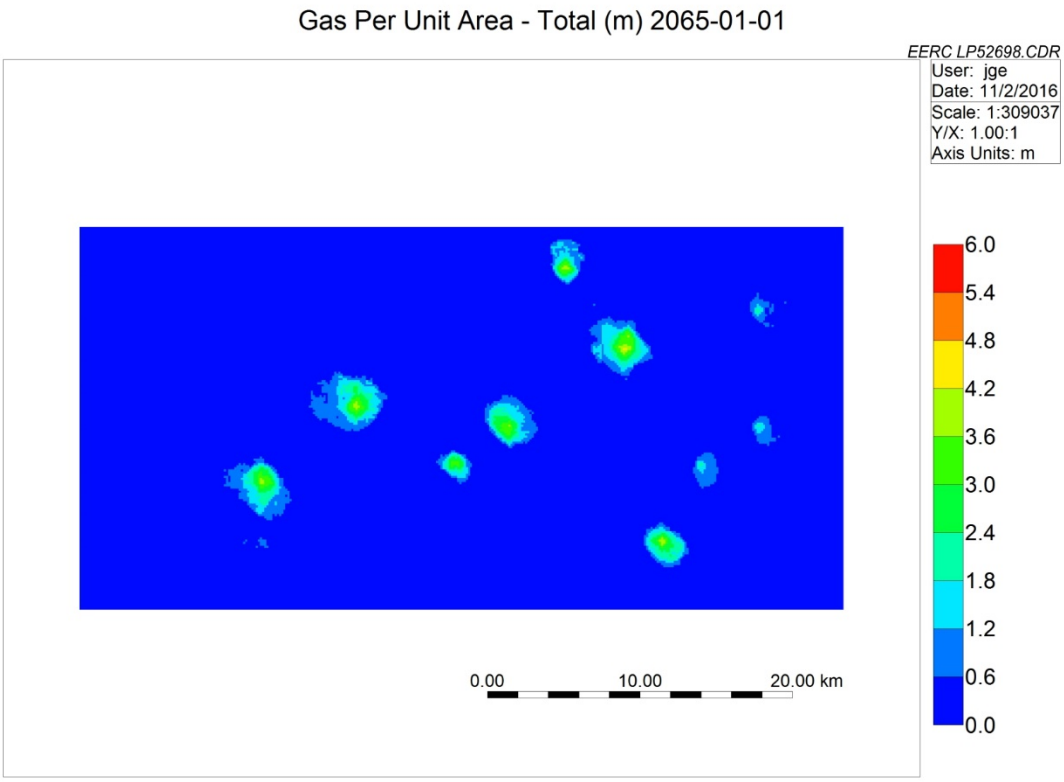

Figure A-13. Case S4: CO_2 footprint (total gas per unit area in meters) after 50 years of injection.

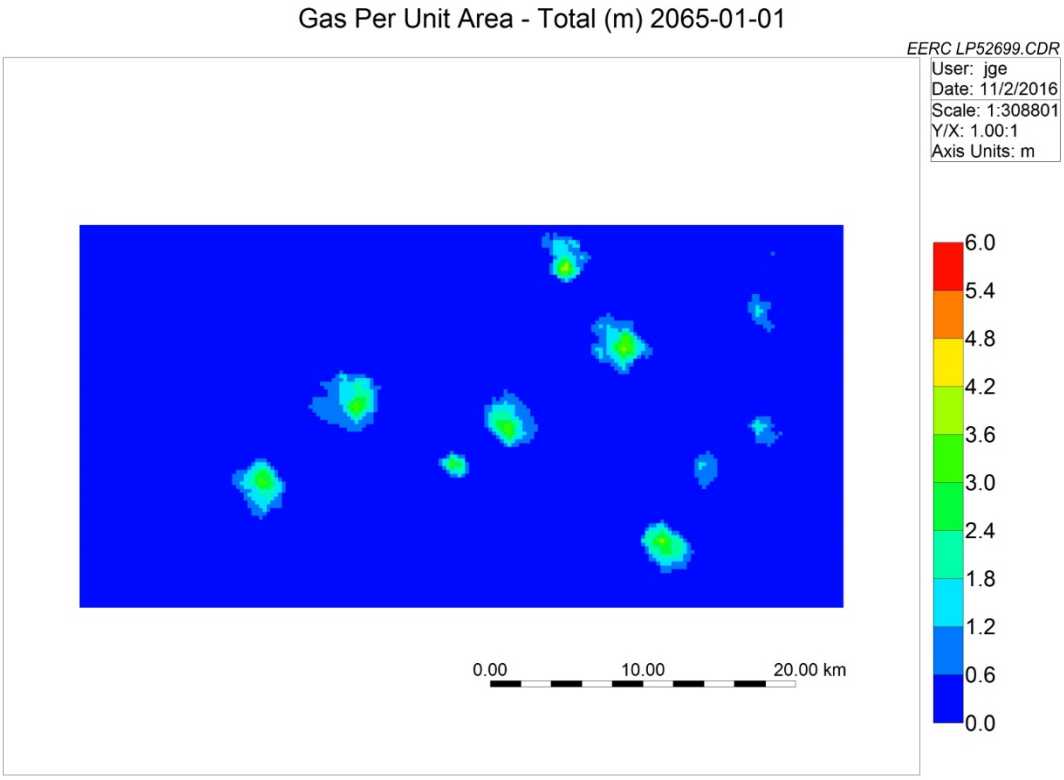

Figure A-14. Case S5: CO_2 footprint (total gas per unit area in meters) after 50 years of injection.

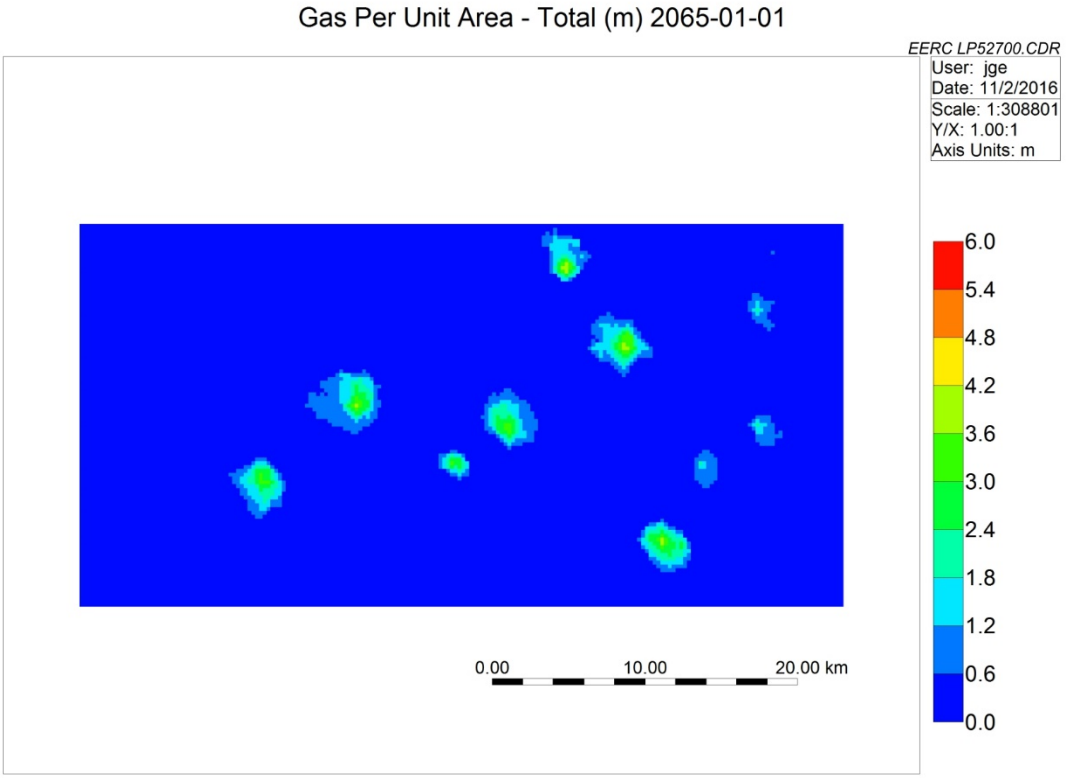

Figure A-15. Case S6: CO_2 footprint (total gas per unit area in meters) after 50 years of injection.

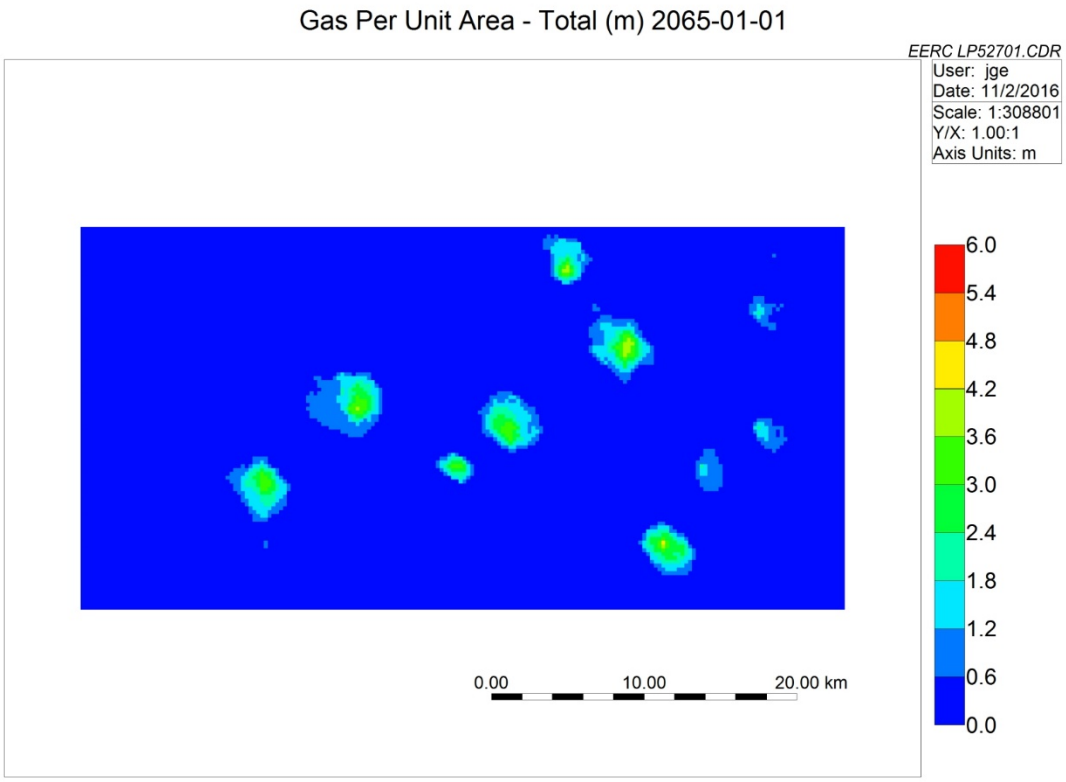

Figure A-16. Case S7: CO_2 footprint (total gas per unit area in meters) after 50 years of injection.

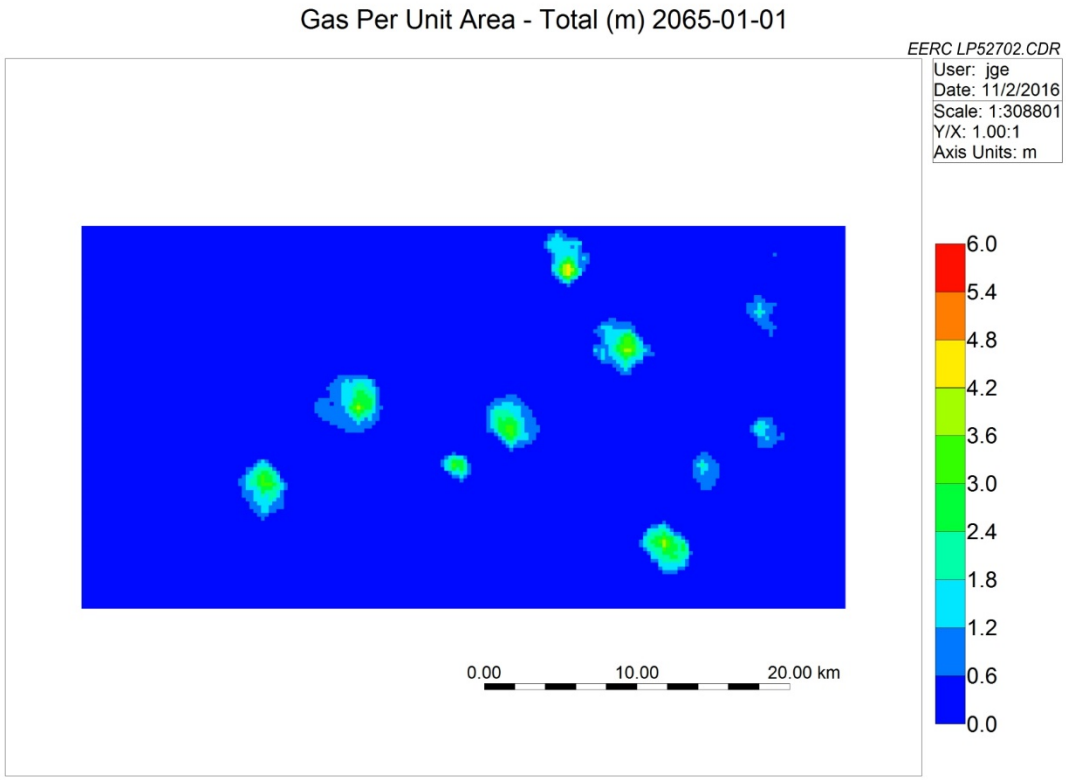

Figure A-17. Case S8: CO_2 footprint (total gas per unit area in meters) after 50 years of injection.

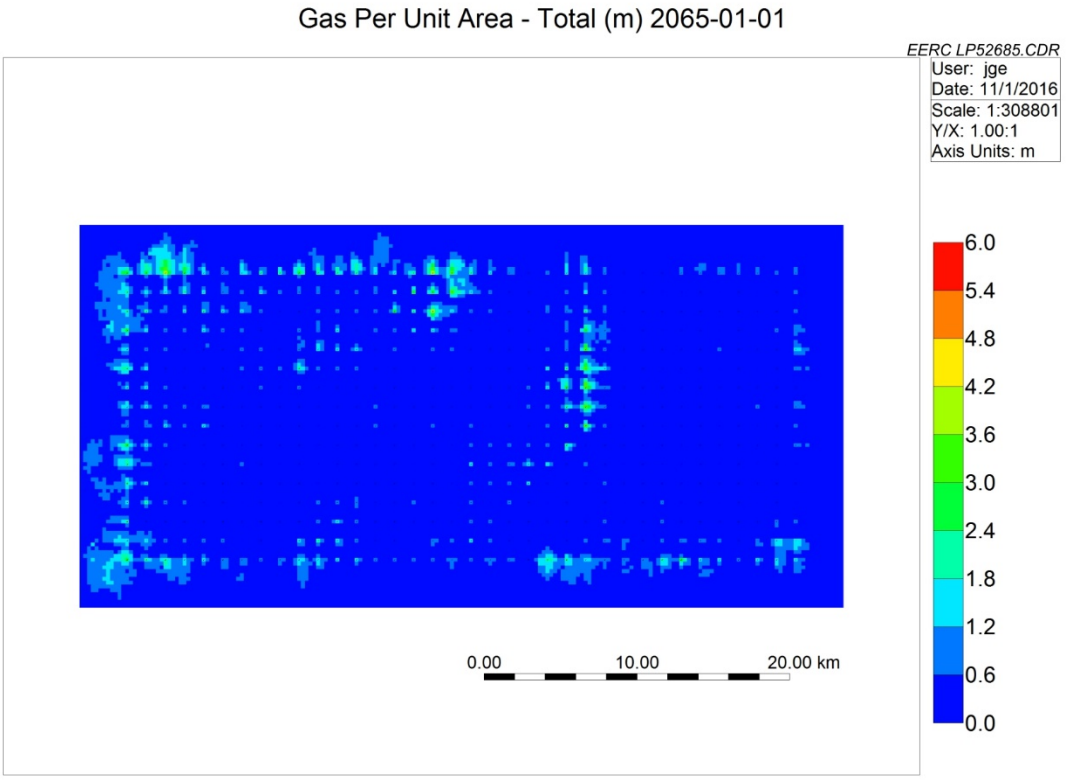

Figure A-18. Case A1: CO_2 footprint (total gas per unit area in meters) after 50 years of injection.

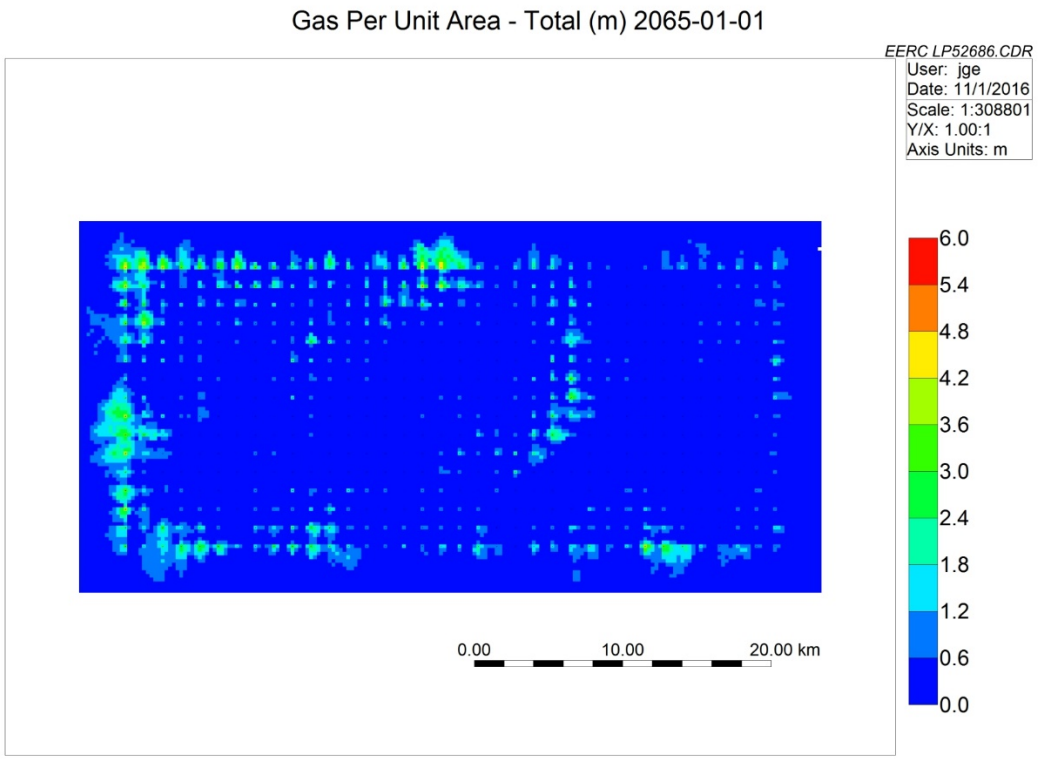

Figure A-19. Case A3: CO_2 footprint (total gas per unit area in meters) after 50 years of injection.

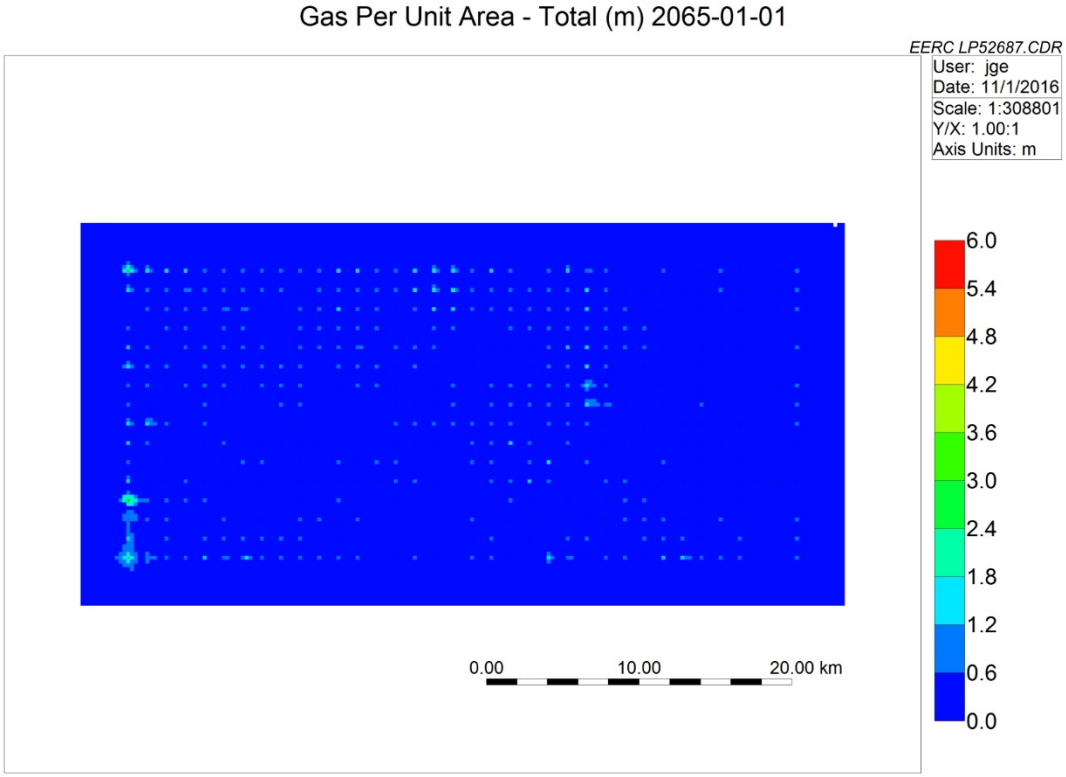

Figure A-20. Case A4: CO_2 footprint (total gas per unit area in meters) after 50 years of injection.

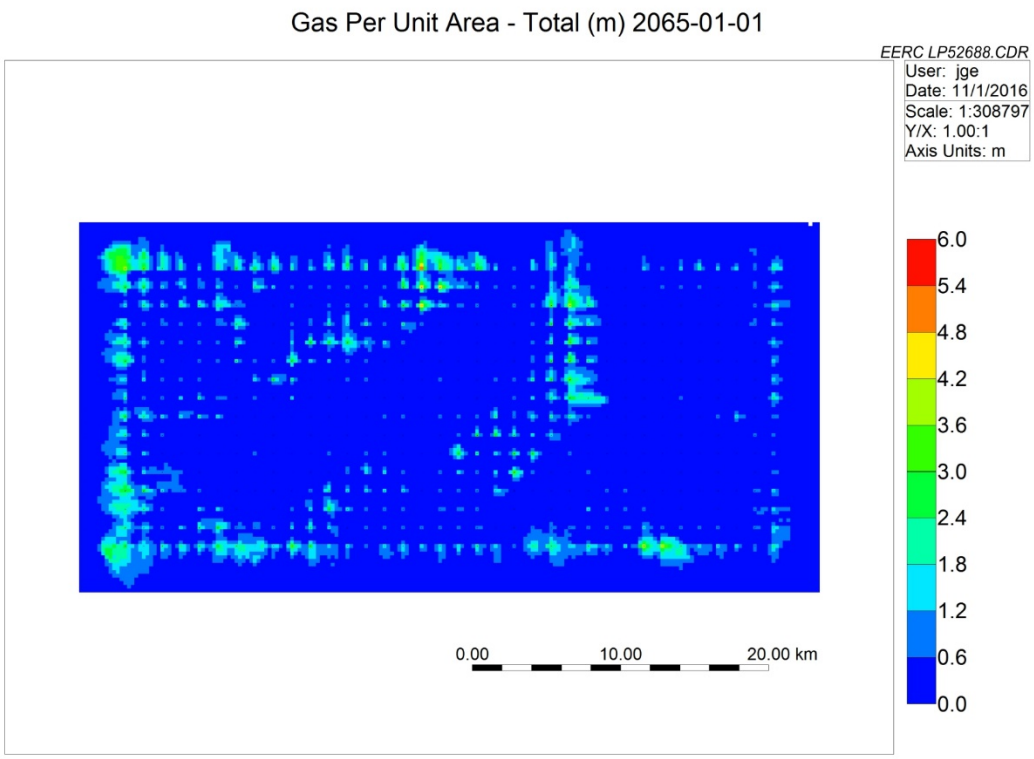

Figure A-21. Case A6: CO_2 footprint (total gas per unit area in meters) after 50 years of injection.

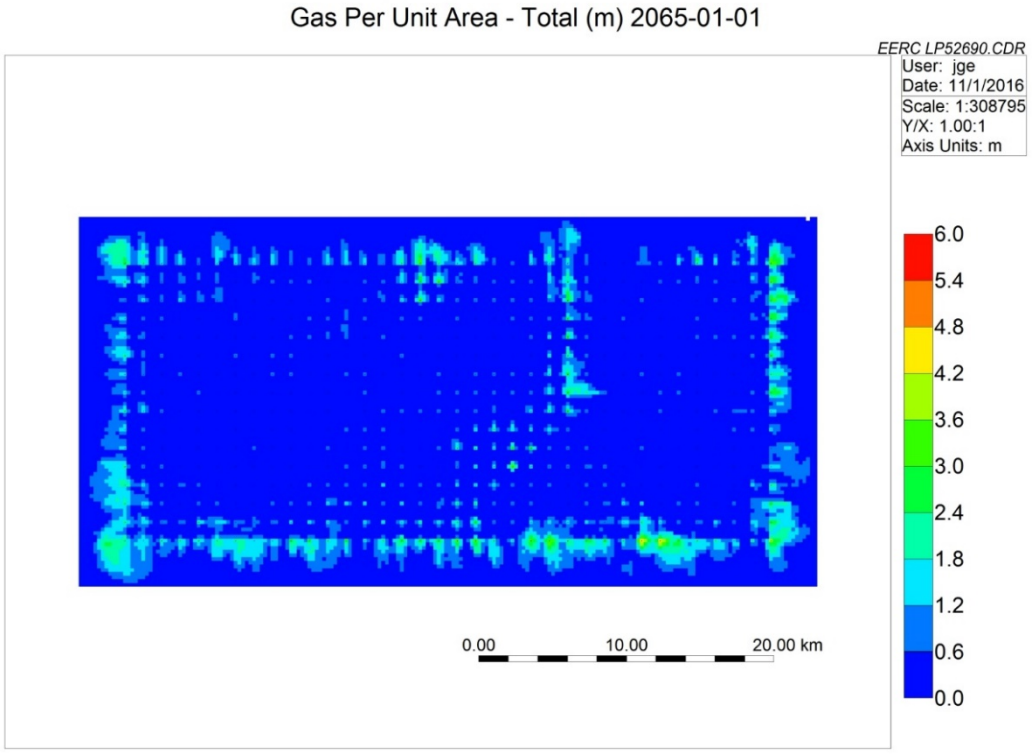

Figure A-22. Case A7: CO_2 footprint (total gas per unit area in meters) after 50 years of injection.

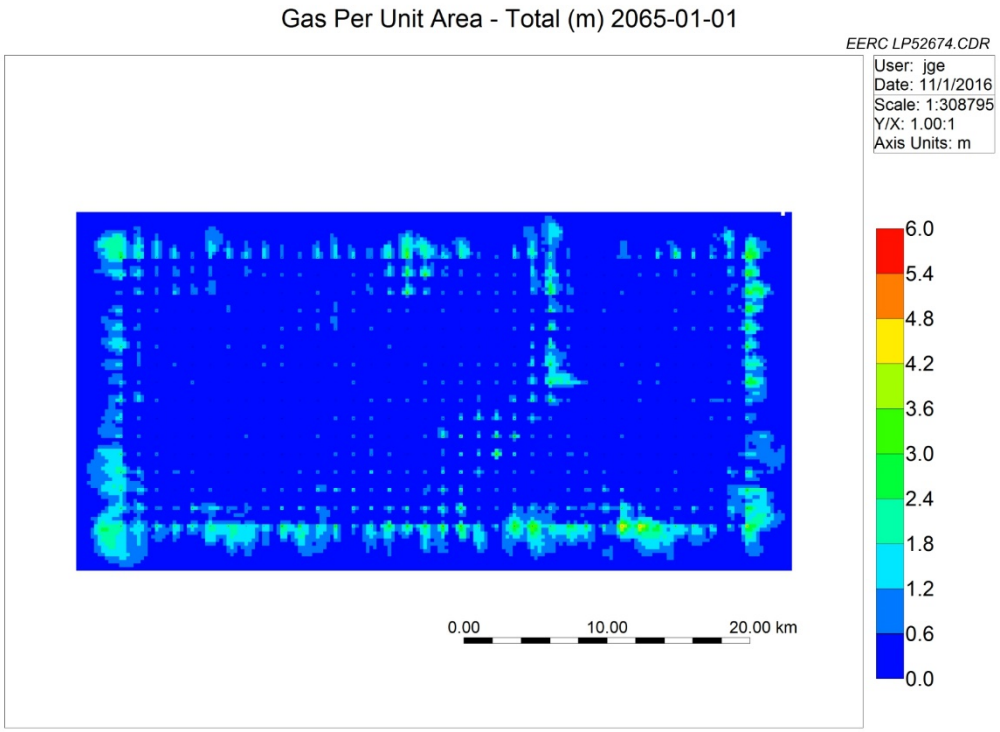

Figure A-23. Case A8: CO_2 footprint (total gas per unit area in meters) after 50 years of injection.

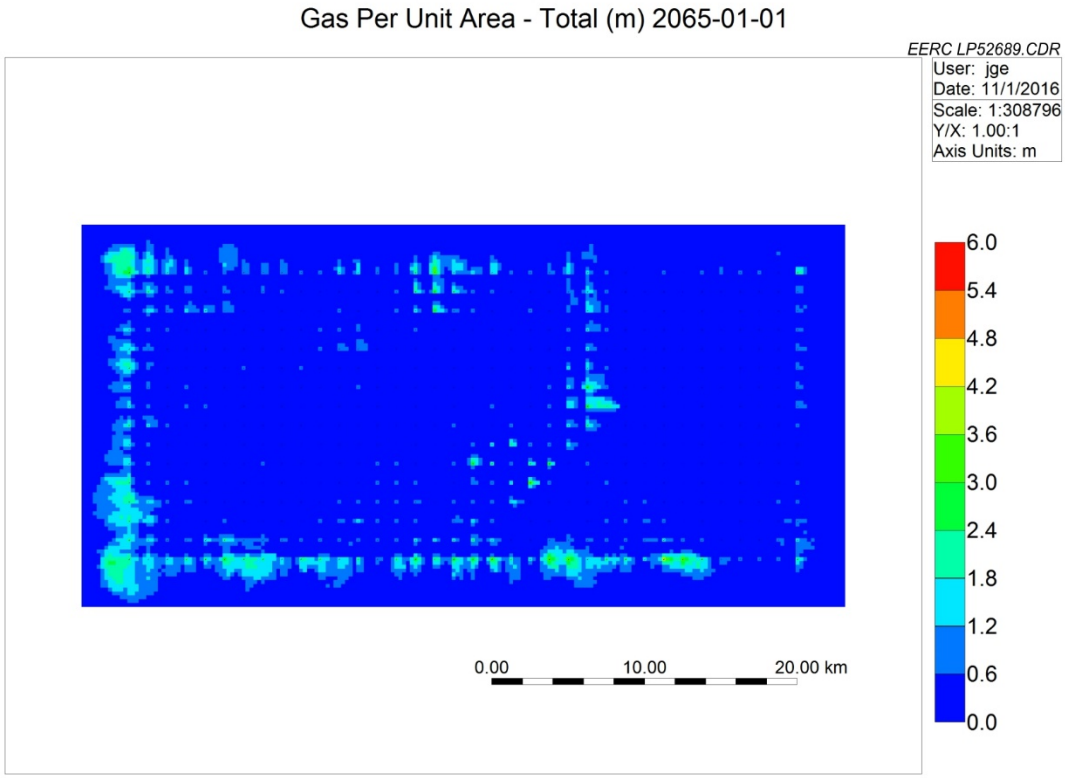

Figure A-24. Case A9: CO_2 footprint (total gas per unit area in meters) after 50 years of injection.

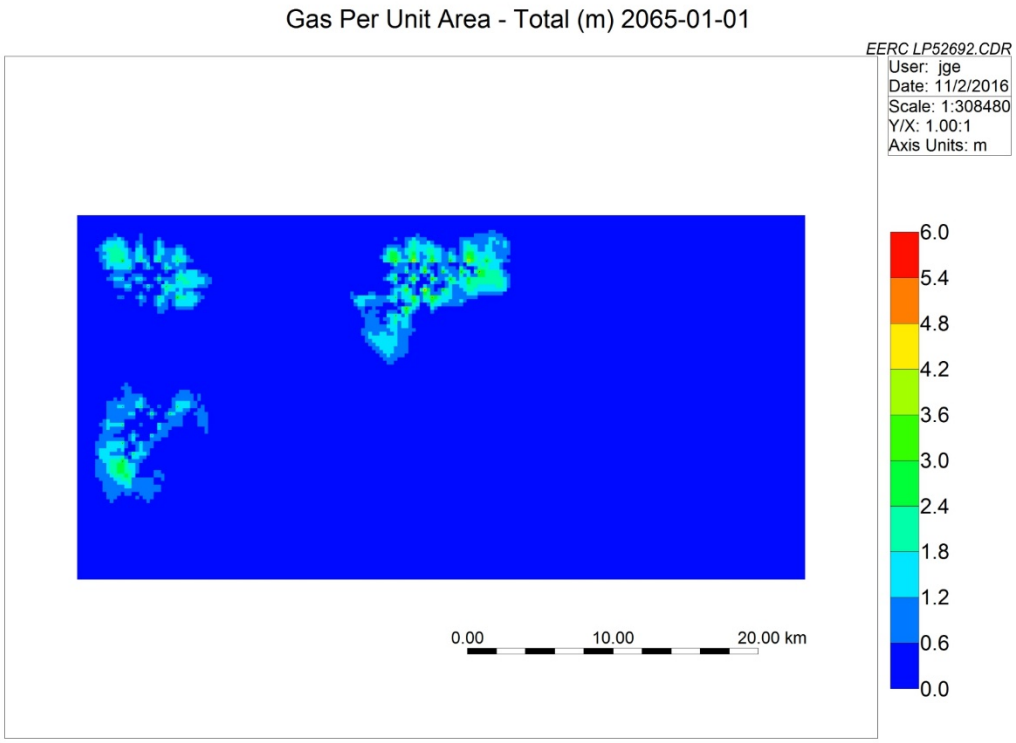

Figure A-25. Case A10: CO_2 footprint (total gas per unit area in meters) after 50 years of injection.

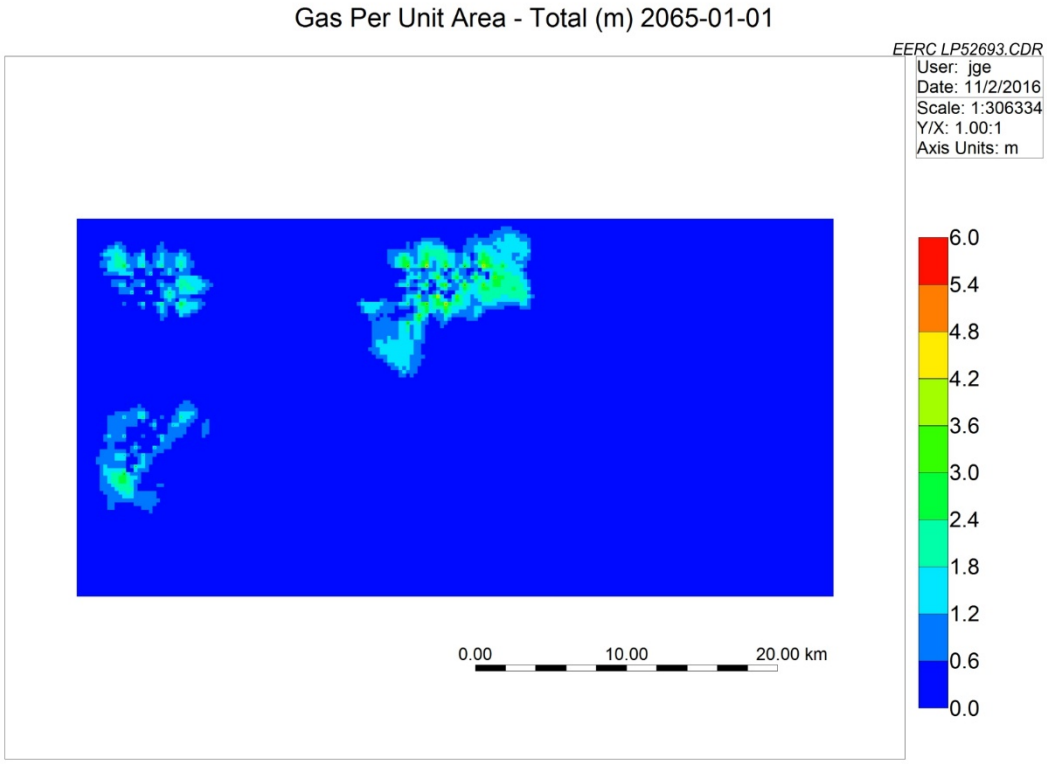

Figure A-26. Case A11: CO_2 footprint (total gas per unit area in meters) after 50 years of injection.

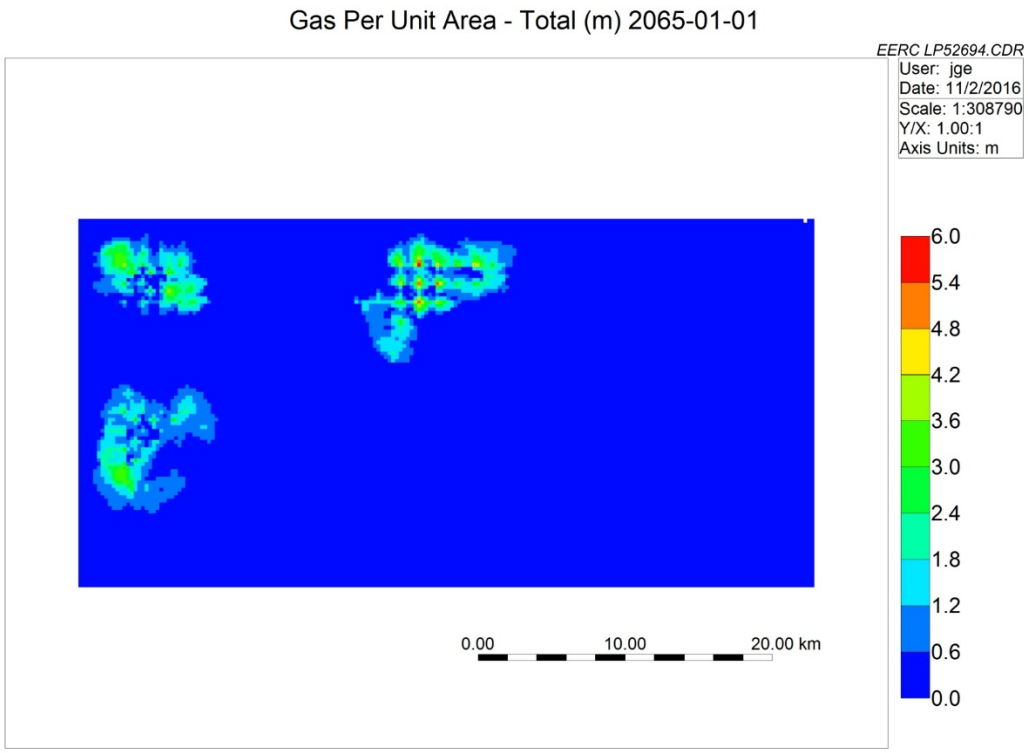

Figure A-27. Case A12: CO_2 footprint (total gas per unit area in meters) after 50 years of injection.

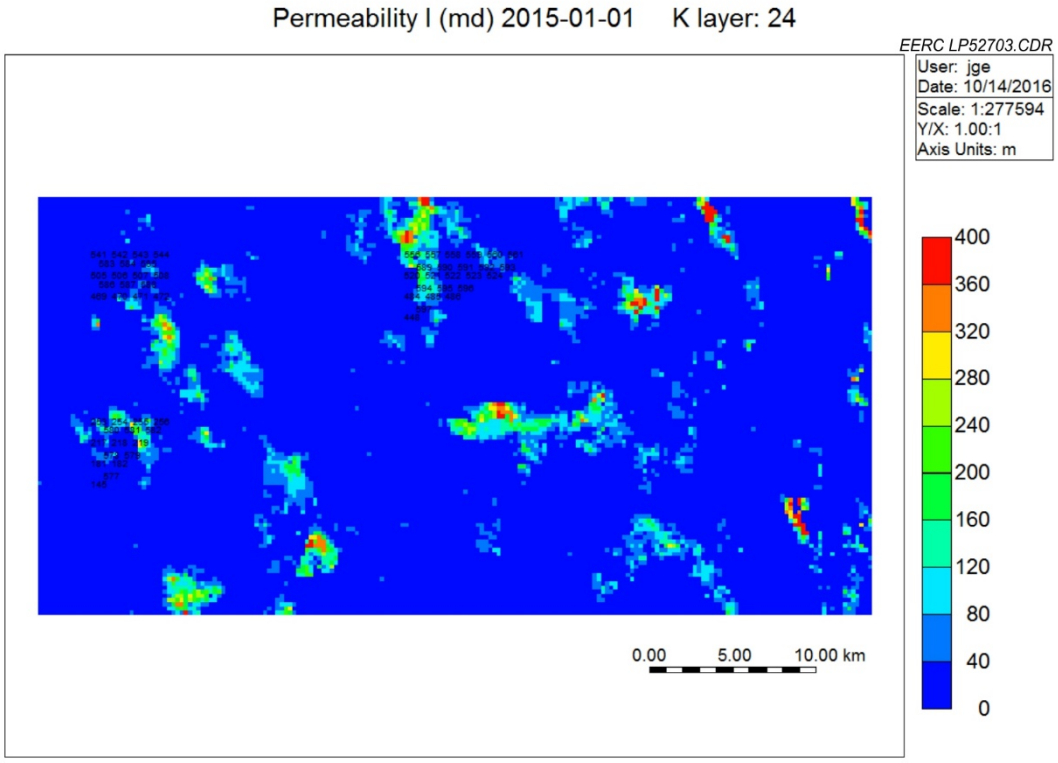

Figure A-28. Location of wells in the concentrated development simulation cases.

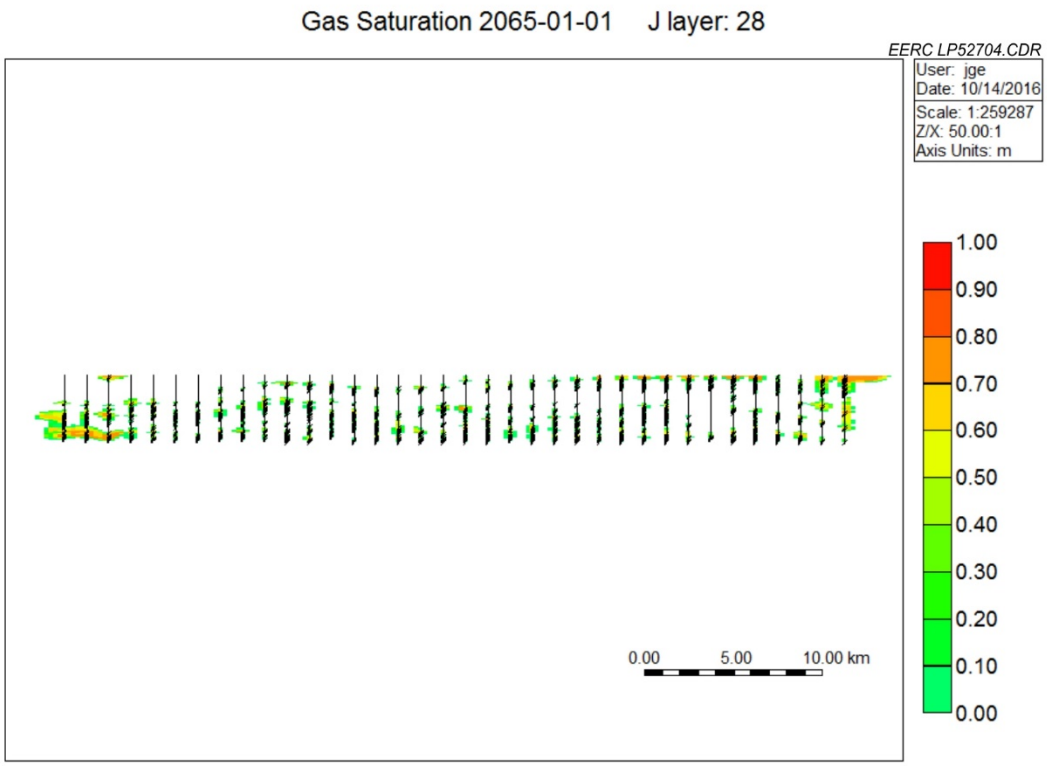

Figure A-29. Case A7: Cross-sectional view (Z/X ratio, 50:1) of CO_2 saturation profiles for flat structure.

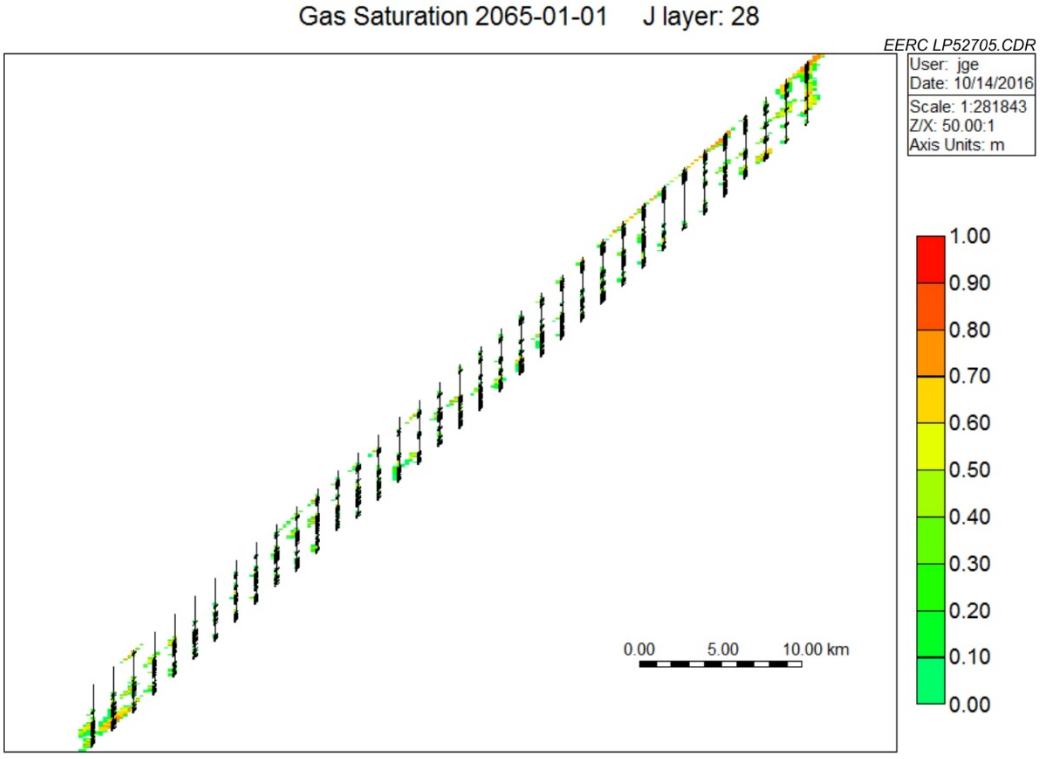

Figure A-30. Case A8: Cross-sectional view (Z/X ratio, 50:1) of CO_2 saturation profiles for monocline structure.

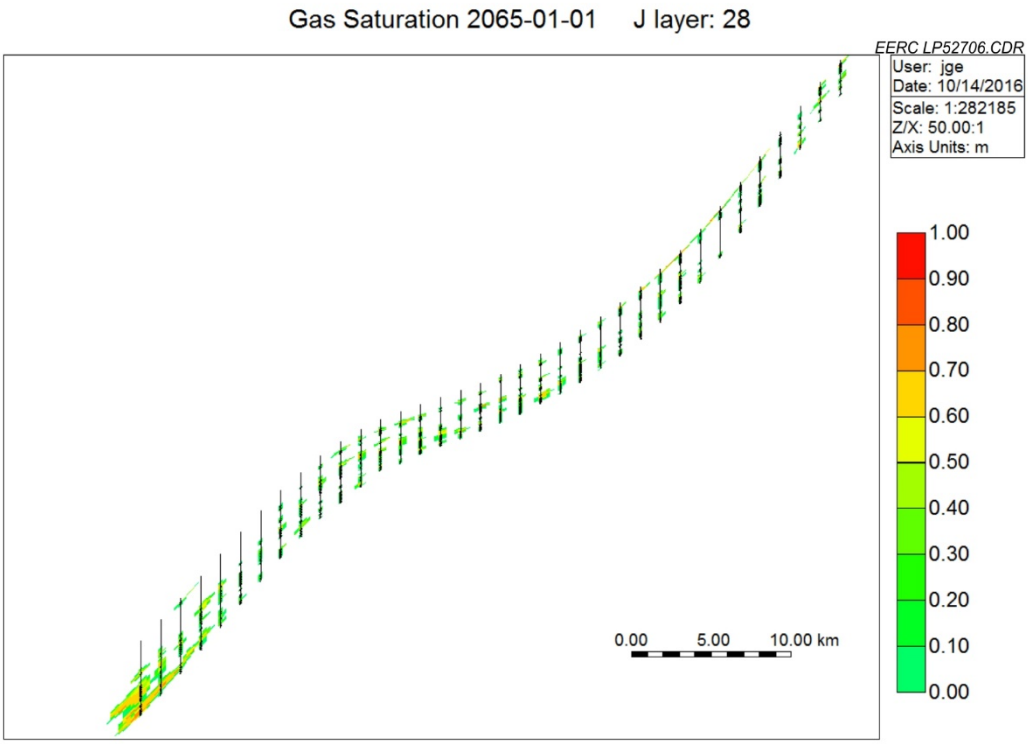

Figure A-31. Case A9: Cross-sectional view (Z/X ratio, 50:1) of CO_2 saturation profiles for trap structure.

REFERENCES

Barati, R., 2011, EORI collaboration in solving the challenges of Minnelusa: Presented at the EOR Commission and Technical Advisory Board Meeting, Laramie, Wyoming, www.uwyo.edu/eori/_files/eroctab_july_2011/reza%20-minelusapres%2007-19-2011%20tab_reza.pdf (accessed November 2016).

Barati R., 2012, Minnelusa core analysis and evaluation project: Presented at the EOR Commission and Technical Advisory Board Meeting, Denver, Colorado, www.uwyo.edu/eori/_files/eorc_tab_jan_2012/reza%20-%20core_project_tab_commission_01-31-2012_clean.pdf (accessed November 2016).

Garcia, R.G., 2005, Reservoir simulation of CO_2 sequestration and enhanced oil recovery in Tensleep Formation, Teapot Dome Field: Master thesis, Texas A&M University.

Pitts, M.J., and Surkalo, H., 1995, Detailed evaluation of the West Kiehl alkaline-surfactant-polymer field project and its application to mature Minnelusa waterfloods: Final technical report, p. 138, www.netl.doe.gov/KMD/cds/disk44/C-Chemical%20Flooding/BC14860_5.pdf (accessed November 2016).

APPENDIX B

ADDITIONAL FIGURES FOR THE BUNTER SIMULATIONS

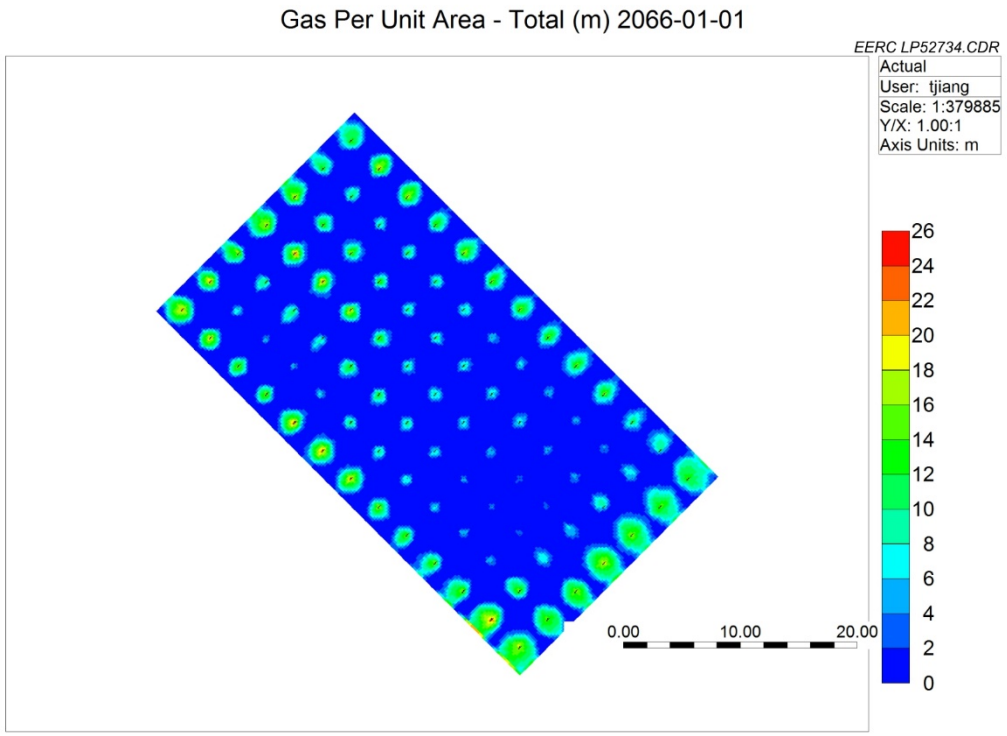

Figure B-1. Case B-A2: CO_2 footprint (total gas per unit area in meters) after 50 years of injection.

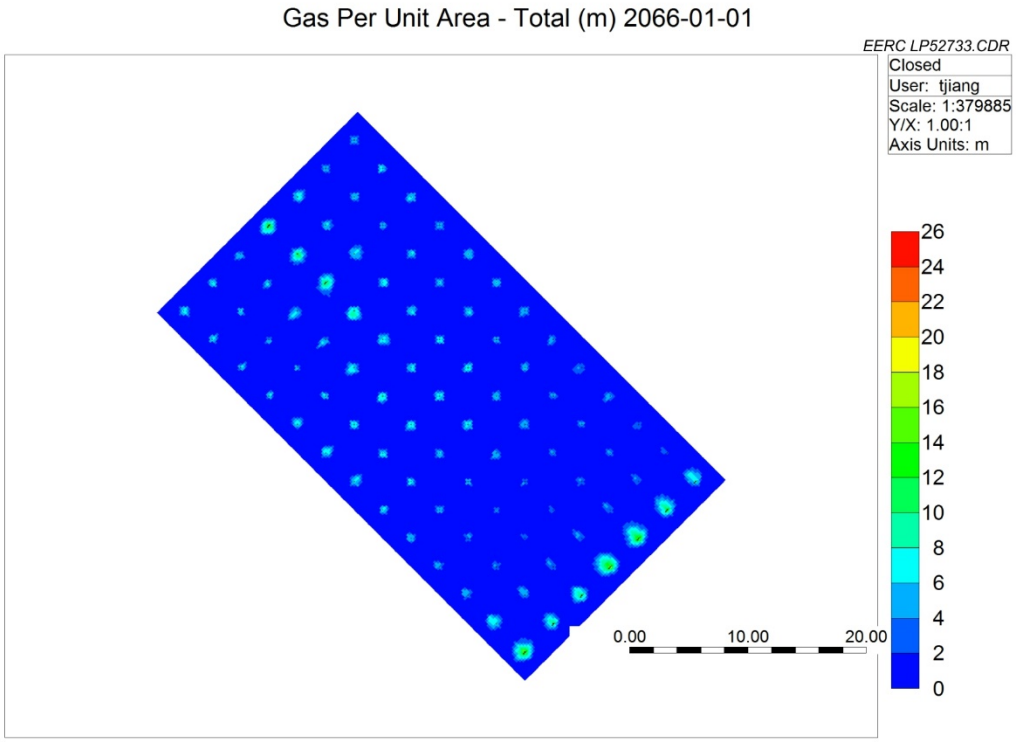

Figure B-2. Case B-A4: CO_2 footprint (total gas per unit area in meters) after 50 years of injection.

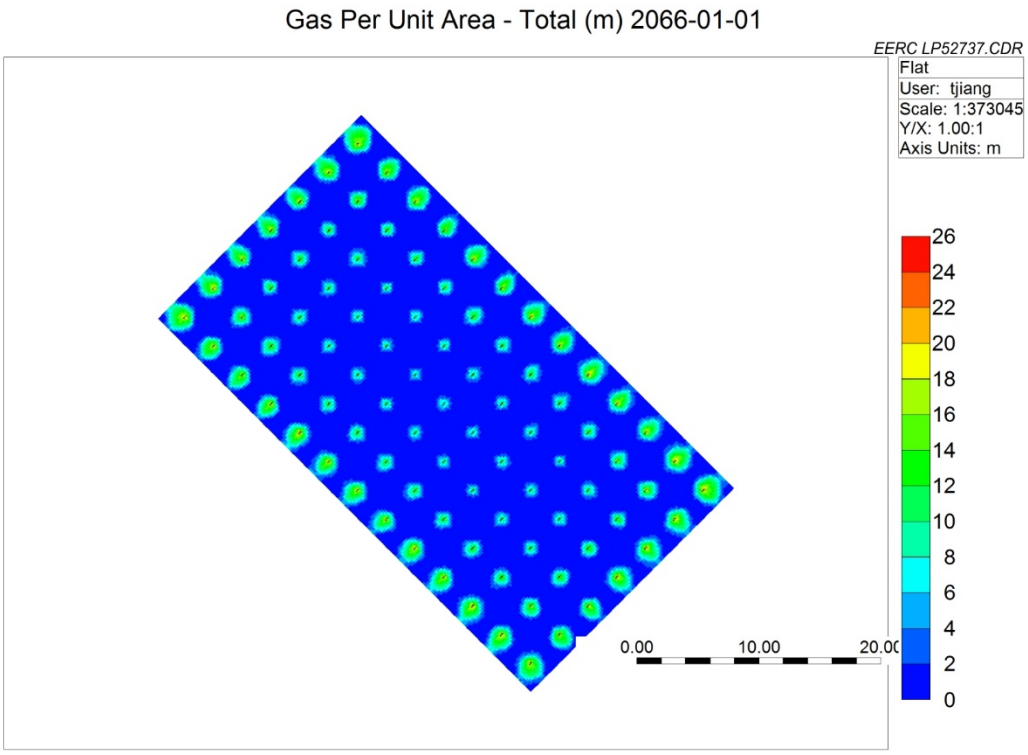

Figure B-3. Case B-A7: CO_2 footprint (total gas per unit area in meters) after 50 years of injection.

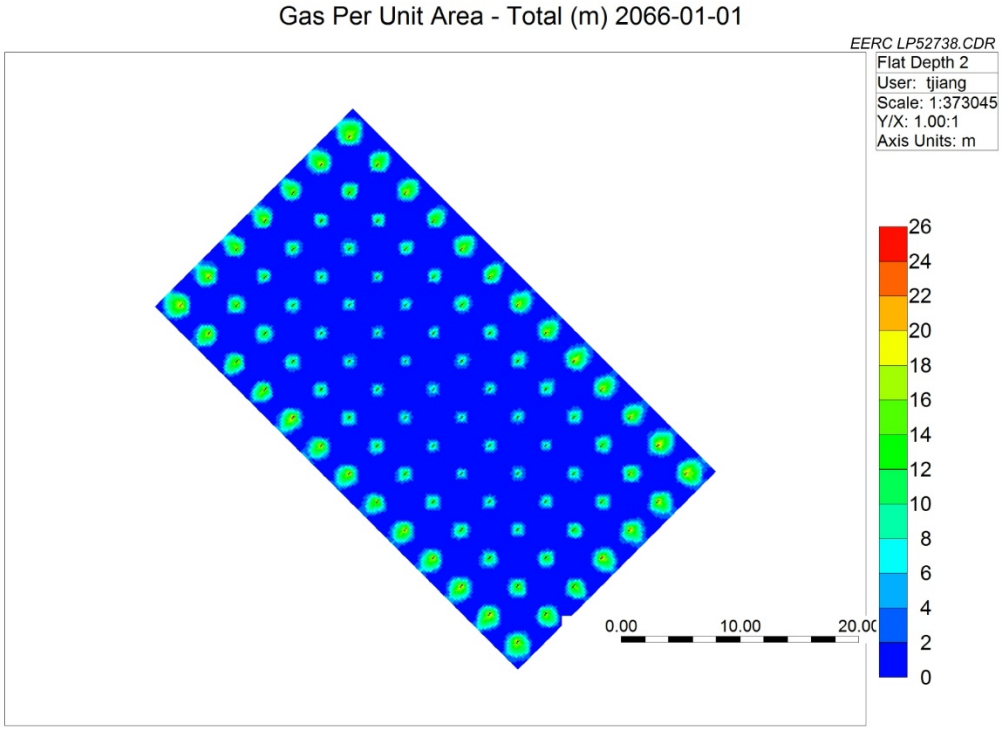

Figure B-4. Case B-A8: CO_2 footprint (total gas per unit area in meters) after 50 years of injection.

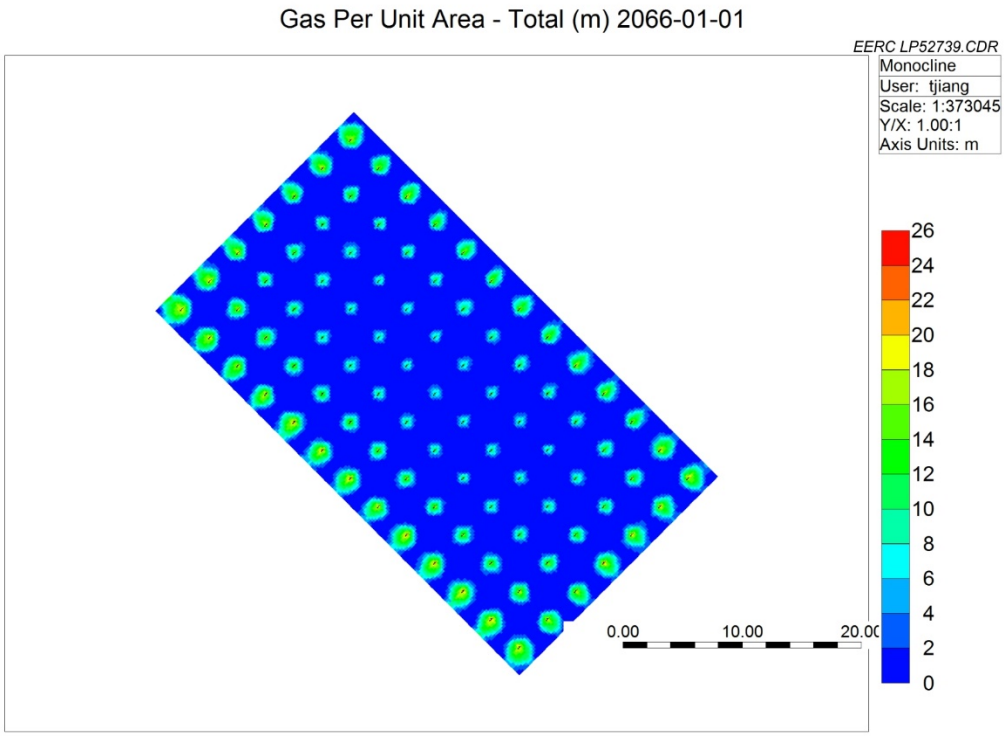

Figure B-5. Case B-A7-1: CO_2 footprint (total gas per unit area in meters) after 50 years of injection.

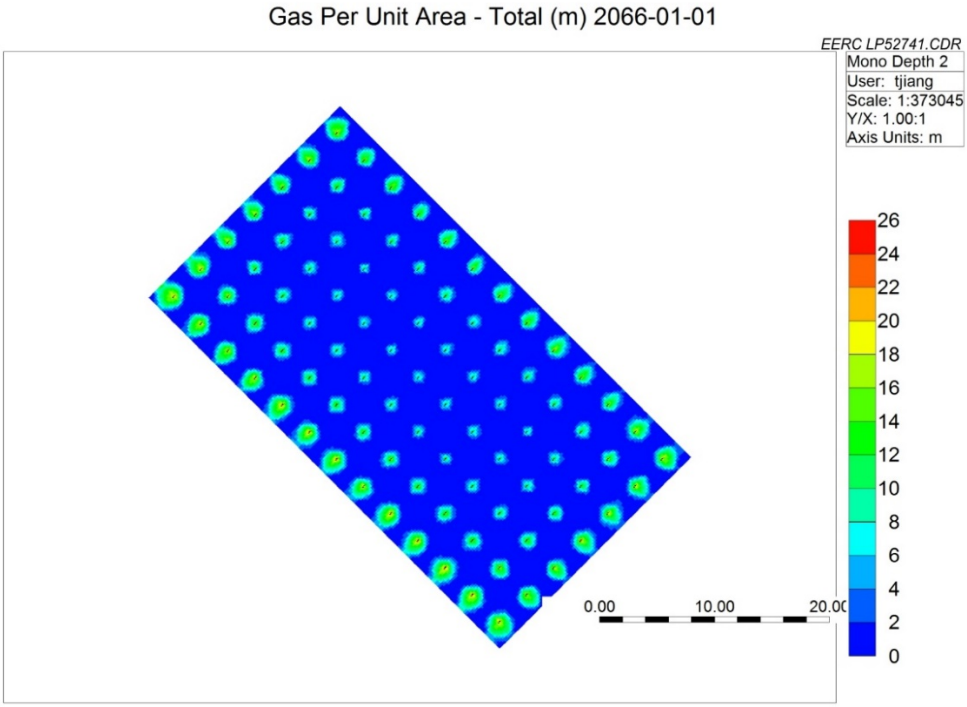

Figure B-6. Case B-A8-1: CO_2 footprint (total gas per unit area in meters) after 50 years of injection.

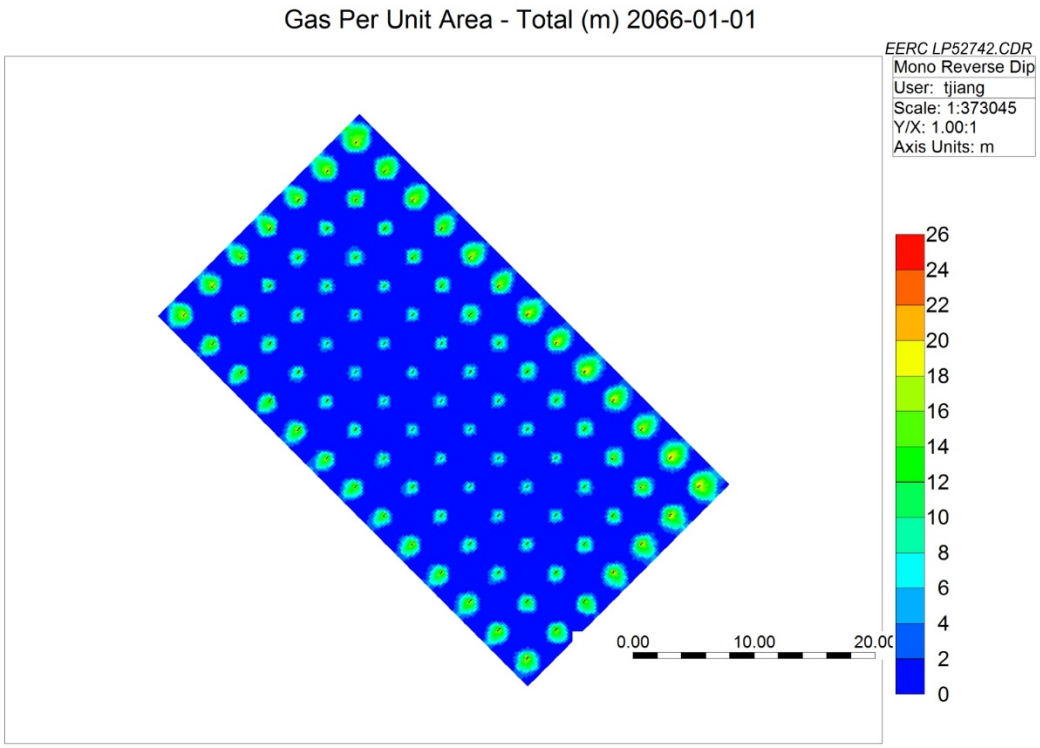

Figure B-7. Case B-A8-2: CO_2 footprint (total gas per unit area in meters) after 50 years of injection.

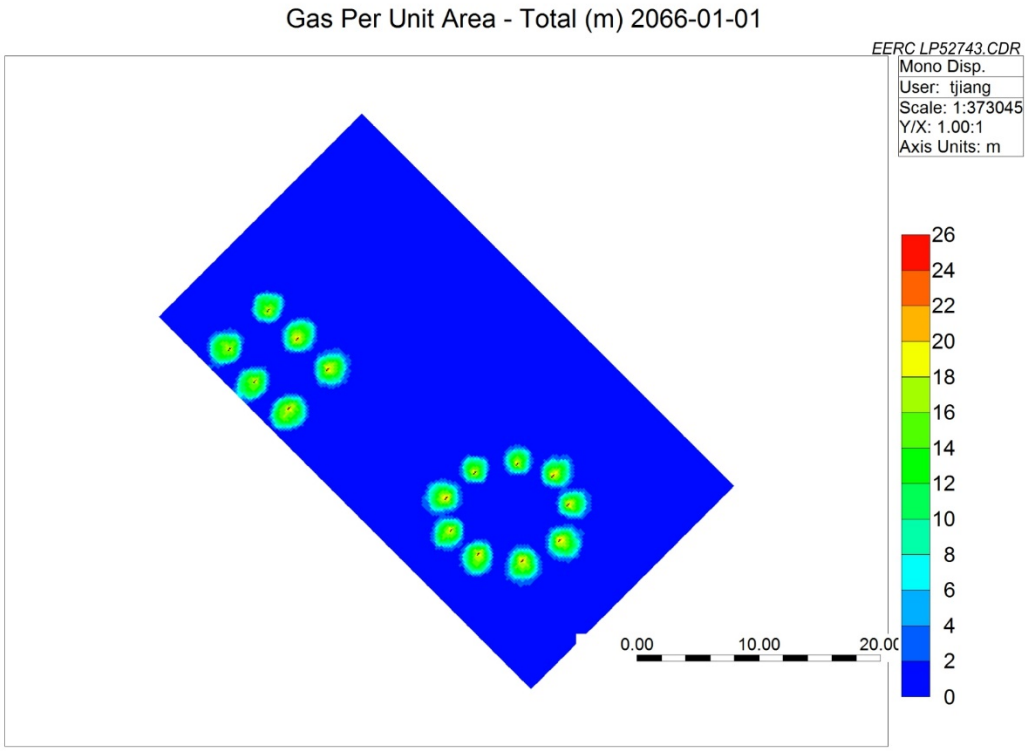

Figure B-8. Case B-A7D: CO_2 footprint (total gas per unit area in meters) after 50 years of injection.

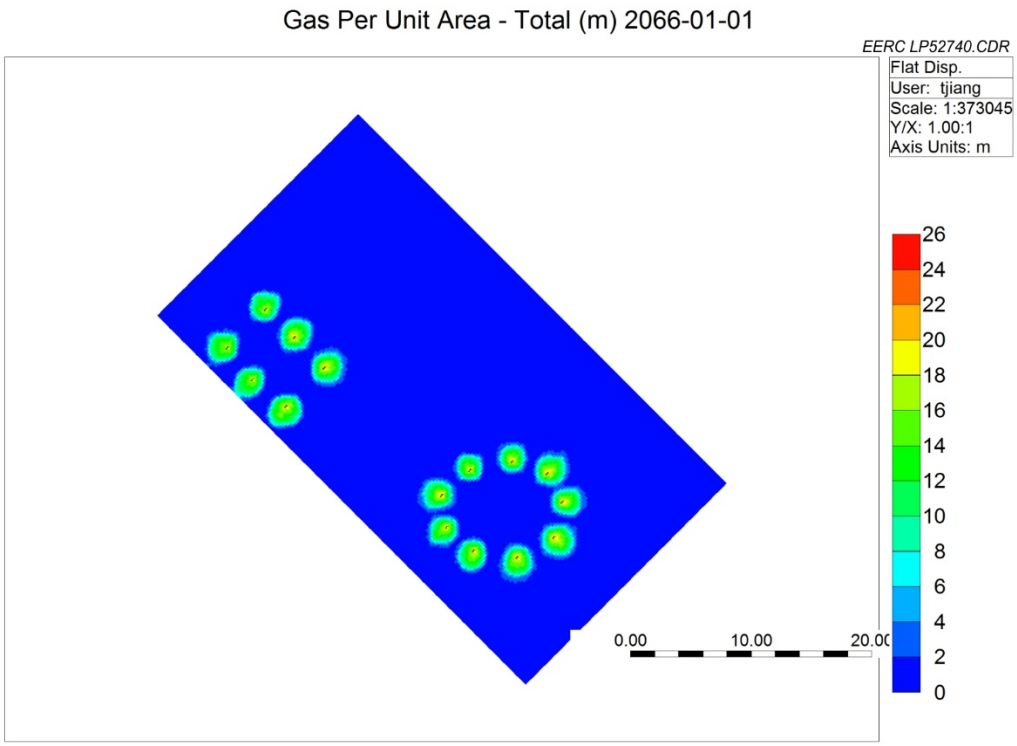

Figure B-9. Case B-A8D: CO_2 footprint (total gas per unit area in meters) after 50 years of injection.

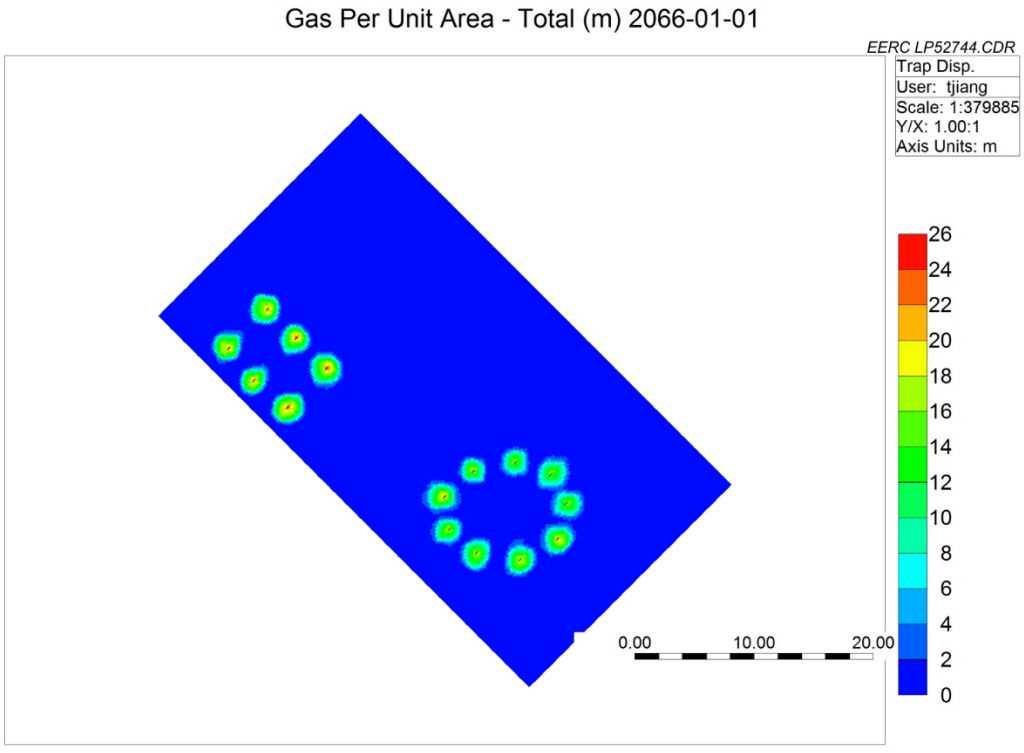

Figure B-10. Case B-A9D: CO_2 footprint (total gas per unit area in meters) after 50 years of injection.

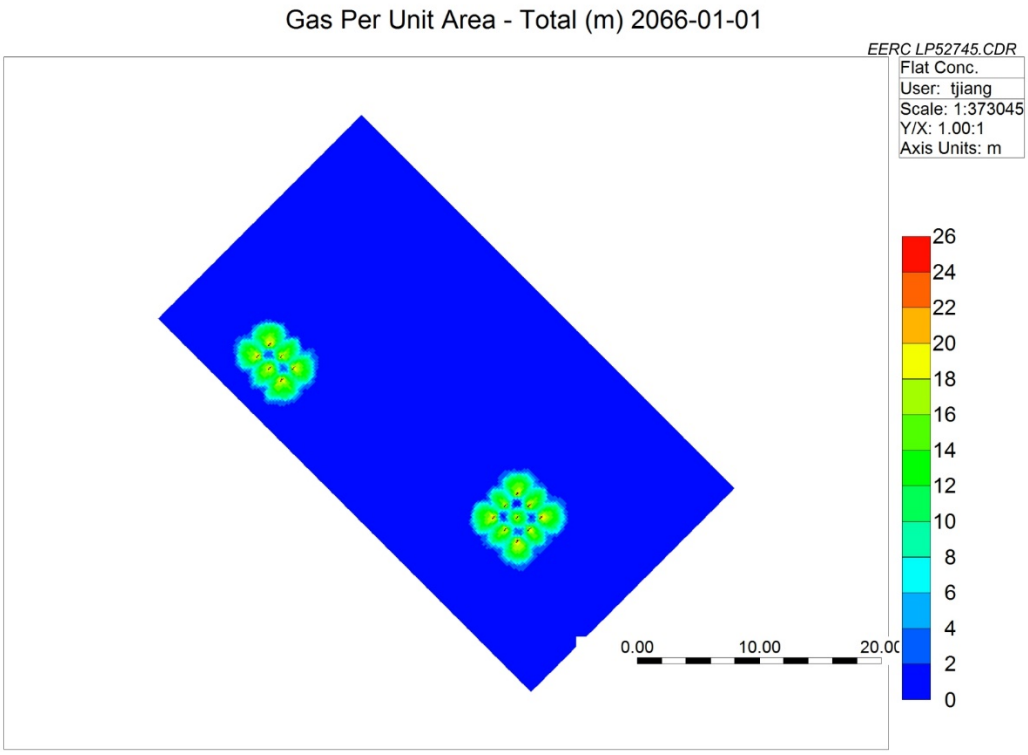

Figure B-11. Case B-A10C: CO_2 footprint (total gas per unit area in meters) after 50 years of injection.

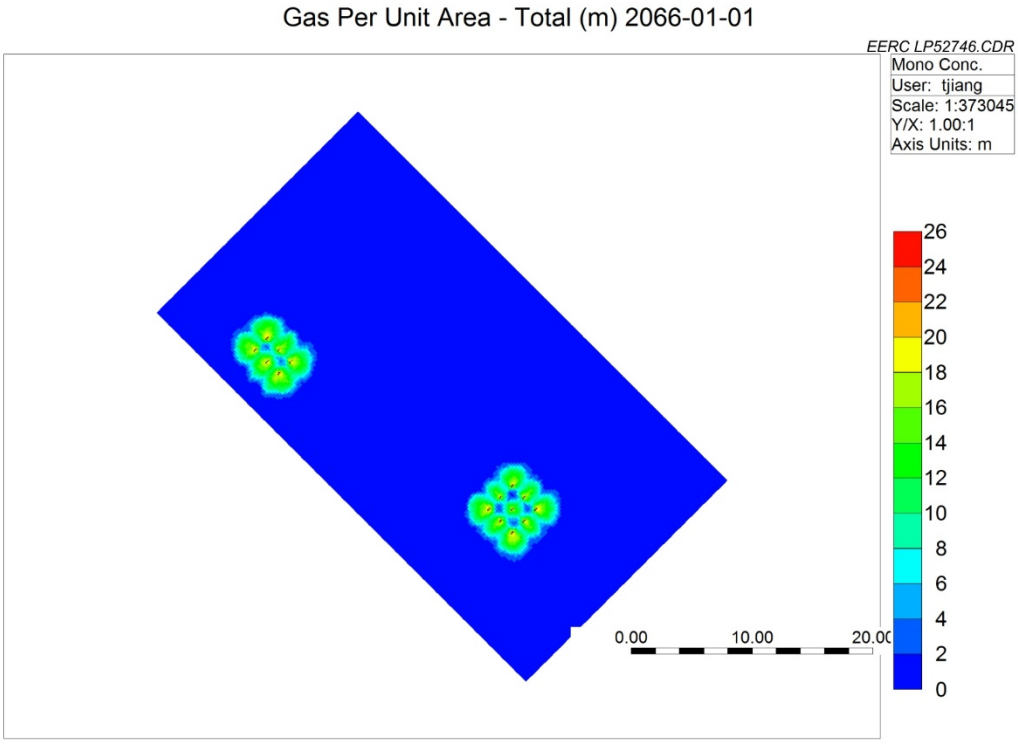

Figure B-12. Case B-A11C: CO_2 footprint (total gas per unit area in meters) after 50 years of injection.

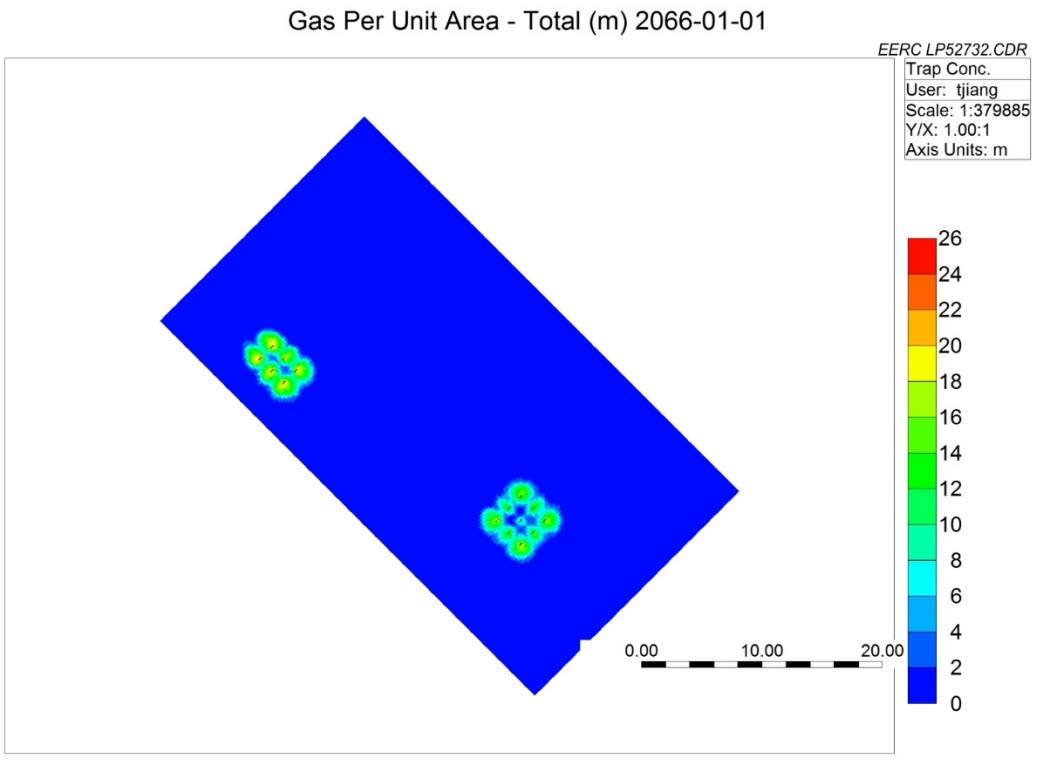

Figure B-13. Case B-A12C: CO_2 footprint (total gas per unit area in meters) after 50 years of injection.

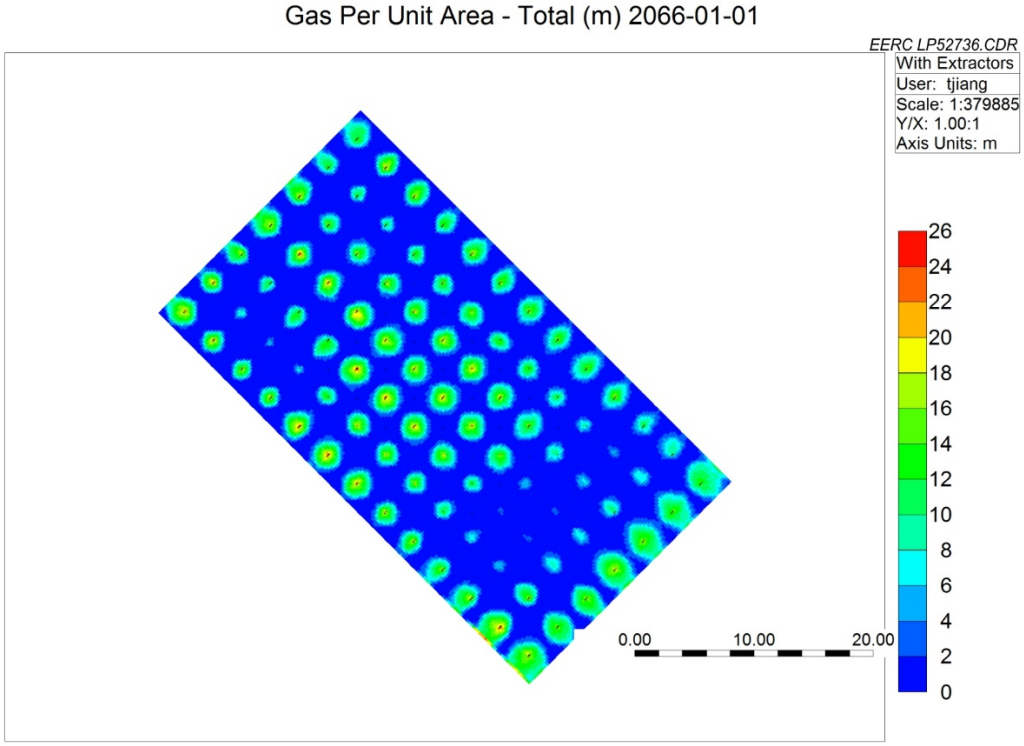

Figure B-14. Case B-A6: CO_2 footprint (total gas per unit area in meters) after 50 years of injection.

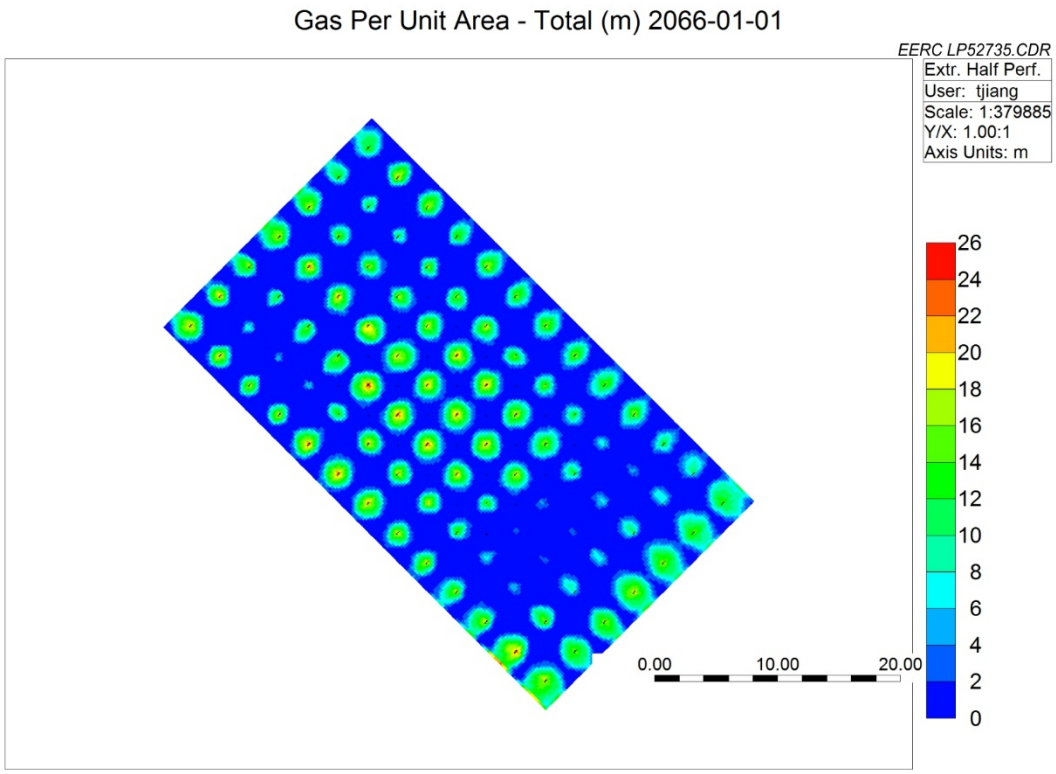

Figure B-15. Case B-A6P: CO_2 footprint (total gas per unit area in meters) after 50 years of injection.

IEA Greenhouse Gas R&D Programme

Pure Offices, Cheltenham Office Park, Hatherley Lane,
Cheltenham, Glos. GL51 6SH, UK

Tel: +44 1242 802911 mail@ieaghg.org
www.ieaghg.org